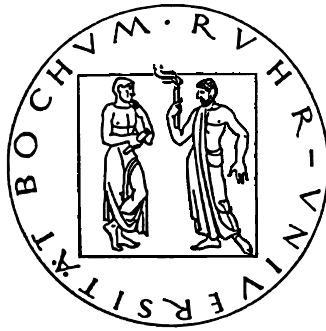# Spatio-temporal Seismicity Clustering

in the Cretan Region

Dissertation

zur Erlangung des akademischen Grades

eines Doktors der Naturwissenschaften

an der Fakultät für Geowissenschaften

der Ruhr Universität Bochum

vorgelegt von

Dirk Becker

aus Hamburg

Hamburg, im Juli 2007

Die vorliegende Arbeit wurde von der Fakultät für Geowissenschaften der Ruhr Universität Bochum als Dissertation im Fach Geophysik zur Erlangung des Grades eines Doktors der Naturwissenschaften anerkannt

1. Gutachter: Prof. Dr. Hans-Peter Harjes
2. Gutachter: PD Dr. habil. Thomas Meier
3. Gutachter: Prof. Dr. Stöckhert

Tag der Disputation: 14. 11. 2007

Abstract

The spatio-temporal seismicity distribution and the seismic energy release in the area of Crete is investigated at different time and length scales utilizing microseismic, instrumental and historic earthquake catalogues either obtained during this work or from the literature. We observe a spatio-temporal clustering of seismicity in the Cretan region over many time and length scales.

During an amphibian microseismicity study conducted between July 2003 and June 2004 the study region in the central and eastern forearc of the Hellenic Subduction Zone (HSZ) exhibited constantly high seismic activity with magnitudes up to $M_L = 4.5$. The large majority of events was located in the southern off-shore region. The southern termination of the interplate seismicity was found at depths of about 20 km in the region of the Strabo trench while the interplate seismicity in the north terminated below the southern Cretan shore at a depth of about 40 km creating a roughly 100 km wide seismogenic zone at the plate contact with rather evenly distributed seismicity and no detectable locked zones. Seismic activity observed at the Strabo trench suggests that it is a structure within the continental Aegean crust.

Intra-plate seismicity off-shore Crete within the Aegean crust on the other hand is concentrated at the Ptolemy and Pliny trench with hardly any seismic activity in between. This hints at a rigid block movement in the forearc without major internal deformation. This block is interpreted as a forearc sliver seperated by the Pliny and Ptolemy trenches. No significant seismic activity was detected towards the south in the thick sedimentary cover of the accretionary prism which seems to deform aseismically.

Seismic activity in the Aegean crust below Crete is mainly confined to the upper about 20 km depth. It follows trends compatible with north-east south-west striking surface structures like the Ierapetra graben. In the region of the Messara graben a southward dipping zone of microseismicity is observed that continues down to the plate contact at about 40 km. Furthermore, seismic clusters with small spatial extent and magnitudes up to $M_L 3.5$ were detected on Crete and close to the northern shoreline of Crete.

A study aimed at finding clusters of microearthquakes showing high correlation coefficients with respect to their waveforms successfully detected clusters in the interplate seismicity as well as in the intraplate seismicity of the continental crust in the region of the transtensional Ptolemy structure. The majority of the clusters are off the southern coast of Crete, in a region of elevated intraplate microseismic activity within the Aegean plate. Clusters in the Gavdos region are located at depths compatible with the plate interface while cluster activity in the region of the Ptolemy trench is distributed along a nearly vertical structure throughout the crust extending down to the plate interface. Most clusters show swarm-like behaviour with seismic activity confined to only a few hours or days, without a dominant earthquake and with a power-law distribution of the inter-event times.

For the largest cluster, precise relocations of the events using travel time differences of P- and S-waves derived from waveform cross correlations reveal migration of the hypocenters. This cluster is located in the region of the Ptolemy trench and migration occurs along the strike of the trench at 500 m/day.

Relocated hypocenters as well as subtle differences in the waveforms suggest an offset between the hypocenters and thus the activation of distinct patches on the rupture surface. The observed microseismicity patterns may be related to fluids being transported along the plate interface and escaping towards the surface in zones of crustal weakness (Ptolemy structure), triggering swarm-like cluster activity along its way.

A study using a formula to calculate the maximum seismic slip on a fault surface incorporating information from earthquake catalogues found a very low seismic coupling for the plate interface in the area of the 365 AD $M_w 8.3$ event. Calculated values are 0.25, 0.1 and less than 0.1 for the last 2000 and 500 years and for the time interval from 1964-1998, respectively. This means that a substantial part of the total slip is accomodated aseismically in the region of the plate contact in the western forearc.

The shallow plate contact of the HSZ south-west of Crete seems to be recently weakly coupled, shows high seismic activity up to magnitudes of about 6, but exhibits the potential to generate larger earthquakes. The behaviour of the plate contact south-west of Crete may be described as conditionally stable.

Contents

List of Figures

List of Tables

X

Preface

...κατα μερως δε γινωνται ωι σεισμωι της γης...
...the earthquakes occur in certain areas...
Aristotle (384 - 322 BC)

As already noted by Aristotle more than 2000 years ago, earthquakes have the tendency to cluster is space. Later on it became apparent that they also tend to cluster in time. Knowledge of the processes gouverning this spatio-temporal seismicity clustering is valuable because it can be used to estimate the location, time and possibly also the magnitude of future earthquakes. However, our knowledge of the underlying mechanisms governing earthquake generation is far from perfect. This is caused on the one hand by the fact that the rupture surface generally is buried within the earth and thus we have in most cases no precise information about rupture surface properties like the sizes of asperities, the distribution on fluids or pore-pressures and the material in contact at the fault zone. For large events there exists the additional problem that we often have no idea how frequently they occur because we are generally not able to observe several cycles of these major events due to the limited timespans covered by instrumental and historic catalogues.

By studying spatio-temporal seismicity patterns spanning several orders of magnitude of the spatial and temporal scales, however, it may be possible to gain some insight into the mechanisms at work. By means of microseismicity studies it is for instance possible to detect the activity of fluids and possible pore-pressure changes and to assess the current state of the rupture surface. Studies of historic and palaeseismological catalogues may answer the question whether large events are abundant on a strongly coupled fault or whether the seismic coupling is weak creating only sporadically large events. Finally, all this might be used to estimate the seismic hazard in a specified region.

1 Introduction

1.1 Patterns in Seismic Activity

A tectonic seismic event can be regarded as a mechanical failure of the medium caused by the accumulation of strain beyond the point of breakage. This stability threshold is determined by the rock properties, the fault surface, the current state of the fault and the rate of strain accumulation. In its most general form this relationship can be expressed by the Coulomb failure criterion which is a measure for the maximum shear stress that can be sustained on an arbitarily oriented surface without failure of the medium (e.g. Scholz, 2002)

$$\tau_{failure} = c + \mu_i(\sigma_n - P_f) \tag{1.1}$$

In this formulation $\tau_{failure}$ is the shear stress above which failure occurrs, c is the cohesion of the medium and thus a measure for its strength, μ_i is the coefficient of internal friction, σ_n the normal stress on the surface and P_f the pore pressure. Already this simple formulation of the failure criterion includes a hint at clustering of seismicity because the cohesion c on a preexisting fault is zero and thus frictional sliding on an already existing fault surface can be described by Amonton's second law (e.g. Scholz, 2002):

$$\tau = \mu_s(\sigma_n - P_f) \tag{1.2}$$

where μ_s is the coefficient of friction which is not identical with the coefficient of internal friction μ_i given above. Because μ_s is generally smaller than μ_i seismicity tends to cluster on already existing rupture surfaces because the initiation of a new crack is only possible if no favourably oriented older fault is present in the region of stress accumulation. Thus most seismic activity occurs along already exising rupture surfaces. The rupture of this fault contact is no longer governed by a bulk property (μ_i) but is now controlled by the contact property of friction (μ_s) which drops from its static to its dynamic value during rupturing. This behaviour is called slip weakening and explains why an initially small

slipping area can grow into a large rupture. This coefficient of friction is governed by the properties of the fault contact which may be subject to spatial and temporal changes. The presence of weak materials like sediments or fault gauge on the rupture surface may significantly lower the value of μ_s thus making the fault more likely to fail and making it less likely to accomodate large tectonic stresses. Because the material present at the fault surface may significantly change over small spatial distances also the seismic behaviour may show sharp spatial changes causing the spatial clustering of seismicity close to areas that deform predominantly aseismic.

Possibly the most important property influencing the behaviour of the rupture surface is the size and number of asperities at the rupture surface. An asperity is envisioned as a part of the fault contact that is locked in the time interval between subsequent seismic events while aseismic sliding may occur in the surrounding regions causing stress accumulation at the perimeter of these asperities (e.g. Kato and Seno, 2003). It is believed that the ratio between asperities and aseismically sliding parts of the rupture surface controls the potential of the rupture zone to create seismic events breaking the entire fault (Bourouis and Bernard, 2007). In case this ratio is high the fault surface may be completely locked and has the potential to accumulate large tectonic stresses. Such a fault surface becomes unstable and may fail seismically in a large dynamic rupture breaking the whole rupture zone (Lay and Kanamori, 1981). After this rupture the distribution of asperities at the fault contact might be changed and thus the seismic behaviour of the rupture surface may differ from the one observed before. If the ratio is low no rupture of the complete fault surface occurs. However, the breaking asperity may cause other changes in its surrounding than the initition of a large dynamic rupture.

Every breakage of an asperity causes a static stress change in its surrounding possibly bringing other parts of the fault surface closer to failure by means of stress loading (e.g. Ziv and Rubin, 2000). This static triggering is observed in aftershock sequences and also used to model microseismic activity in earthquake swarms using special trigger models (e.g. Ogata, 1983; Hainzl, 2004). Furthermore large earthquakes have the potential to create large positive changes in Coulomb stress (ΔCS) to load the adjacent fault segment and bring it closer to the point of failure. An example for this fault stress loading from other events may be seen along the North-Anatolian-Fault-Zone where the large events show a westward migration (e.g. Tokszös et al., 1979). Also dynamic triggering may occur when a passing seismic wave sufficiently lowers the effective normal stress to initiate a seismic event (West et al., 2005). Furthermore, in the case that fluids are present at the fault surface, a seismic event has the potential to change the pore pressure in its

vicinity leading to a possible overpressurization of adjacent fault areas (e.g. Miller and Olgaard, 1997; Yamashita, 1999). Also new pore space can be created in this process. A pore-pressure change can also be introduced into the system from the outside. This can happen either artificially e.g. during hydrofrac experiments (Bourouis and Bernard, 2007) or naturally e.g. by the intrusion of hydrothermal fluids (Parotidis et al., 2003). In both cases the increased pore-pressure reduces the effective normal stress on the rupture surface making shear failure more likely. All these processes and properties mentioned above have the potential to cause a spatio-temporal clustering of seismicity by either triggering subsequent earthquakes or modifying the properties at the fault surface in such a way that seismic failure is more likely than in adjacent areas.

The spatio-temporal clustering of seismic activity and energy release resulting from these processes and variable properties can be observed on all length and time scales. A quick look at a map depicting the worldwide earthquake distribution for the last 30 years or so will show that seismic activity is not randomly distributed over the surface of the earth but closely follows the plate boundaries with the largest activity concentrated in subduction zones. On the other end of the length scale acoustic emissions in a stressed rock sample align along planes of weakness favourably oriented with respect to the acting shear stresses indicating microcracking in the rock sample (e.g. Lockner et al., 1991) which may lead to macroscopic failure.

Also temporal clustering of events seems to be present on all length and time scales involved in natural seismicity. Bufe and Perkins (2005) found a highly significant worldwide clustering of events with moment magnitudes larger then $M_w = 8.6$ for the time period 1950-1965 when evaluating a complete worldwide catalog of events spanning the time period 1901-2001. For the Eastern Mediterranean a phase of elevated seismic activity, called the EBTP (Early Byzantine Tectonic Paroxysm), is observed between the middle of the fourth and the middle of the sixth century (Pirazzoli et al., 1996; Fig. 1.1).

On smaller spatio-temporal scales earthquake swarms and clusters of highly similar events are observed which are concentrated in space and time but lack the characteristics of a mainshock-aftershock sequence. They are a well known phenomenon in regions of volcanic or hydrothermal activity (e.g. Got et al., 1994; Kurz et al., 2004) but are also observed in the subduction zone environment (e.g. Igarashi et al., 2003) and for regions of strike-slip events (e.g. Nadeau et al., 1995). The duration of this activity is also highly variable ranging from only a few hours or days (e.g. Igarashi et al., 2003) to several months (e.g. Fischer and Horalek, 2000), with the longer time sequences in general indicative of a larger active volume. These differences may be attributed to different
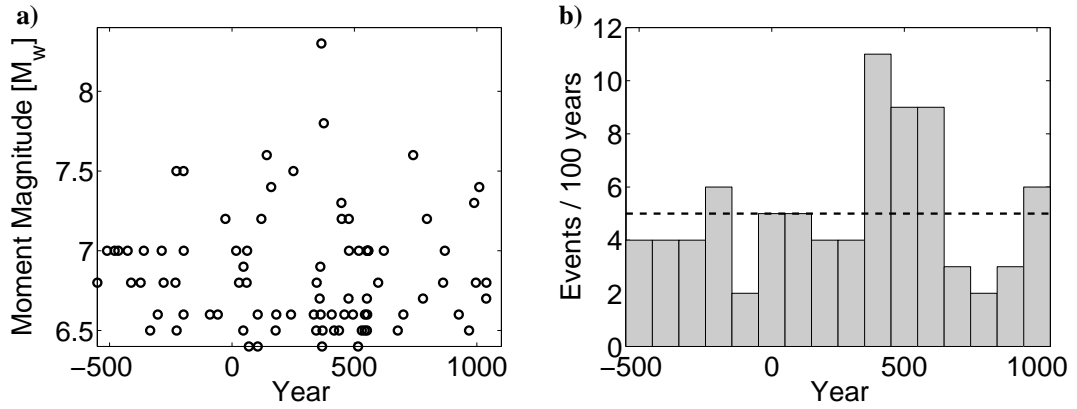
Figure 1.1: Apparent seismicity clustering in the Eastern Mediterranean during the so called EBTP. a) Magnitude-time plot for events with $M_w \geq 6.5$ in the Eastern Mediterranean according to the catalogue by Papazachos et al. (2000). b) Histogram for the events in a) with 100 year bins. Broken horizontal line indicates the mean of 5 events per century.
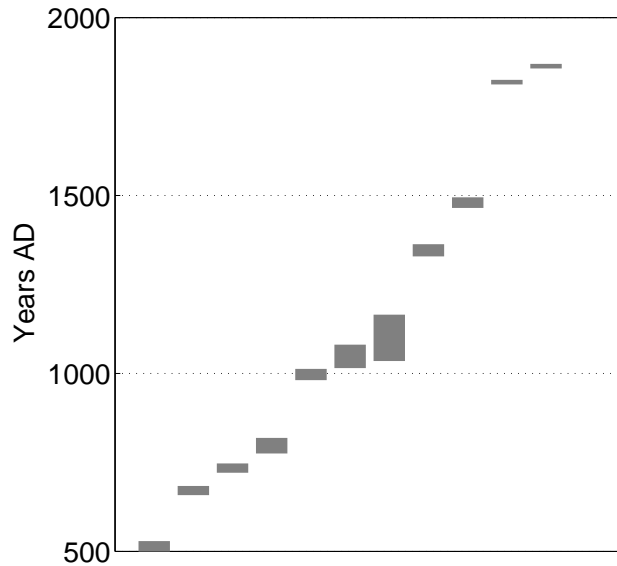
Figure 1.2: Fault ruptures of the Mojave section of the San Andreas fault at Pallett Creek

underlying trigger mechanisms or greatly differing porosities and permeabilities in the seismically active volume.

There are several possible physical models which may explain the presence of earthquake swarms and clusters of highly similar events. Yamashita (1999) proposes a model in which the fault slip of a seismic event is creating new porosity in the surrounding medium which may be filled by fluid from a source region thus reducing the effetive normal stress which may lead to the following failure of this patch of the rupture surface. Parotidis et al. (2003) suggest the idea of pore-pressure diffusion by ascending fluids which encounter patches of different diffusivity and criticality on their way. Ziv und Rubin (2000) investigate the contribution of static stress transfer caused by previous events. Although they only deal with events of magnitude $M_w \geq 4.5$ they are not able to find a lower threshold value for the triggering effect of an event and so it may also be relevant for even smaller events which are much tighter clustered.

The great variability of properties governing the seismic coupling of the rupture surface in conjunction with external influences like static and dynamic stress loading seems to be the reason why simple models of earthquake recurrence based on the idea of tectonic loading up to the point of failure (e.g. elastic rebound theory; Reid, 1911) generally fail to explain the observed seismicity patterns. In consequence this means that a simple recurrence model for earthquakes is in most cases questionable. This can e.g. be seen by the fact that the long anticipated Parkfield event did not materialize within the predicted time window (Roeloffs and Langbein, 1994) although the preceding sequence of events was regarded by many seismologists as a perfect example for a series of periodically occuring events (e.g. Bakun and Lindh, 1985). One possible explanation for the time delay of the Parkfield event which finally struck in September 2004 with respect to the statistically predicted time interval is the occurrence of two nearby thrust events which may have taken some of the stress load from the Parkfield section of the San Andreas Fault (Miller, 1996). Interestingly, other parts of the San Andreas Fault seem to be gouverned by interchanging periods of event clusters and seismic gaps (Sieh et al., 1989; Fig. 1.2). Ben-Zion et al. (1999) tries to explain this behaviour with the concept of mode switching on the fault where the system switches back and forth between periods of large characteristic events and periods with smaller magnitude events.

1.2 Seismicity Databases

In order to study spatio-temporal seismicity patterns it is necessary to have access to earthquake hypocenters which are as precise as possible. The catalogue used for quantifying these patterns should be homogeneous in both, space and time. Furthermore a low magnitude of completeness of the respective catalogue is desirable to study small scale patterns like seismic swarm activity, the precise aftershock activity of major events, seismic sequences prior to a mainshock or the current microseismic activity on known rupture surfaces. With sufficiently high temporal and spatial resolution of the dataset it might be possible to infer the underlying physical processes governing the seismicity distribution. To gain a complete picture of the seismic cycle and the seismic activity in the seismogenic region between major events it is necessary to combine seismicity information gained from different sources ranging from microseismicity studies to palaeoseismological information. Fig. 1.3 shows the different magnitude and time scales covered by the available datasets. For comparison Fig. 1.4 plots the lengthscale of different seismic and aseismic activities of a rupture surface versus their expected time of activity or recurrence, respectively. The length scale in this plot corresponds to one specific event, i.e. either a megathrust or silent slip event or one member of the aftershock or swarm sequence. The whole extent of an aftershock area might of course be larger than the rupture area of the main event and the seismogenic volume activated during swarm activity can also be tens to hundreds of km^3. The time scale for the megathrust and 'repeating events' in Fig. 1.4 refers to their return intervals while for the aftershock and swarm sequences as well as the silent slip events it refers to time duration of one sequence or event. Aftershock sequences of exceptionally large events, however, might be much longer than indicated in this figure spanning decades or even more than hundred years (e.g. Ogata, 1989).

While microseismic studies have a low completeness magnitude which depends on the station spacing and the ambient noise level within the network the recording time is generally limited to only a few months although there are studies which tried to monitor the microseismic activity of a region for several years to find systematic patterns in microseismic activity (Deshcherevsky and Zhuravlev, 2004). Despite the short recording period of these networks it is possible to image the seismogenic zones in seismically very active regions. These studies are able to reproduce the geometry of seismic faults and plate contacts even when operated for only a few weeks or months (e.g. Meier et al., 2004a). Microseismicity studies can also be utilized to predict the location of the next major event by mapping variations in the b-values on the rupture surface (Schorlemmer and Wiemer, 2005). However
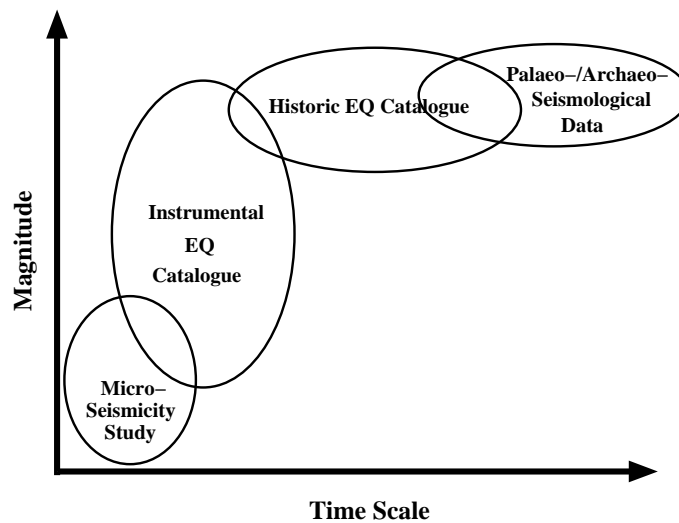
Figure 1.3: Magnitudes and times covered by earthquake catalogues

they may fail to identify rupture surfaces which are locked during the time of observation when the surrounding deforms aseismically or which exhibit only sparse seimic activity below the detection threshold of the network. Furthermore, temporary studies are generally limited to smaller magnitudes because the return period of larger events is much longer than the normal operation period of a microseismic network. These studies also have a local or at best regional focus and concentrate only on a specific area with magnitudes of completeness quickly increasing outside the networks. This sometimes prohibits the characterization of large events which may exhibit activity patterns differing from those observed in microseismic activity and spanning a rupture area of several thousand km^2 which is often beyond the extent of the microseismically surveyed region. Nevertheless microseismic studies allow a glimpse at the present state of the rupture surface in seismically active zones as has been done for numerous regions within the last 20 years (e.g. Igarashi et al., 2003; Meier et al, 2004a).

Catalogues of instrumental seismicty generally span a time period of approximately 100 years since the start of the continuous recording of seismicity with seismometres at the beginning of the 20th century. Due to the uneven distribution of seismic stations before the installation of the WorldWideStandardizedSeismographNetwork (WWSSN) there was a highly heterogeneous data set of global earthquakes. The installation of the WWSSN in the 1960s (http://www.iris.edu/about/GSN/map_wwssn.html) for the first time led to a global catalogue with more or less uniform magnitudes of completeness.

These stations are however confined to continents and islands and thus only provide a lim-
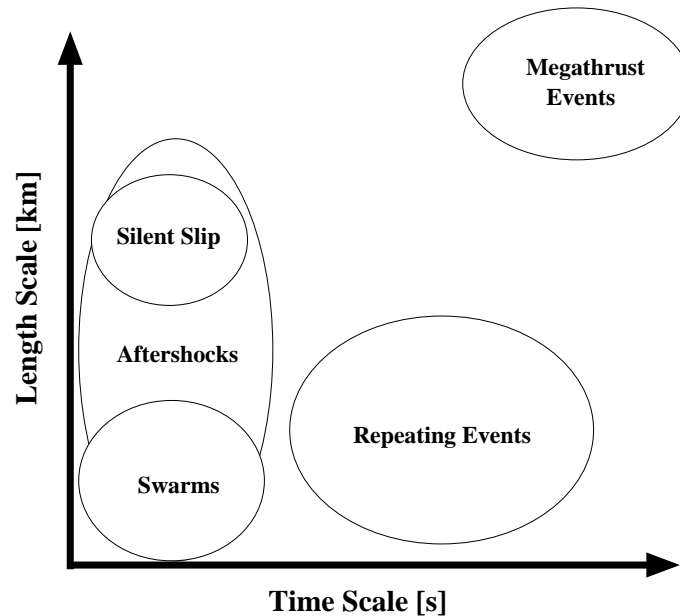
Figure 1.4: Spatio-temporal seismicity patterns

ited coverage for the world oceans and for instance the seismicity at the mid ocean ridges. However, the catalogues obtained by global or regional seismological networks generally span a time period of several decades with completeness magnitudes of 5 or better and thus form a valuable database of seismicity information. Although the covered time span is generally much shorter than the return period of the largest events within the region these catalogues may allow the estimation of return periods even for these events given a reliable database of medium sized activity. Furthermore these catalogues can cover several seismicity cycles for events with magnitude $M_w = 5 - 6$ in seismically active regions. It is also possible to study changes is seismic energy release utilizing these catalogues which may hint at seismic gaps or accelerating seismic energy release (e.g. Wyss and Baer, 1981; Papazachos et al., 2004). This information can be utilized to estimate the probability of a future major event.

Sometimes information about the largest events in a region can only be obtained from historic earthquake catalogues or, in case such catalogues are absent, from palaeoseismological or archaeoseismological studies. These studies tend to underestimate the number of intermediate and deep events because such events generally do not create as much destruction as shallow events or produce the surface ruptures or subsidence/uplift needed for paleoseismological studies.

While historic earthquake records contain the written account of a seismic event and thus

need the existence of a culture with written records, palaeoseismological studies can also be obtained for regions which were not populated when the seismic event occurred or only populated by civilizations without written history. Both catalogues allow the continuation of the seismicity record further into the past and thus allow a better estimation of the seismic energy release and possible changes in energy release or clustering of major seismic activity in the past. These catalogues also have their intrinsic drawbacks. Historic earthquake catalogues are always biased with respect to the population distribution and thus miss events in uninhabited regions which may nevertheless pose a high seismic risk while the palaeoseismological investigations are restricted to events which produced geological markers (e.g. stream offsets, fault scarps, shoreline changes) which were preserved since the day of the seismic event. Furthermore historic earthquake catalogues have very large uncertainties for the earthquake parameters because these parameters are at best estimated from macroseismicity maps with only sparse data. This is however not the case when additional information about surface rupture is provided that can be correlated with active fault traces. When considering palaeoseismological data the accuracy with which the earthquake can be located depends on the geological evidence used in the study. Stream offsets and fault scarps directly map the fault trace while coastline subsidence or uplift do not provide as good constraints about the epicenter of the event.

Archaeoseismology investigates the damages inflicated on man-made structures by a seismic event and may sometimes lead to information about events predating the historic earthquake catalogues. This subdiscipline of seismology is especially valuable in the Mediterranean region with its long historic record of ancient civilazations producing a record of seismicity dating back almost 4000 years (Stiros and Jones, 1996).

Combinig all these different earthquake catalogues and thereby utilizing their specific advantages may lead to a better understanding of the seismic activity with respect to its location and temporal as well as spatial characteristics.

1.3 The study region

This is only a short introduction into the general setting of the study region. Further information relating to specific topics dealt with in this work can be found in the introductory parts of the following chapters.

The general tectonic setting of the Aegean region is depicted in Fig. 1.5. The opening of the Red Sea which is transferred along the Dead Sea Tranform (DST) drives the Arabian plate

northward which causes the Anatolian microplate to escape in a westward direction. This movement gives rise to large right-lateral strike-slip earthquakes along the North Anatolian Fault Zone (NAFZ) where a relative motion of about 25mm/a is observed across the fault. A diffuse shear zone in the North Aegean Trough (NAT) which forms the border between the Aegean and the Adriatic plate (Scordilis et al., 1985) transforms this westward motion into the southward motion of the Aegean plate. While the south-west Aegean plate seems to move as a rather rigid miroplate according to GPS studies (McClusky et al., 2000) the region towards the east is goverend by N-S extension (Fig. 1.5). Towards the north in the area containing the NAT and the westward continuation of the NAFZ a region of mixed strike-slip and extensional behaviour exists.

A possible explanation for the observation that the plate velocity of the south-west Aegean microplate is larger than that of the Anatolian plate (Fig. 1.5) is the slab pull of the downgoing African lithosphere causing a roll back of the Hellenic Subduction Zone (Jolivet, 2002). A further contribution to the overall relative motion between the African and the Aegean plate comes from the small north-westward motion of Africa with respect to stable Europa. The velocities of all plate motions were determined by McClusky et al. (2000) and can by found in Fig. 1.5.

This convergent movement between the African and Aegean plate is accomodated by thrust events in the Hellenic subduction zone while the whole Hellenic Arc is simultaneously experiencing arc parallel extension (Armijo et al., 1992) which is evident from earthquake focal mechanisms (Papazachos and Papazachou, 1997; Jost et al., 2002) as well as from surface data (Duermeijer et al., 1998) and manifested in roughly north-south trending normal faults. Furthermore the island of Crete is in a rapid exhumation process (Meulenkamp et al., 1994; Lambeck, 1995) with especially high uplift rates in Western Crete. Due to the increasingly oblique angle of subduction towards central and eastern Crete transtensional structures within the continental Aegean plate are formed that dominate the bathymetry south of eastern Crete (Kahle et al., 1998; Kahle et al., 2000; Bohnhoff et al., 2005). These so called Ptolemy, Pliny and Strabo trenches constitue a graben system in the off-shore region that is continued towards the west in the Ionian trench. It is believed that the Ptolemy, Pliny and Strabo trenches in the east accomodate left-lateral relative motion. All these processes and movements must be reflected in the seismicity patterns of the Cretan region and possible models explaining them.

Fig. 1.6 shows a combination of historic (triangles), instrumental (circles) and microseismicity catalogues (squares) for the Cretan region to give an idea of the event distribution contained within the different catalogues. The instrumental ISC data (Engdahl et al., 1998)
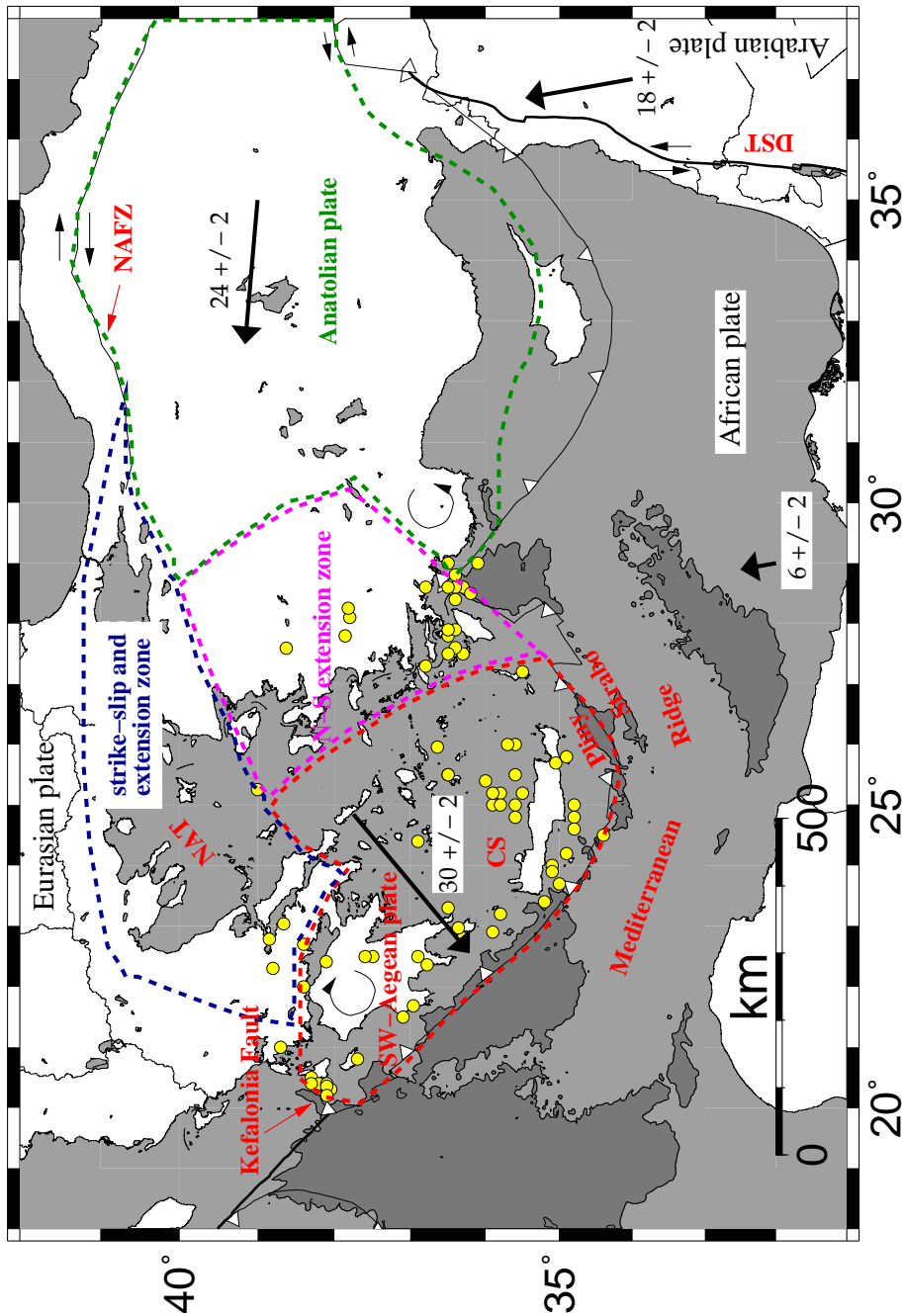
Figure 1.5: General tectonic and dynamic setting of the Aegean region. Velocities of plate motions are given in mm/a and regions with colour-coded borders are those given by McClusky et al. (2000) and are explained in the text. Yellow dots depict historic seismicity in the region of Greece during the time-interval 550 BC - 1999 AD with $M_w \geq 7$ given in the catalogue of Papazachos et al. (2000). Regions with a waterdepth exceeding 3000m are shaded in dark grey.

reveals the general trends in the Aegean seismicity with strong shallow seismic activity following the curvature of the Hellenic Arc and thus mapping the interplate seismicity of the subduction zone. To the west the Hellenic subduction zone is limited by the highly active Kefalonia Transform Fault (Fig. 1.5). Towards the east shallow seismicity related to the plate contact can be traced up to the Turkish coast. The depth distribution of the events on the concave side of the Hellenic trench allows one to follow the Benioff zone of the subduction to depths of up to 160km. The deepest activity can be observed in the eastern part of the volcanic island arc in the region of Kos and Nysiros which also forms a region of elevated seismic activity (region in the upper right corner of Fig. 1.6). The western part of the Benioff zone can only be traced to a depth of 100km below the volcanic center of Milos. This coincides with the observation that the dip angle of the oceanic slab increases from west to east (e.g. Knappmeyer and Harjes, 1999). The continental crust in the Cretan Sea (CS) generally exhibits only low seismic activity indicating that this region is only weakly deforming. However, the historic catalogue compiled by Papazachos et al. (2000a) reveals strong intermediate depth activity in that region which is captured neither in the instrumental dataset nor in the microseismicity studies (Becker, 2000; Meier et al., 2004a) due to their long recurrence intervals. When comparing the large events from the historic catalogue with instrumental data, several similarities in the event distribution can be observed (activity in the western Hellenic Arc, clustering of events in the east between Kos and Rhodes). However, also remarkable difference can be observed (lack of events with $M_w \geq 6.0$ in the Pliny-Strabo region and rather high activity in the Cretan Sea) which can not be readily explained. The distribution of the observed microseismicity is strongly influenced by the fact that stations were confined to the land areas of the study region and thus were not able to map microseismic activity e.g. in the Pliny and Strabo trenches. Because of the low detection threshold of the microseismicity surveys they are on the other hand able to map seismically active structures not discernable in the historic and instrumental seismicity records due to their much higher thresholds.

In order to gain insight into the seismicity patterns on different time and length scales it is thus necessary to evaluate historic, instrumental and microseismic activity in a complementary way to be able to assess the seismicity patterns both quantitatively and qualitatively. This includes the need of precise event location and relative relocation in order to obtain the spatial distribution of the recorded seismicity with the needed resolution.

This work consists of three seperate and independant studies dealing with different aspects of the spatio-temporal seismicity variability and seismic energy release in the vicinity of Crete spanning different time and length scales and utilizing seismic activity covering a
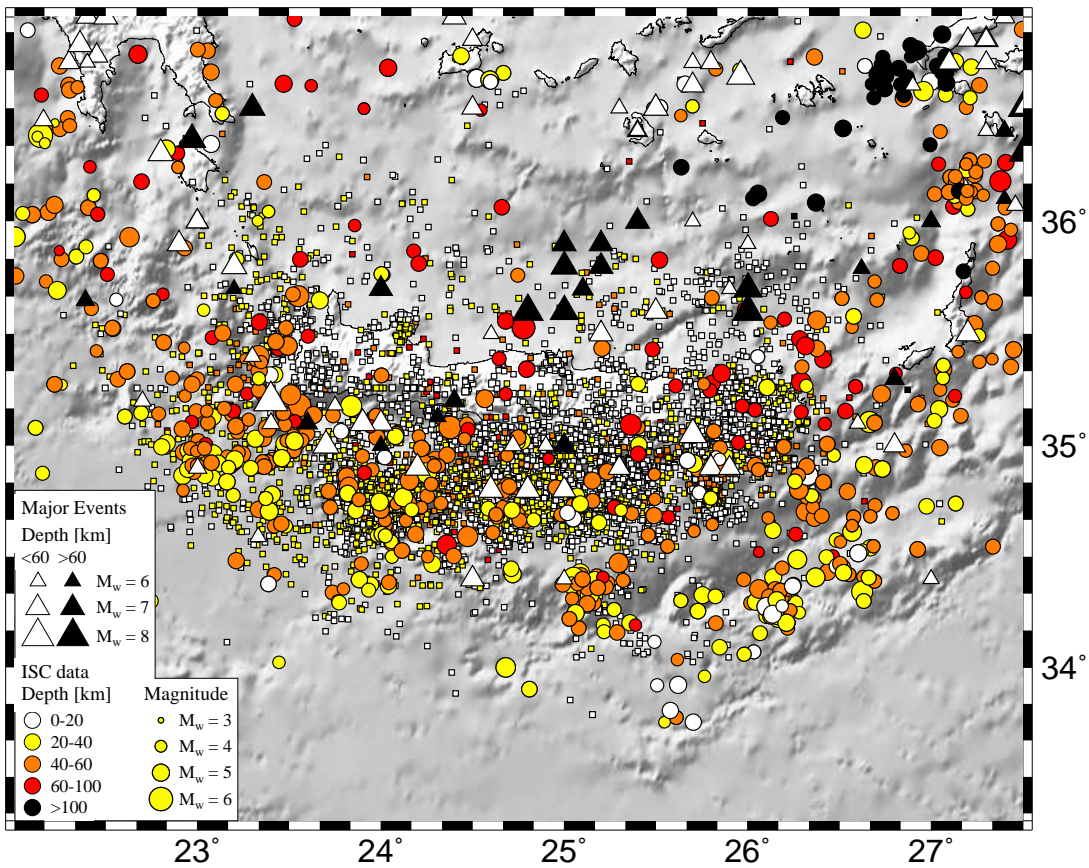
Figure 1.6: Seismicity recorded in microseismicity (squares), instrumental (circles) and historic (triangles) catalogues of the Cretan region. The same depth scale is used for all three catalogues.

magnitude range from $M_w 0$ up to $M_w \geq 8$. Although each study is complete in itself they are in many aspects complementary and taken together they give a clearer picture of the spatio-temporal seismicity clustering in the area of Crete. The first study evaluates the microseismicity recorded by an amphibian network (LIBNET) in the central and eastern forearc of the HSZ and its tectonic and dynamic implications. The second part of the work consists of a study dealing with the identification of events with similar waveforms (clusters) in the Cretan region. The spatial distribution of the detectect clusters is used to infer a model for the fluid circulation in the Hellenic forearc region and the temporal migration of cluster events is studied and interpreted. In the final study a formula is derived to estimate the maximum seismic slip on a rupture surface from events given in a seismicity catalogue. This formula is applied to the plate contact in the vicinity of the large 365 AD event south-west of Crete in order to estimate the seismic slip coupling for different time intervals. Furthermore, the temporal and spatial variability of the seismic energy release as given by historic and instrumental catalogues for that region is investigated.

2 Seismicity at the convergent plate boundary off-shore Crete observed by an amphibian network

2.1 Summary

The seismically active zones in the region of the convergent plate boundary of the Hellenic Subduction Zone (HSZ) on- and off-shore eastern Crete are located and investigated using an amphibian network of seismometers. The sea-based part of the network, the Libyan Sea Network (LIBNET), consisted of up to six Ocean Bottom Seismometers (OBS) while the on-shore complement was made up of five short period seismometers and the regional permanent broad-band stations on Crete and the surrounding islands. Thus, the whole intracrustal off- and on-shore graben system in central and eastern Crete consisting of the so called Strabo, Pliny and Ptolemy trenches as well as the Messara graben was covered by the network.

During the observation period from July 2003 - June 2004 the study region exhibited constantly high seismic activity with magnitudes up to $M_L = 4.5$. More than 2500 local and regional events were detected by the network and located using different velocity models and location techniques. Most of the seismic activity is located off-shore central and eastern Crete in the Libyan Sea while the on-shore region exhibits a considerably lower seismic activity. The downdip termination of seismicity related to the plate contact of the subducting African and overriding Aegean plates is found roughly below the southern shoreline of Crete at depths of 40 km while the updip limit of this seismically active zone is observed in the region of the Strabo trench slightly below 20 km depth thus constituting a seismogenic zone of 100 km width. Seismicity at the plate contact is more or less randomly distributed and no indication for locked zones were observed.

While in the region of the Ptolemy trench high seismic activity is observed from the sur-

face down to the plate contact, the continental Aeagean crust towards the south between the Ptolemy and Pliny trenches lacks significant seismic activity. Further activity within the Aegean crust is found in the region of the Pliny trench. This hints at a rigid block movement in the forearc between the Ptolemy and Pliny trench without major internal deformation. This block can be interpreted as a forearc sliver separated by the two trenches. Interplate as well as intraplate seismicity continues southwards to the region of the Strabo trench that represents the southern termination of the interplate seismogenic zone. The accretionary prism to the south showed practically no seismic activity during the observation period and seems to be deforming aseismically.

Seismic activity in the Aegean crust below Crete is mainly confined to the upper about 20 km depth. It follows trends compatible with north-east south-west striking surface structures like the Ierapetra graben. In the region of the Messara graben a southward dipping zone of microseismicity is observed that continues down to the plate contact at about 40 km. Furthermore, seismic clusters with small spatial extent and magnitudes up to M_L 3.5 were detected on Crete and close to the northern shoreline of Crete.

Completeness magnitudes of the recorded seismicity vary between 1.5 on Crete and the adjacent off-shore area of the Ptolemy trench and values of up to 2.5 in the vicinity of the Strabo trench. B-values found in the Aegean crust are about 1.0 with slighly higher values towards the south-east at the Pliny trench whereas b-values for seismic activity around the plate contact are slightly lower at about 0.8.

2.2 Introduction

2.2.1 Tectonic setting of the HSZ

The HSZ is the seismically most active region in Europe. This high seismic activity is caused by the subduction of the oceanic African lithosphere beneath the continental Anatolian-Aegean lithosphere as indicated by Benioff zones (Papazachos and Comninakis, 1971; Makropoulos and Burton, 1984; Papazachos et al., 2000) and seismic tomography (Spakman et al., 1988; Spakman et al., 1993; Papazachos and Nolet, 1997). According to Thomson et al. (1998) the current active margin south of Crete was initiated approximately 15 Ma ago following earlier subduction of oceanic basins north of the present day active margin and accretion of continental terranes to Eurasia (Dercourt et al., 1986; Gealey, 1988). According to neotectonic reconstructions, this active margin

migrated approximately 400-500 km to the south-west during the last 15 Ma (ten Veen and Meijer, 1998; ten Veen and Kleinspehn, 2003). The retreat of the active margin is caused by slab-pull of the downgoing African lithosphere (Angelier et al., 1982; LePichon et al., 1995; Laigle et al., 2004). In the same time-interval, the African plate approached Eurasia by about 150 km (Dercourt et al., 1986; Gealey, 1988; Facenna et al., 2003). At present the Aegean plate moves towards the south-west with an approximate velocity of 3.0-3.5 cm/a with respect to stable Eurasia while the African plate exhibits a northward drift of less than 1 cm/a within the same reference frame (McClusky et al., 2000).

The Hellenic Subduction Zone in the region of western Crete seems to enter the phase of continent-continent collision (ten Veen and Kleinspehn, 2003) with the passive continental margin of Africa entering the subduction (Meier et al., 2004b). While subduction in western Crete occurs almost normal to the continental margin of the Aegean plate, subduction becomes more and more oblique towards the east (LePichon et al., 1995). This oblique subduction and the roll back of the downgoing slab are likely causes for the transtensional structures within the continental Aegean lithosphere which dominate the bathymetry south of eastern Crete (Kahle et al., 1998; Kahle et al., 2000; Bohnhoff et al., 2005). These structures are indicated in Fig. 2.1 by solid lines. In the vicinity of the northernmost off-shore trench (Ptolemy) steeply dipping faults were imaged in active seismic studies of the region (Bohnhoff et al., 2001) while swath-mapping and seismic reflection profiles in the region of the Pliny and Strabo trenches show en echelon troughs and normal faulting (e.g. Huchon et al., 1982; LePichon et al., 1982; Huguen et al., 2001). Towards the west this graben system continues in the Ionian trench which is interpreted as an extensional structure within the Aegean lithosphere (Lallemant et al., 1994) that shows currently little microseismic activity (Meier et al., 2004a). All these so called trenches are interpreted as structures within the continental Aegean crust while the active continental margin is found further south buried below a thick sedimentary cover (Lallemant et al., 1994; Mascle et al., 1999; Huguen et al., 2001).

2.2.2 Seismicity of the HSZ

For the area of the HSZ an exhaustive historic catalogue (Papazachos et al., 2000), spanning the last 2500 years, as well as a number of microseismicity studies investigating the entire (Hatzfeld et al., 1993) or parts of the forearc (e.g. Delibasis et al., 1999; Becker, 2000; Meier et al., 2004b) are available in addition to global catalogues covering the second half
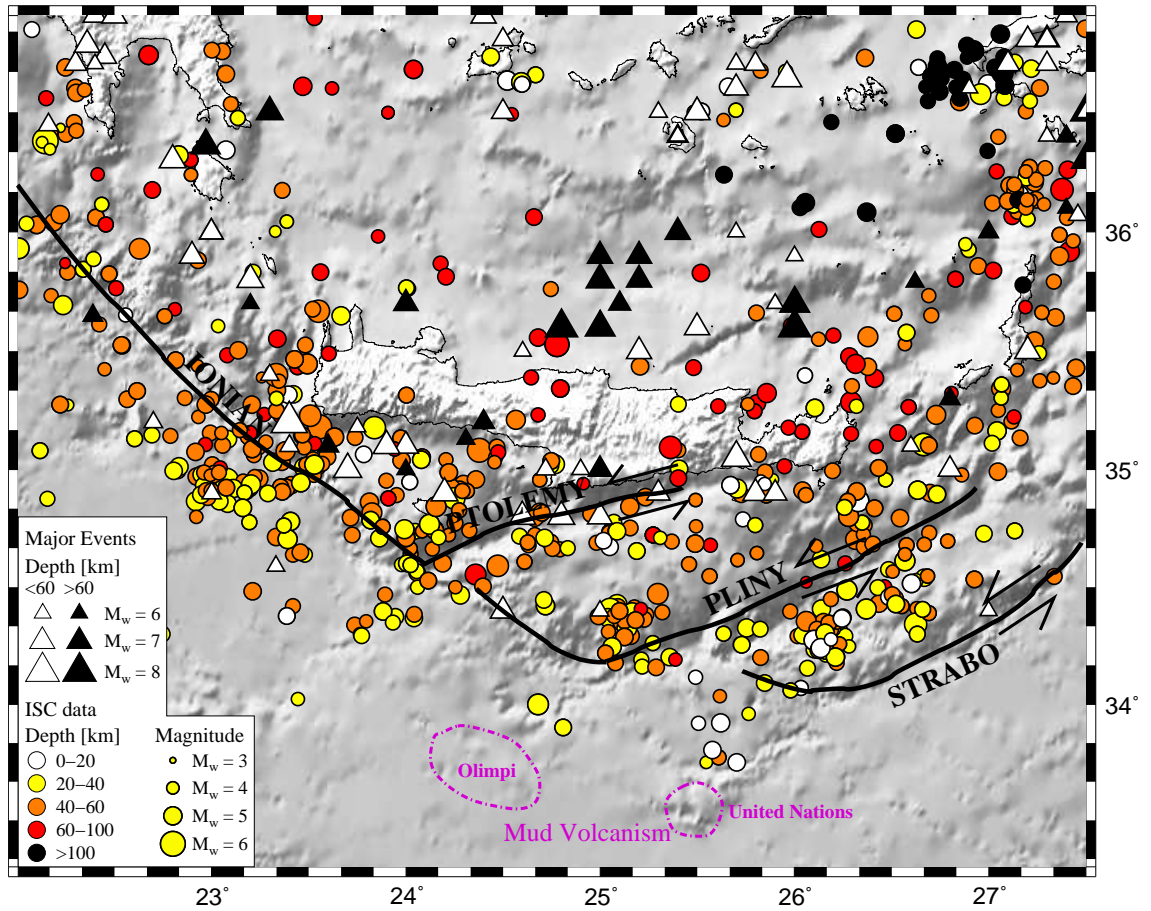
Figure 2.1: Historic and instrumental seismicity recorded at the convergent plate boundary of the Hellenic Subduction Zone. Major seismicity (triangles) with magnitudes $M_w \geq 6.0$ spans the time period 550 BC - 1999 AD (Papazachos et al., 2000) while circles represent the relocated seismicity according to the ISC catalogue for the time period 1963-1999 (Engdahl et al., 1998). Solid black lines indicate the locations of the Ionian, Ptolemy, Pliny and Strabo trenches as seen in the bathymetry and arrows indicate sense of displacement of the transtensional structures (e.g. Kahle et al., 2000; tenVeen and Kleinspehn, 2003). Mud volcano fields in the accretionary prism south of the Pliny and Strabo trenches are indicated by broken lines (Galindo-Zaldivar et al., 1996; Cifci et al., 1997).

of the 20th century (e.g. Engdahl et al., 1998). This allows the study of seismic activity over several time and length scales and faciliates the identification of possible temporal and spatial changes of the seismic activity.

The first order trend of seismic activity in the the HSZ is caused by the seismogenic part of the plate contact. This seismicity follows the amphitheatrically curved shape of the subduction zone from the Kefalonia fault in the west to the Turkish coast north-east of Rhodes in the east. Fig. 2.1 depicts this activity in the vicinity of Crete. Towards the north, the Benioff zone seismicity of the HSZ can be traced to depths of up to 180 km in the eastern part close to Rhodes and depths of approximately 100 km below Milos in the west using the relocated ISC catalogue (Engdahl et al., 1998; Fig. 2.1). From inspection of Fig. 2.1 it can be seen that this intermediate depth seismicity is much stronger in the central and eastern part of the Cretan Sea north of Crete when compared to the west. This holds both for historic and instrumental data although no large events with $M_w \geq 6.5$ are found in the instrumental database.

The largest historically documented event with a magnitude of $M_w\,8.3$ (Papazachos et al., 2000; Stiros, 2001) occured in 365 AD in the western forearc of the subduction zone south-west of Crete and caused coastline uplifts of up to 9 m on western Crete and up to 2.5 m on the adjacent island of Antikythira (Pirazzoli, 1996; Stiros, 2001). This event presumably ruptured the plate interface between the African and Aegean plates (Papazachos and Papazachou, 1997; Papazachos et al., 1999) on a lateral extent of 300 km from south of central Crete up to 22°E (Papazachos, 1996). The eastern part of this area exhibits strong current seismicity (Fig. 2.1).

In instrumental seismicity data (Engdahl et al., 1998) crustal activity within the Aeagean plate is found in the central and eastern off-shore region south of Crete in the vicinity of the Ptolemy trench and further south between the Pliny and Strabo trench. Also historic catalogues (Papazachos et al., 2000) show shallow seismic activity in that area although it is generally not possible to discriminate between intra- and interplate activity for these historic events. Remarkably, almost all of the shallow strong historic activity with magnitudes of $M_w \geq 6$ locates close to the Cretan shore in the area of the Ptolemy trench or even on-shore while the medium sized instrumental activity which is generally in the range of $M_w 3.5 - 5$ is found in its majority further south between Pliny and Strabo. Most of this shallow activity is likely caused by relative movements along transtensional structures caused by the oblique subduction and slab roll-back (Kahle et al., 2000; Bohnhoff et al., 2005). In the western off-shore area, seismicity is generally confined to the plate interface with low seismic activity at the Ionian trench. Historic and instrumental data

show a good agreement in this region. Seismicity on Crete itself is generally low with a trend of increasing activity towards the east and some strong histroric events along the south coast of central and eastern Crete. Towards the north in the Cretan Sea hardly any shallow seismic activity is observed and most of the seismicity is of intermediate depth (70 - 300 km). Interestingly, this strong intermediate depth seismicity north of Crete with $M_w \geq 7$ earthquakes is much stronger in the eastern part and not recognizable in the instrumental dataset.

Microseismicity studies in the forearc of the HSZ complement the historic and instrumental data sets. Several microseismic studies were conducted on the islands of Crete and Gavdos with temporary short period networks to study the distribution of microseismic activity in the region. In 1988 a study of microseismic activity covering the whole southern Aegean Sea recorded only sparse microseismic activity on-shore Crete while most activity occured south of Crete between the Pliny trench and the coast (Hatzfeld et al., 1993). A study conducted in 1995 in central Crete (Delibasis et al., 1999) however found significant microseismic activity in the Messara graben, the Heraklion Basin as well as in the southern off-shore region of the Ptolemy trench. This latter activity was also observed during a 2000/1 field campaign aimed at studying the microseismic activity in central Crete (Meier et al., 2004a). Field campaings in the years 1996-2002 mapped microseismic activity at the plate interface (Meier et al., 2004a) and found an offset between the southern border of the Aegean lithosphere and the southern border of active interplate seismicity. Most of the off-shore activity in the western part originated at the plate contact with only little activity in the Ionian trench. A microseismic study in eastern Crete in early 1999 found abundant activity on-shore eastern Crete as well as in the southern off-shore region (Becker, 2000).

The only OBS network operated to study microseismicity so far consisted of five analogue OBS stations that were deployed southeast of Crete for 8 days in July 1988 and recorded around 1000 microearthquakes of which more than 140 were located (Kovachev et al., 1991; Kovachev et al., 1992). The authors interpreted the spatial distribution of the hypocenters as an en-echelon positioning of the subduction zone manifested bathymetrically in the Strabo- and Pliny-trenches.

The increased availability of digital OBS stations with longer recording times during the last two decades led to a number of earthquake studies using amphibian networks in different subduction zones to better constrain the subduction related seismic activity with respect to updip and downdip limit of the seismogenic zone, activity within the overriding crust, seismic events within the downgoing lithosphere and spatial variability of this

activity (e.g. Husen et al., 1999; DeShon et al., 2003).

In this paper microseismicity recorded by an amphibian network installed in the region of central and eastern Crete in the Hellenic forearc between June 2003 and May 2004 is evaluated. The study aims to supplement earlier microseismicity studies in the region which were limited to on-shore station locations on Crete and the surrounding islands. The amphibian network for the first time covers the whole trench system south of central and eastern Crete. This should significantly improve the hypocentre determination and especially give a better depth control of the events when compared to solely land-based networks. Furthermore, the detection threshold for off-shore events is lowered and thus active structures should become apparent even in this short observation period of less than one year.

After describing the experimental setup and the data processing the influence of the velocity model on the hypocentre location is investigated and the location uncertainties are estimated. The results of an initial location run using a velocity model which was derived in an earlier microseismicity study in the region (Meier et al., 2004a) is compared with the results obtained by simultaneous inversion for a velocity model and station corrections using the VELEST software package (Kissling et al., 1994) and the locations obtained by applying a probabilistic earthquake location scheme to a 3-D velocity model using the NonLinLoc software (Lomax et al., 2000). The resultant distribution of the microseismic activity obtained in this study is interpreted in the regional tectonic framework and event statistics like a- and b-values are used to interpret the seismic activity.

2.3 Experimental Setup and Data Processing

The initial station distribution of the amphibian network was chosen in such a way that the whole central and eastern off-shore trench system in the region of Crete as well as the supposed southern border of the Aegean plate were covered by the network. To meet this objective, one OBS was placed south of the Strabo trench at a location presumably on top of the oceanic African lithosphere as suggested by refraction seismic studies (Brönner, 2003). With this station layout a lower detection threshold, a better location accuracy for crustal seismicity within the Aegean plate as well as better depth constraints for events at the plate boundary can be expected when compared to land based networks or networks of regional or global scale. Thus, the identification of active structures within the continental Aegean crust south of Crete as well as the determination of the updip limit of interplate

seismicity becomes possible. Furthermore, it permits a glimps at the accretionary complex to the south with its mud volcanism (Kopf, 2002).

The off-shore part of the LIBNET project was organized in five separate observation phases during which up to 8 OBS stations were deployed simultaneously for a recording period of up to 60 days. After each phase the stations were recovered, the raw data saved, the OBS stations checked, batteries changed and the stations redeployed. Except for one OBS in the last observation phase which was equipped with a CME-40 broad-band sensor all OBS stations were equipped with SM-6 B-coil geophones with a natural frequency of 4.5 Hz. Data registration was performed on SEDIS data loggers. Seismic data was sampled at 128 Hz or 250 Hz, respectively, and converted to miniseed format for further data processing. A clock drift correction was applied to the data after station recovery. Due to the loss of OBS stations and hardware failures a maximum of 6 stations produced usable data records simultaneously.

The land based short period local network at the south coast of Crete consisted of 5 Mark L4-3D seismometers and PDAS-100 data loggers operated at 50 Hz sampling frequency. The permanent broad-band stations incorporated in the data analysis are equipped either with STS-2 Streckeisen seismometers or Lennartz LE-20/3D sensors and are operated by the GEOFON network (Hanka et al., 1994), the National observatory of Athens (NOA) and MEDNET, respectively. Data from these stations were provided by the GEOFON data centre in Potsdam, Germany (http://www.gfz-potsdam.de/geofon/).

The initial network geometry spanning the entire transtensional system off-shore southeastern Crete was used for the first three deployments while the latter two phases used a modified network geometry with a denser station coverage further north (Fig. 2.2). This change was performed because the data quality of the OBS stations deteriorated with increasing distance from the island of Crete (Fig. 2.3). The densification of the OBS network in the last two phases as well as higher data recovery rates for those phases lowered the detection threshold for events in the seismically very active off-shore region between Crete and the Strabo trench further.

During data processing continuous waveforms from LIBNET stations and the temporary short period on-shore stations present in mini-seed format were filtered between 2 and 20 Hz and a STA/LTA trigger (Robinson, 1967) was applied for event detection. The subsequent application of a coincidence trigger required a minimum of 3 stations triggering within 19 seconds. This rather long time interval was chosen due to the large inter-station distances and the assumption of low seismic velocities within the thick sedimentary cover. Seismic activity was strong during the whole observation campaign with occasional bursts
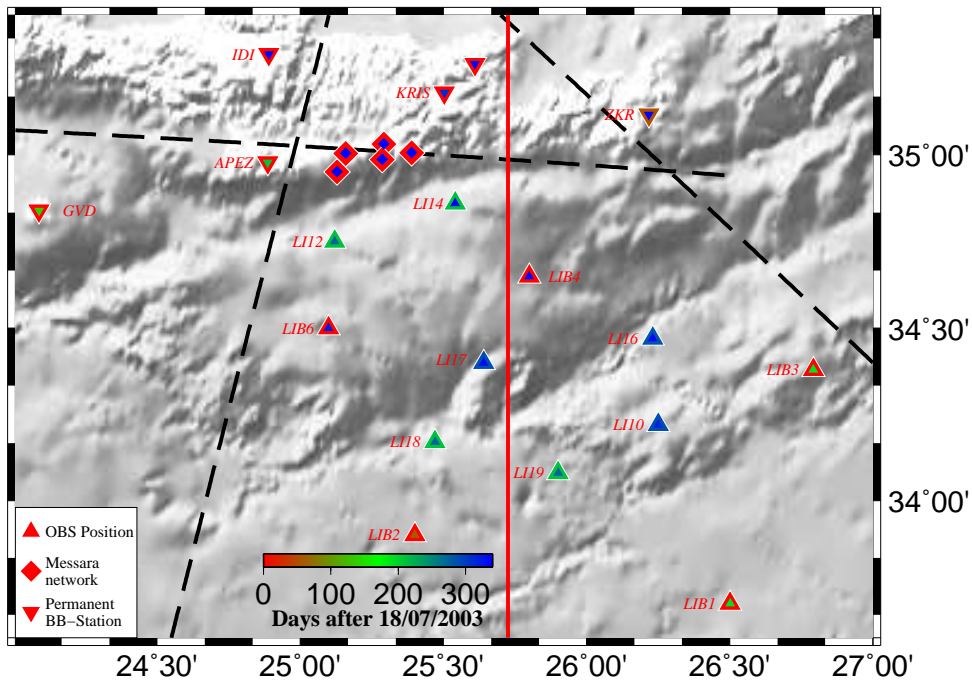
Figure 2.2: Configuration of the amphibian network. Triangles mark the OBS locations of LIBNET, diamonds the temporary short period on-shore stations and inverted triangles the permanent broad-band stations from the GEOFON-, NOA- and MEDNET-networks. Data from these stations was provided by the GEOFON project (Hanka et al., 1994). Colour-coding of the symbol outline indicates begin of recording while the colour in the symbols interior indicates end of recording. Broken lines indicate locations of refraction seismic lines (Bohnhoff et al., 2001; Brönner, 2003) which were used in the construction of the 3-D velocity model for probabilistic earthquake location and red line is orientation of profile through this 3-D velocity model depicted in Fig. 2.11.

Event with Ml=2.8 at 34.0427N/25.3294E and 13 km depth
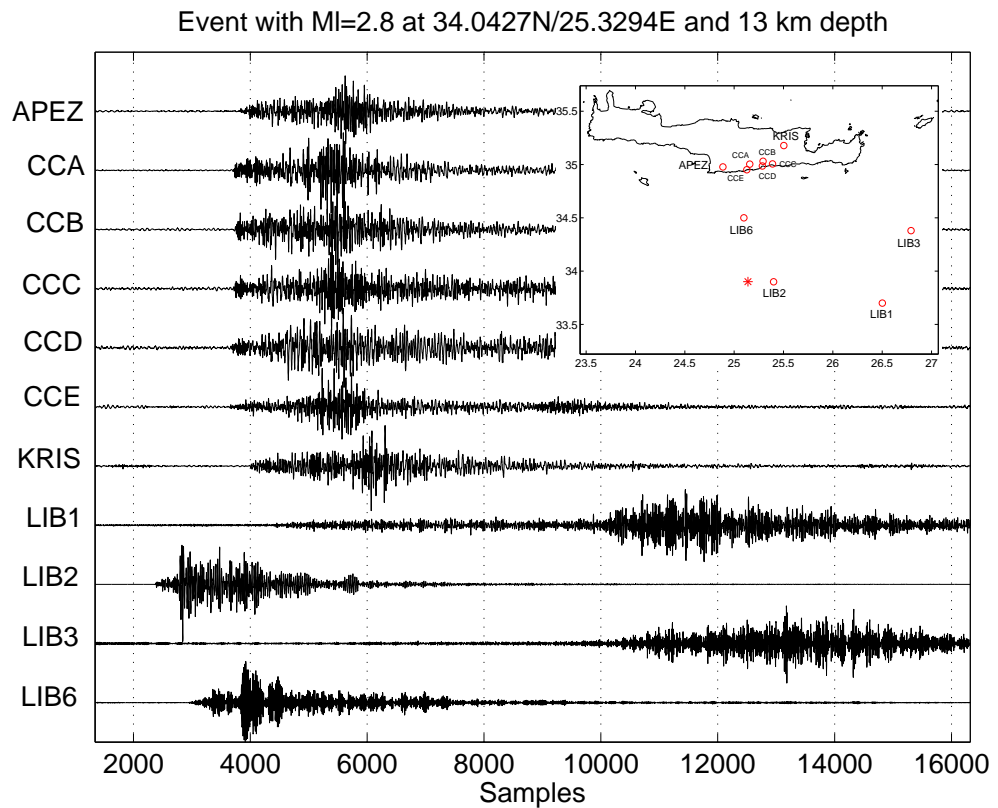
Figure 2.3: Waveform examples from an southern off-shore event recorded by LIBNET. Data passband filtered between 1 and 10 Hz. Note the marked difference in signal quality between different OBS stations and the long signal coda at stations LIB1 and LIB3 which is typical for many OBS stations to the south of the study region positioned on the thick sedimentary cover of the accretionary complex.

of activity consisting of more than 100 events recorded within 24 hours. However, these events were often small and only recorded at one or two stations and thus not included in the further data processing because their evaluation was beyond the scope of this paper. Most of this high seismic activity was found off-shore Crete in the region of the Ptolemy trench. This region between Crete and the Pliny trench also marks the area with the best OBS data quality while stations further south exhibited considerably lower signal to noise ratios (SNRs) and often very long signal coda (Fig. 2.3). The bad data quality might be explained by the thick, water saturated sediment cover present in the southern part which also prevented signal penetration during active seismic experiments in the region (Brönner, 2003). The few intra-slab events detected below Crete and further to the north under the Sea of Crete, on the other hand, exhibit high SNRs on the OBS stations (Fig. 2.4) and indicate the waveguide qualities of the subducting African slab.

The triggering procedure led to the identification of 3257 potential events for the 5 recording phases covering the time period July 2003 - June 2004. After visual inspection and elimination of teleseismic and multiple triggered events a total of 2686 local and regional events were processed and 17173 P- and 15995 S-phase onsets were picked manually during the data analysis.

2.4 Event Location Procedure

In order to investigate the influence of the velocity model on the seismicity distribution and to find the most reliable hypocentre locations different velocity models and location schemes were adopted. Firstly, the 2686 detected local and regional events were located using a velocity model derived in earlier microseismicity studies of the region (Meier et al., 2004, Tab. 1) modified by incorporating information from active seismic studies (Bohnhoff et al., 20001; Brönner, 2003) using the hypoinverse2000 location software (Klein, 2002). To account for the larger study region compared to this earlier investigation and possibly very low velocities below the southernmost stations, it was attempted to find a minimum 1-D velocity model with corresponding station corrections for the amphibian network by applying the VELEST inversion software (Kissling et al., 1994) to the dataset. In a final test a simple 3-D velocity model was constructed based on passive and active seismic studies of the region (Bohnhoff et al., 20001; Brönner, 2003; Endrun et al., 2004) and a probabilistic event location utilizing the NonLinLoc software package (Lomax, 2000) was performed. With this test the influence of the slab and the horizontally varying velocity
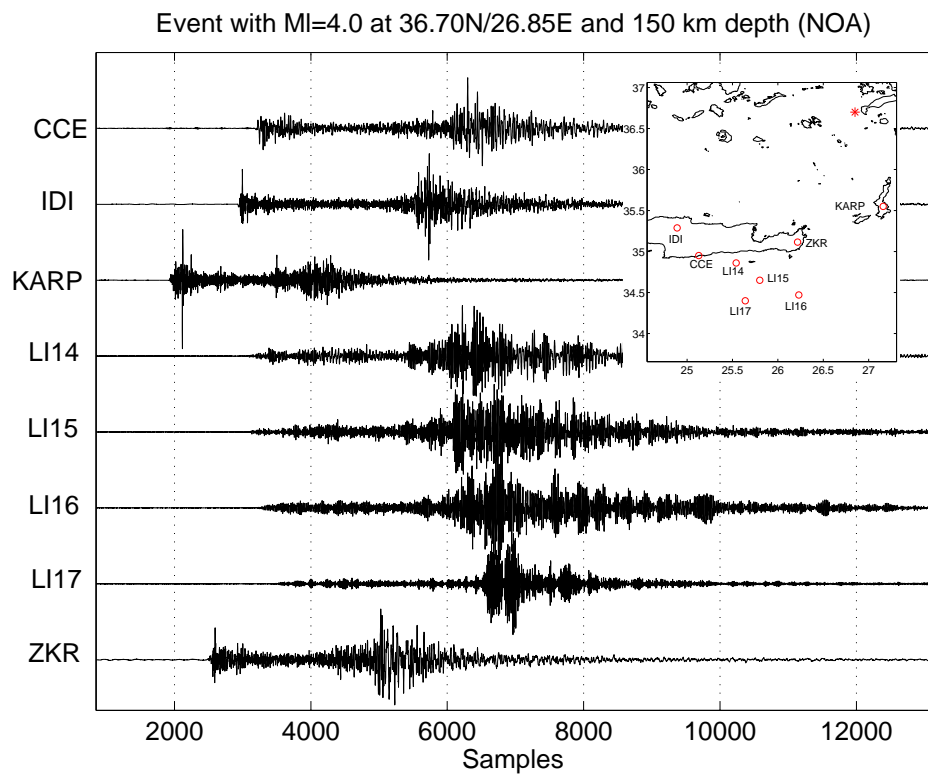
Figure 2.4: Waveform examples from an event within the subducting African slab north of Crete. Data passband filtered between 1 and 10 Hz. Note the high signal to noise ratio for the OBS stations south of Crete indicative of the waveguide qualities of the subducting African slab.

Depth [km]	v_p [km/s]
0.00	5.10
1.00	5.51
3.00	5.80
5.00	6.16
15.00	6.28
20.00	6.67
30.00	7.61
35.00	8.00
90.00	8.35

Table 2.1: Initial velocity model from Meier et al. (2004a) and modified according to active seismic information (Bohnhoff et al., 20001; Brönner, 2003). Depth is top of respective layer. v_p/v_s ratio is set to 1.78.

structure on the seismicity distribution was investigated. Furthermore, the model space is more completely sampled and the danger of getting stuck in local minima close to the initial event location is excluded by this approach. This threefold location approach was chosen to estimate the location accuracy of the event hypocentres and to get an idea of the order of the errors of the finally adopted hypocentre solutions.

2.4.1 Initial Event Location

Initial event locations were computed using the hypoinverse2000 location software (Klein, 2002) and a velocity model obtained during earlier seismological and seismic studies in the region (Bohnhoff et al., 2001; Brönner, 2003; Meier et al., 2004; Tab. 1). This velocity model is very similar to the one derived by Meier et al. (2004a) in a microseismicity study for the region of central Crete which was obtained by solving for a minimum 1-D model using the VELEST inversion software (Kissling et al., 1994). Two of the on-shore stations of this earlier study were also reequipped with short period sensors in our amphibian study. A v_p/v_s velocity ratio of 1.78 was adopted after evaluation of Waditi plots for events within the network. Delay times of the OBS stations were estimated according to the depth of the respective station. The starting depth was varied between 5 and 150 km
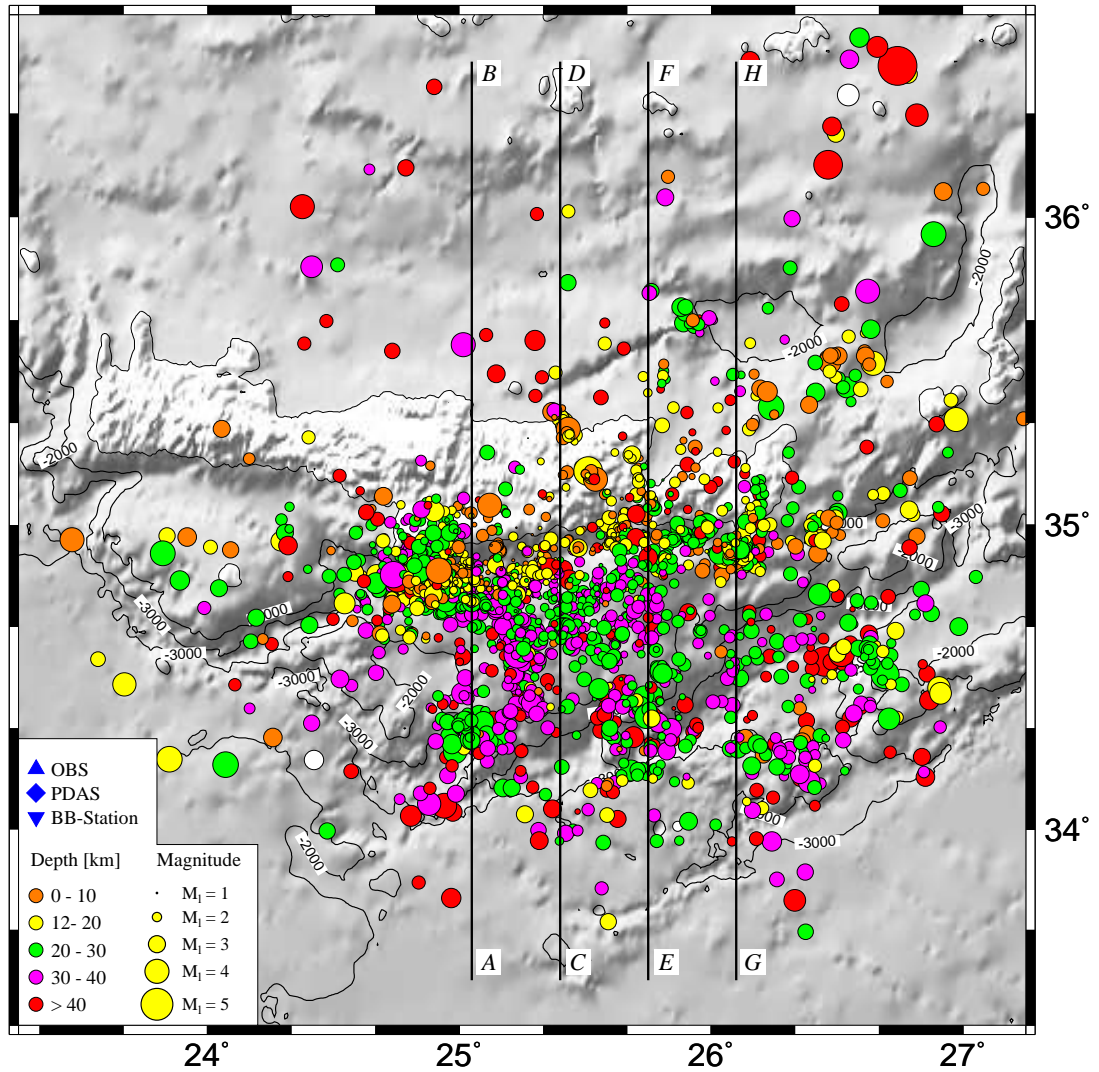
Figure 2.5: Initial locations of earthquakes detected with the LIBNET network between July 2003 and June 2004 using a velocity model derived in earlier studies (Meier et al., 2004a) of the region and station corrections according to station altitude. All events which converged towards a final solution within 40 iteration steps and with free depth are depicted.

and the hypocentre calculation was terminated after 40 iterations. The solution with the smallest rms value and location uncertainty was adopted as hypocentre. The step size was 5 km down to 40 km depth and increasingly larger below. This approach was chosen to more completely sample the depth space and avoid termination of the location program in a local minimum. It significantly increased the number of events converging to a low rms solution within the given number of iterations when compared to a single location run with just one fixed starting depth.

Fig. 2.5 contains all 2411 events for which the hypocentre solution converged within 40 iterations and for which the depth was not fixed by the location program. This means that events with large rms values and considerable location uncertainties are still present in the data set. However, inspection of subsets containing only events with small rms values and location uncertainties show that these events do not compromise the general conclusions. Fig. 2.6 shows cross-sections of the events in Fig. 2.5 projected on the profiles indicated in that figure. Obvious is the strong crustal activity at the south coast of Crete and the inter-plate seismicity further to the south.

2.4.2 Velocity model inversion using VELEST

Because the velocity model used for the initial event location was derived for a land based network of much smaller extent an inversion for a new minimum 1-D velocity model using the VELEST inversion algorithm is performed. Furthermore, the simultaneous inversion for station corrections can account for near surface velocity anomalies in the vicinity of the recording stations.

The inversion scheme simultaneously solves for velocity model and station corrections by a least squares formulation minimizing the weighted missfit between predicted and observed arrival times. Details and limitations of this inversion procedure can be found in Kissling et al. (1994). This results in a minimum 1-D velocity model with corresponding station corrections and hypocentre locations. Inversion for the minimum 1-D velocity model is done using version 3.3 of the VELEST software. As input, 435 events from the initial hypoinverse2000 location with at least 6 P readings, an azimutal gap of no more than 180 degrees, an rms value of less than 0.7 s and horizontal and vertical errors of no more than 10 and 15 kilometers, respectively, as indicated by the hypoinverse2000 routine (see Fig. 2.7a), were used. As reference station the on-shore station CCD at the southern shore of Crete was chosen because it has a nearly continuous record of events and in contrast to the OBS
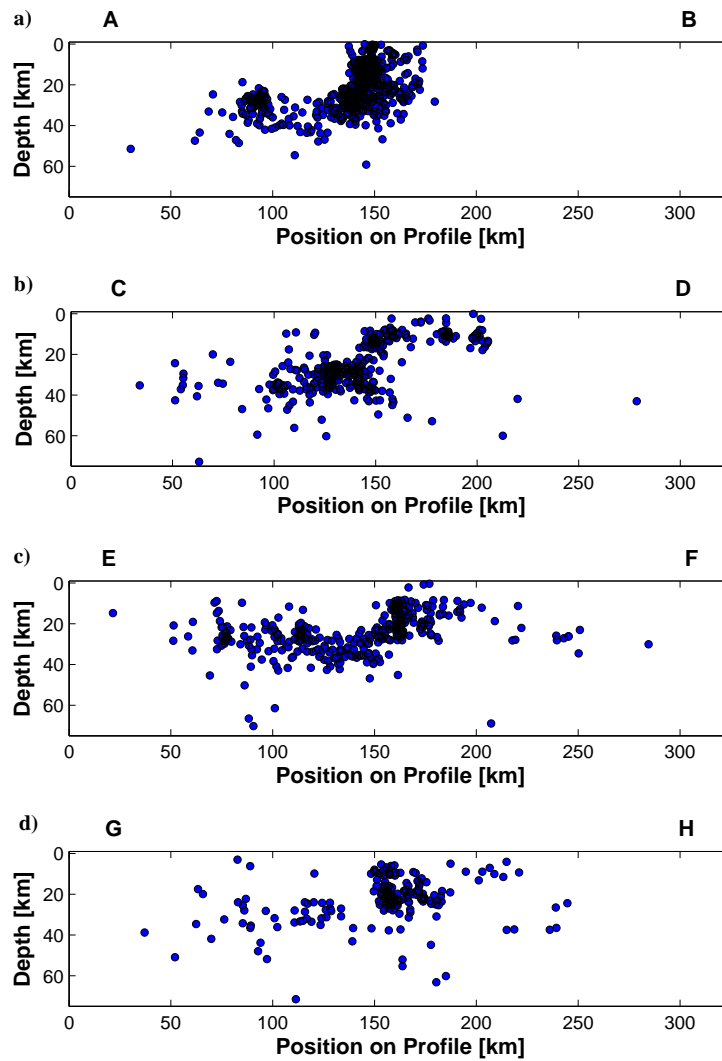
Figure 2.6: Cross-sections depicting the events shown in Fig. 2.5 projected onto lines indicated in that picture. The width of the selected area for projection is 15 km towards both sides of the lines in Fig. 2.5
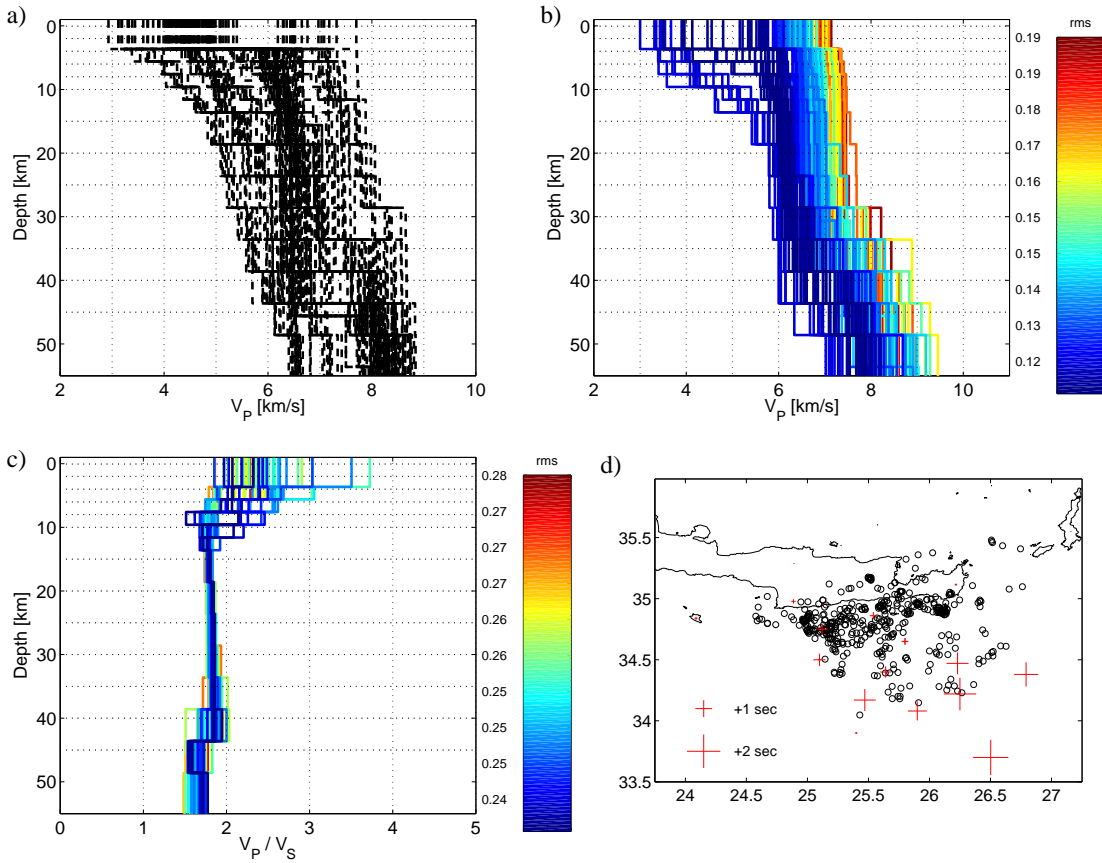
Figure 2.7: Results from the VELEST 1-D velocity inversion. a) Initial P-velocity models used in the inversion scheme sampling a wide range of the model space. b) Resultant P-velocity models colour coded according to their rms-misfits. c) v_p/v_s-ratios obtained by the inversion runs. d) Plot of station corrections obtained for the minimum 1-D model. Also plotted are the epicentres of the 435 events used for the inversion procedure.

Depth [km]	v_p [km/s]
-0.9	4.64
3.65	5.25
5.6	5.67
7.6	5.80
9.6	5.89
11.6	6.02
13.6	6.12
18.6	6.14
23.6	6.19
28.6	6.28
33.6	6.48
38.6	6.84
43.6	7.46
48.6	7.75

Table 2.2: Final minimum 1-D velocity model obtained by VELEST inversion. Because VELEST incorporates station altitude the model starts at 0.9 km above sealevel. The large thickness of the first layer is due to the fact that the deepest OBS was 3.6 km below sealevel and had to be contained within this layer.

stations which were repeatedly deployed its position never changed. The inversion was started with more than 100 different initial velocity models which were chosen in order to sample a broad range of the model space. No low-velocity layers were permitted in these models to avoid possible instabilities of the solutions. All starting velocity models used in the inversion runs are shown in Fig. 2.7a. During the inversion hypocenter and station files were updated after each VELEST run and after 5 VELEST runs all available events were relocated and those satisfying the above mentioned criteria were reselected for the next run of the inversion. Fig. 2.7b shows the resultant velocity models colour-coded according to the model misfit. The velocity model is best resolved between 15 and 35 km depth where the P-velocity is of the order of 6 km/s. At shallower depths the velocity models with the smallest rms misfits indicate P-velocities around 4.5 km/s and below. Due to the strong heterogeneity of the uppermost kilometers in the region of the amphibian network there is no clear convergence of the velocity models in their upper part. For the lower part, velocities increase to values of 8.0 km/s. Because no single model
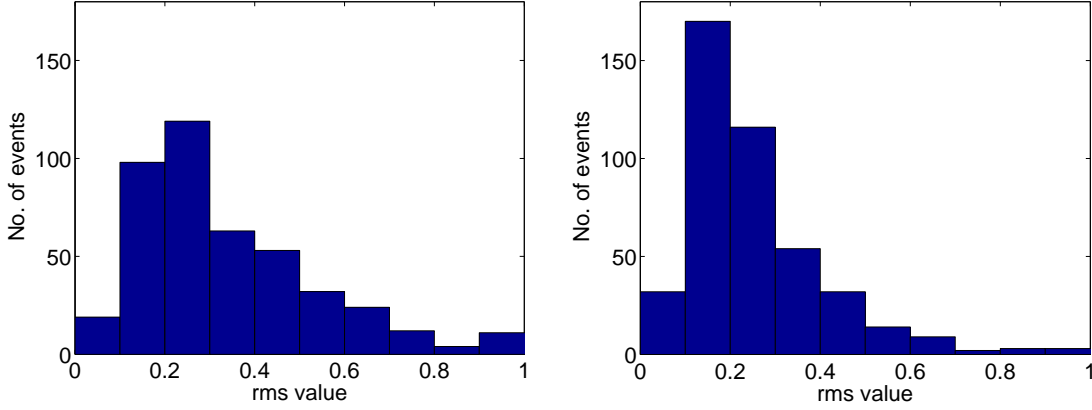
Figure 2.8: Comparison of rms misfits for the VELEST input velocity model (left) and the final 1-D minimum velocity model with corresponding station corrections (right). The v_p/v_s ratio for both models is 1.78 for the whole depth range in agreement with evaluations of Wadati plots. The events are the 435 earthquakes used for the VELEST inversion.

performed signifanctly better than the rest, the arithmetic mean of the 10 models with the lowest rms was adopted as minimum 1-D velocity model. To obtain station corrections for this velocity model, the initial 435 events used in the inversion were taken to invert for station corrections assuming a constant v_p/v_s ratio of 1.78. Final earthquake locations were computed by running VELEST in 'single event mode'. The computed average rms misfit for these final station locations using the new minimum 1-D velocity model with corresponding station corrections is 0.26 s. This is a significant improvement when compared with the initial velocity model which showed an rms misfit of 0.35 s in average for the same 435 events. Fig. 2.8 compares these two misfits before and after applying the VELEST inversion scheme.

In an attempt to solve for idependent S-velocity models the 52 P-models with the lowest rms misfit obtained in the inversion above are taken as initial S-velocity models by using a constant v_p/v_s ratio of 1.78 to invert for both P- and S-velocity models. The inversion procedure is the same as described for the minimum P-velocity model. The P- and S-velocity models and corresponding station corrections obtained from this approach however fail to significantly improve the average rms misfit. Using the P- and S-velocity model with the best fit to the data results in an average rms misfit of 0.24. Because this rather complicated model with strong changes in the v_p/v_s ratio does not significantly improve the misfit obtained with the much simpler minimum 1-D velocity model with constant v_p/v_s

ratio this model is rejected. Thus, the v_p model described above as the minimum 1-D model in conjunction with a v_p/v_s ratio of 1.78 compatible with the initial velocity model was adopted as final result of the VELEST inversion. However, some general trends of the v_s velocity models can be estimated from the inversion. In the best constrained depth range between 15 and 35 kilometres the v_p/v_s ratio is alsmost constant around 1.78-1.80 with a slight increase towards larger depths (Fig. 2.7c). Towards shallower depths we observe a large scatter in the obtained v_p/v_s ratio with values generally above 2 and sometimes as high as 3.5 indicating low resulution. At depths of 40 km or more where the African mantle lithosphere is expected south of Crete the S-wave velocity seems to be rather fast when compared with v_p showing a ratio of less than 1.7. However, due to the small number of raypaths within this depth range, the results are not very well constrained. Calculated station corrections (Fig. 2.7d) show increasingly positive values towards the south-east while values for stations close to the south coast of Crete are comparable to on-shore stations. Locating all events with this updated velocity model and the new station corrections resulted in improved mean rms values.

 Locations obtained with the updated velocity model and the new station corrections (Figs. 2.9 and 2.10) show a very similar distribution when compared with the locations obtained with the initial velocity model (Figs. 2.5 and 2.6). However, the new earthquake locations generally tend to cluster more spatially and events in the southern off-shore region between Pliny and Strabo locate at shallower depths compatible with the large positve station corrections found for stations in this area caused by the thick sedimentary cover. Many events in that region (e.g. Fig. 2.10 Profile E-F) are now found at depths supposedly belonging to the Aegean crust.

2.4.3 3-D velocity model and probabilistic event location

In order to investigate the influence of the slab and the thick sedimentary cover in the southern part of the network on the seismicity distribution a simple 3-D velocity model based on a priori velocity information from refraction seismic studies (Bohnhoff et al., 2001; Brönner, 2003) as well as seismological receiver function and surface wave dispersion studies (Endrun et al., 2004) is constructed. The constructed velocity model has a dimension of 360 x 275 x 91 km in longitude, latitude and depth, respectively and starts at an altitude of one kilometer to contain all recording stations within its dimensions. Islands are modelled as blocks being superimposed on a background velocity
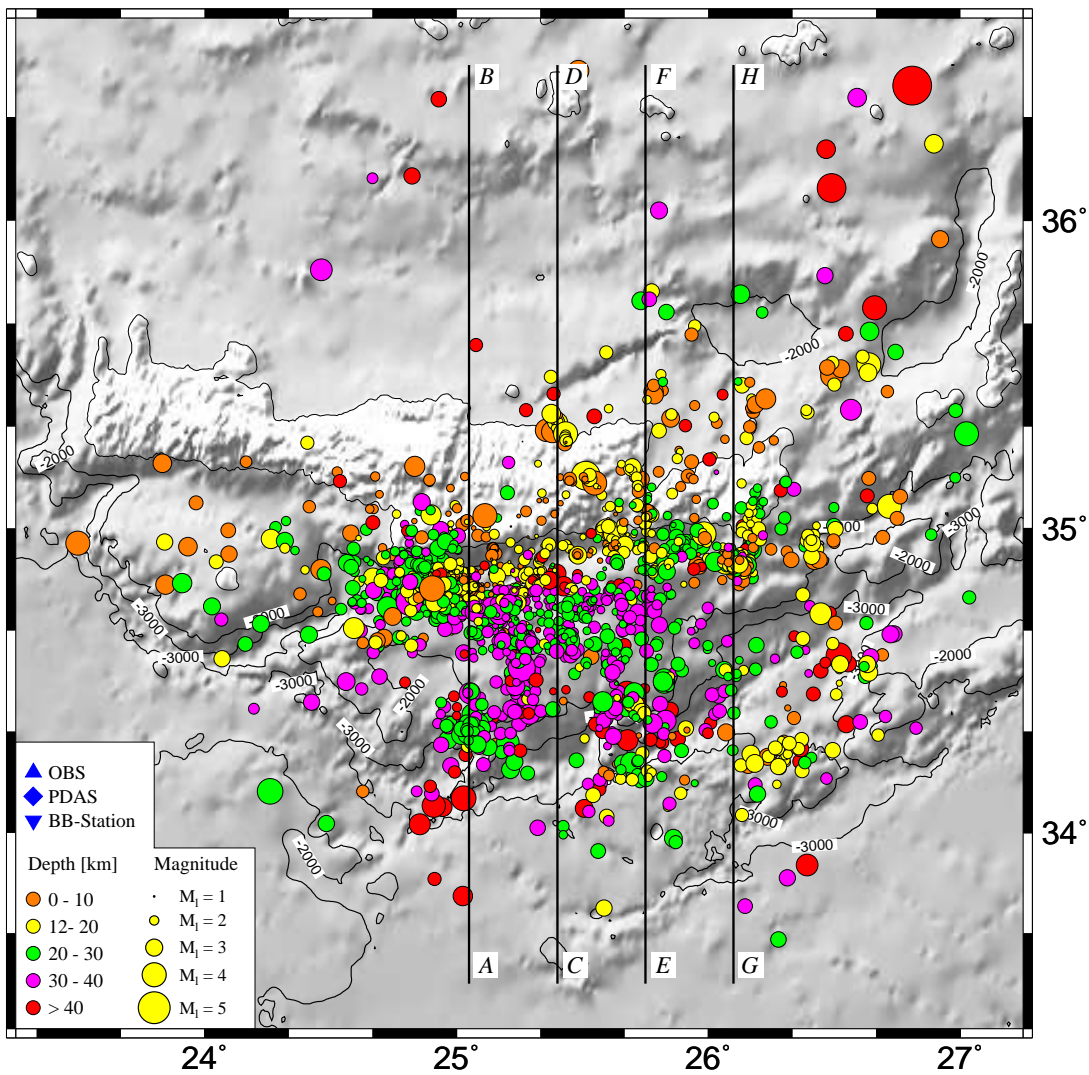
Figure 2.9: Mapview of the updated event locations using the minimum 1-D velocity model and the station corrections obtained by the VELEST inversion.
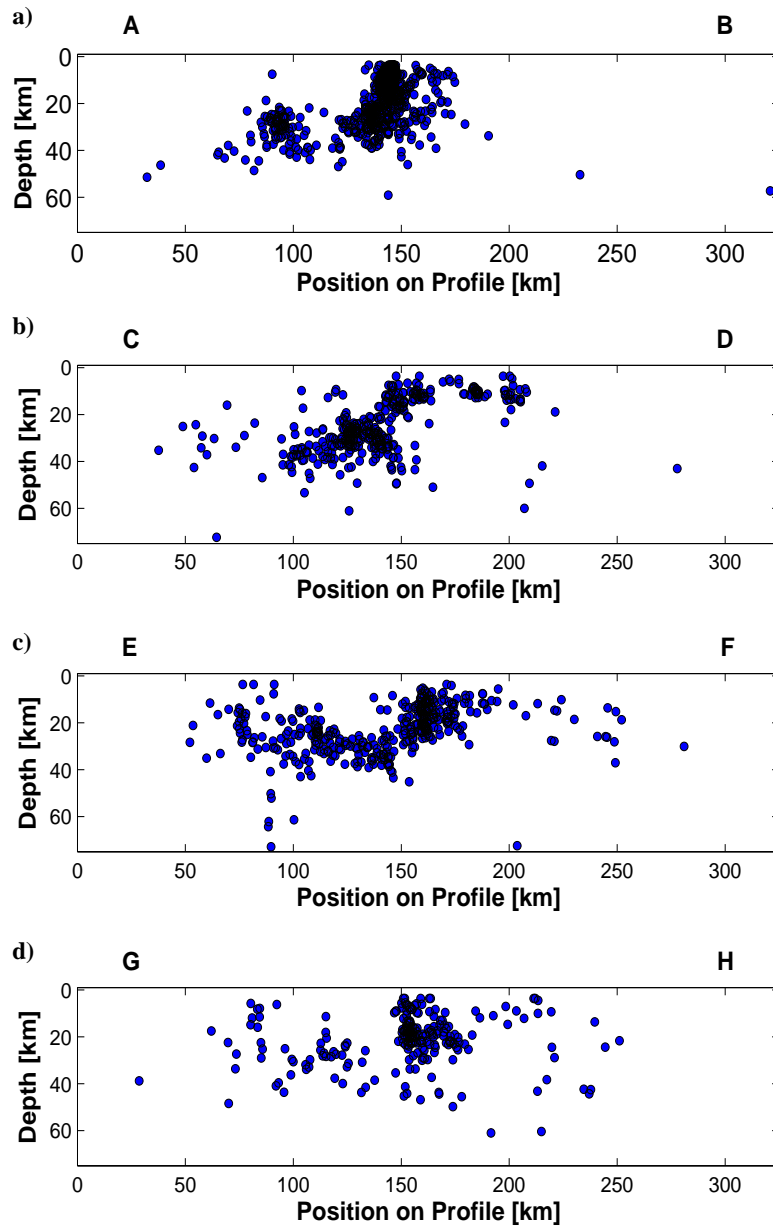
Figure 2.10: Cross-sections depicting the events shown in Fig. 2.9 projected onto lines indicated in that picture. The width of the selected area for projection is 15 km towards both sides of the lines in Fig. 2.9
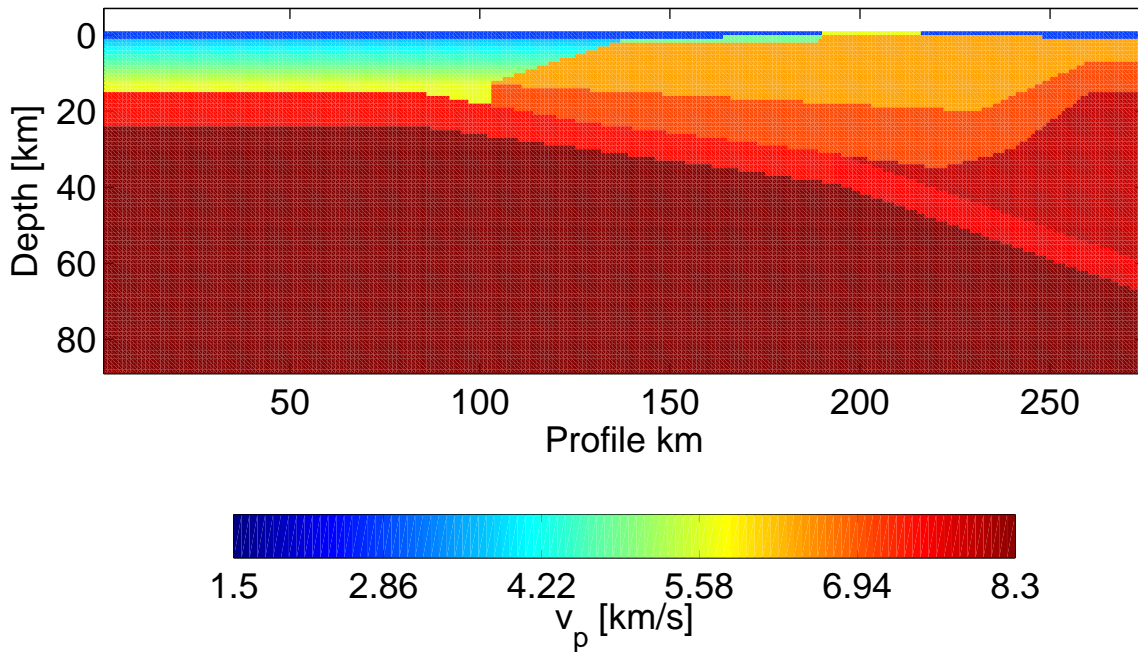
Figure 2.11: Cross-section through 3-D velocity model used for the probabilistic earthquake location with the NonLinLoc code (Lomax, 2000). Location of the profile is is that of profiles E to F in the crosssections above.

model. The curvature of the subduction zone is not modelled in this simple approach. This velocity model (Fig. 2.11), which tries to mimic the effect of the thick sedimentary cover in the south by incorporating low P-velocities and large v_p/v_s ratios indicated by the above discussed inversion approach and a gently dipping African slab, is used in conjunction with the probabilistic NonLinLoc earthquake location program (Lomax, 2000) to solve for earthquake hypocenters.

The travel-time calculation in NonLinLoc is performed by an Eikonal finite-difference scheme (Podvin and Lecomte, 1991) and results are stored for each station seperately in 3-D travel time grid files. To locate the earthquakes the probabilistic Oct-tree search is used. This procedure starts with a global sampling of the search space using a coarse grid and than finds the maximum likelihood hypocentre by mapping the probability density function of the earthquake location by increasingly finer sampling of the search space. This probabilistic approach samples a wider region of the solution space than the gradient methods used in the 1-D location schemes and also allows an estimation of the location uncertainties.

Results of this location scheme are depicted in Figs. 2.12 and 2.13. The general trend of

the seismicity distribution is comparable to those obtained by the 1-D velocity models. The area in which seismicity is located is truncated by the edges of the velocity model which are found roughly at 33.25 and 35.68°N and 23.25 and 27.2°E. These borders are not exactly parallel to meridians because a rectangular grid with constant grid spacing is transferred to geographical coordinates. Earthquakes outside these boundaries are projected onto the edges of the velocity model with large rms values and are removed from the catalogue. Seismicity in the on-shore area and close to the Cretan shoreline in the south shows a distribution resembling that of the 1-D velocity models. Locations towards the south, however, are not as tightly clustered as in the two models above and are generally found at much shallower depths.

To compare the data misfit and location uncertainties found with this simple 3-D velocity model the NonLinLoc routine is initialized with the minimum 1-D velocity model and corresponding station corrections and the Oct-tree search algorithm is used to calculate the hypocentres (Fig. 2.14). Fig. 2.15 compares the rms misfit and the largest axis of the error ellipsoid obtained for the 3-D model and the minimum 1-D velocity model, respectively. Both velocity models produce similar results. While there are more events with very small rms values of less than 0.1 s for the 3-D model the number of events with rms ≤ 0.3 s is larger for the minimum 1-D velocity model. Furthermore the length of the largest half axis of the error ellipsoid is smaller for the minimum 1-D velocity model when compared to the 3-D velocity model.

Thus, locations obtained by applying the minimum 1-D velocity model and corresponding station corrections found in this study seem to be on average better constrained than those obtained by the other two approaches. The inferior performance of the 3-D velocity model when compared with the simpler minimum 1-D velocity model might be explained by the insufficient knowledge of the velocity structure in the off-shore region.

2.4.4 Error estimation

Location accuracy for well resolved events recorded by the network is of the order of less than 5 km for horizontal directions and slightly worse than that in vertical direction. This is also roughly the amount by which these hypocentres move when using the different velocity models and location schemes. This is generally true for events north of the Pliny trench where the different velocity models produce similar results due to the fact that 1-D and 3-D velocity models do not differ much. Events locating further south however
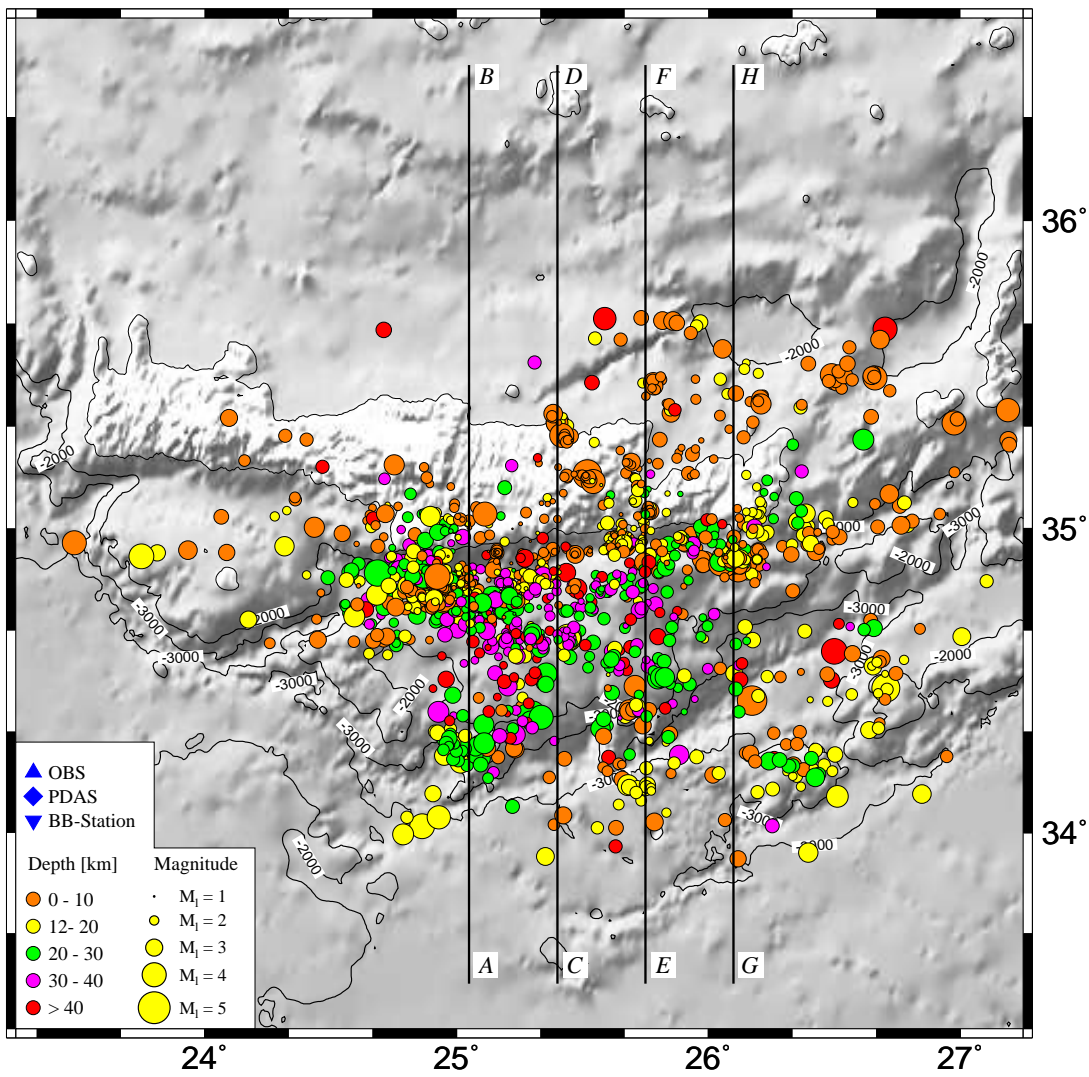
Figure 2.12: Mapview of event locations obtained with the 3-D velocity model and probabilistic location technique.
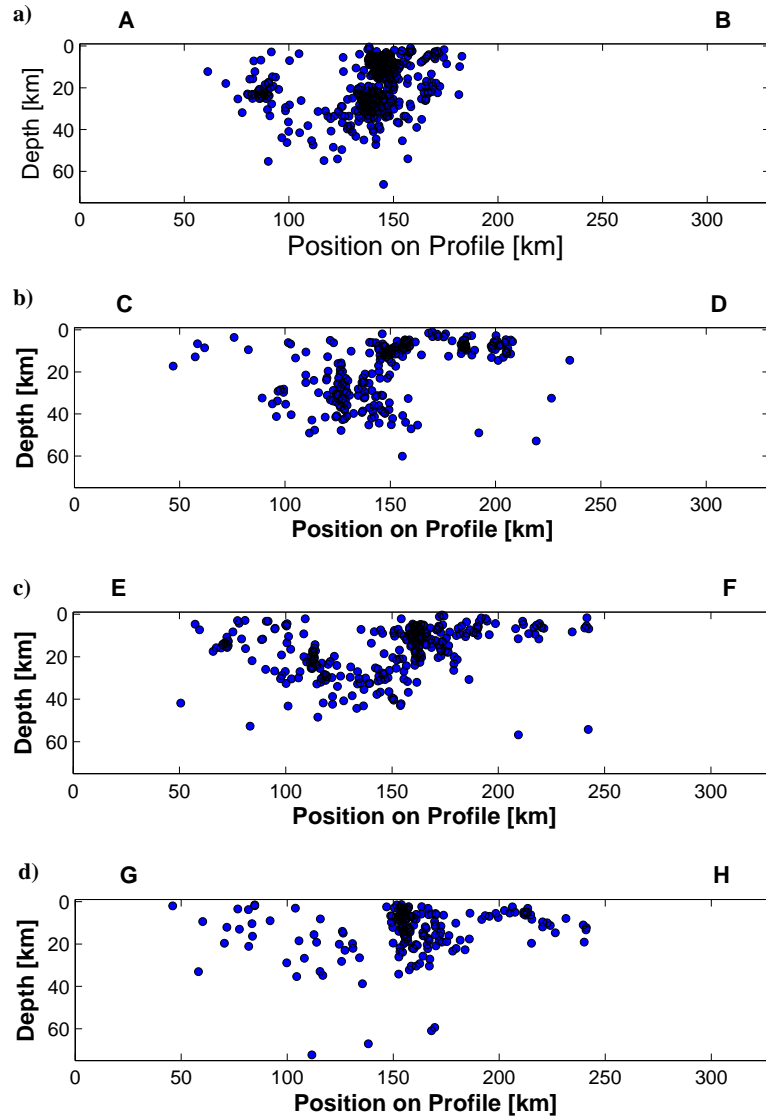
Figure 2.13: Cross-sections of the events shown in Fig. 2.12 projected onto lines indicated in that picture. The width of the selected area for projection is 15 km towards both sides of the lines in Fig. 2.12

are generally less well constrained (Fig. 2.16) which might be explained by a worse fit of the velocity model to the true situation, a less dense station coverage and the fact that the data quality of the southern stations is not as good as that of the norther ones making proper phase identification and picking more difficult. The general observation that events between the Strabo and Pliny trench also locate at crustal depths however is not compromised by this larger location uncertainty because also well constrained events are found in that region and the number of events located at depths larger than the expected plate interface is considerably lower than the number of events found above. This observed distribution contrasts with a random distribution of events around the plate contact expected for a situation in which inter-plate earthquake locations are compromised by large location uncertainties. An idea of the expected error ellipsoids of events recorded by the network can be gained from Fig. 2.16. In this figure a subset of the final earthquake catalogue is plotted with error ellipsoids obtained by mapping the probability density function for the minimum 1-D model in probabilistic earthquake location mode. Generally error ellipsoids point with their longest axis towards the centre of the recording network as expected. The vertical error is considerably larger than the horizontal one for less well constrained events and those at the edges or outside the amphibian network. The general trends in the seismicity distribution however remain the same.

The following sections will use the event locations obtained with the minimum 1-D velocity model in probabilistic earthquake location mode to discuss the microseismicity distribution and its tectonic implications.

2.5 Seismicity Distribution

The strongest seismic activity is found in the southern off-shore region of central and eastern Crete (Fig. 2.9) where the Ptolemy trench constitutes an especially active structure. This pattern was also observed in earlier microseimicity studies of the region (e.g. Meier et al., 2004a). Activity in the Ptolemy structure is observed from near surface depths down to the presumed plate interface at approximately 40 km depth (Figs. 2.14a-d). Towards the south of the Ptolemy trench there is a sharp drop in the crustal activity of the overriding Aegean plate and seismiciy is nearly exclusively found at the presumed plate interface (Figs. 2.14a-d). The inter-plate microseismicity shows a rather even distribution through-

out the whole off-shore part of the seismic network. The only marked exception is a cluster of events in the region of the Pliny trench around 34.4°N/25°E were the trench changes its strike direction from south-east in the west to north-east towards the east. This region of elevated seismic activity is also found in the instrumental ISC catalogue (Fig. 2.1) and seems to correlate with the point where the subduction direction of the downgoing plate with respect to the margin of the Aegean plate changes from normal towards the west to oblique towards the east of this point. Some of this activity, however, might locate at crustal depths within the Aegean plate.

The pattern of strong crustal activity in the Ptolemy trench and absence of crustal microseismic activity towards the south of this structure is observed in the whole study region from off-shore Messara in the west up to the eastern shore-line of Crete in the east (Fig. 2.10d) where seismic activity between the southern coast of Crete and the small island of Koufonissi towards the south is comparable from its depth extent to that found further west. Following the seismic activity further to the south, indications for activity within the Aegean plate between the Pliny and Strabo trench can be found (Fig. 2.9, Fig. 2.14c). Seismic activity, inter-plate as well as intra-plate, terminates almost completely at the Strabo trench and the accretionary complex to the south is practically devoid of any microseismic activity.

On-shore seismicity is less pronounced than the strong off-shore activity. One of the most prominent regions in terms of seismic activity is the area of the Messara graben where fault scarps cutting Quartenary deposits are observed in the field (Monaco and Tortorici, 2004). Observed microseismicity in the Messara basin spans the whole depth interval from the surface to 40 km (cross-section A-B in Fig. 2.14). Also shallow microseismic activity in the Ierapetra graben on-shore Crete and a roughly north-south trending structure adjacent to the south-east coast of Crete with hypocentre depths between 10 and 30 km was observed during the observation period. Both structures are known from geologic and seabeam observations as locations of active quartenary normal faults (Angelier et al., 1982; Armijo et al., 1992). Generally, the region east of the Ierapetra graben exhibits stronger seismic activity than the region to the west. However, there are two spots of significant earthquake clustering to the west of the Ierapetra graben in the vincinity of the permanent broad-band station at Kristallenia (labeled KRIS in Fig. 2.2) and further north at the coast. These locations exhibit cluster-like activity with magnitudes up to $M_L 3.5$.

Only little intermediate depth seismic activity within the subducting African lithosphere was observed during the study period. The deepest events reaching more than 100 km were located in the north-east. Activity in the slab below the island of Crete was also very
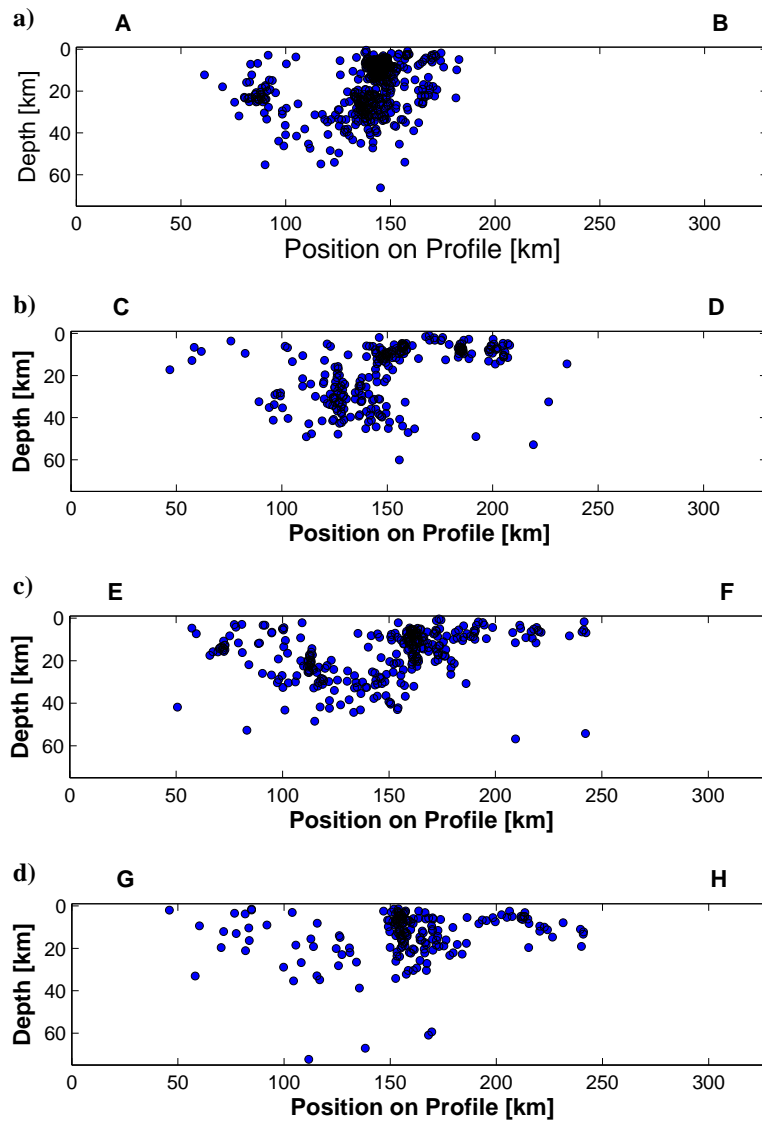
Figure 2.14: Cross-sectional views depicting the events located with the minimum 1-D velocity model and probabilistic location technique.
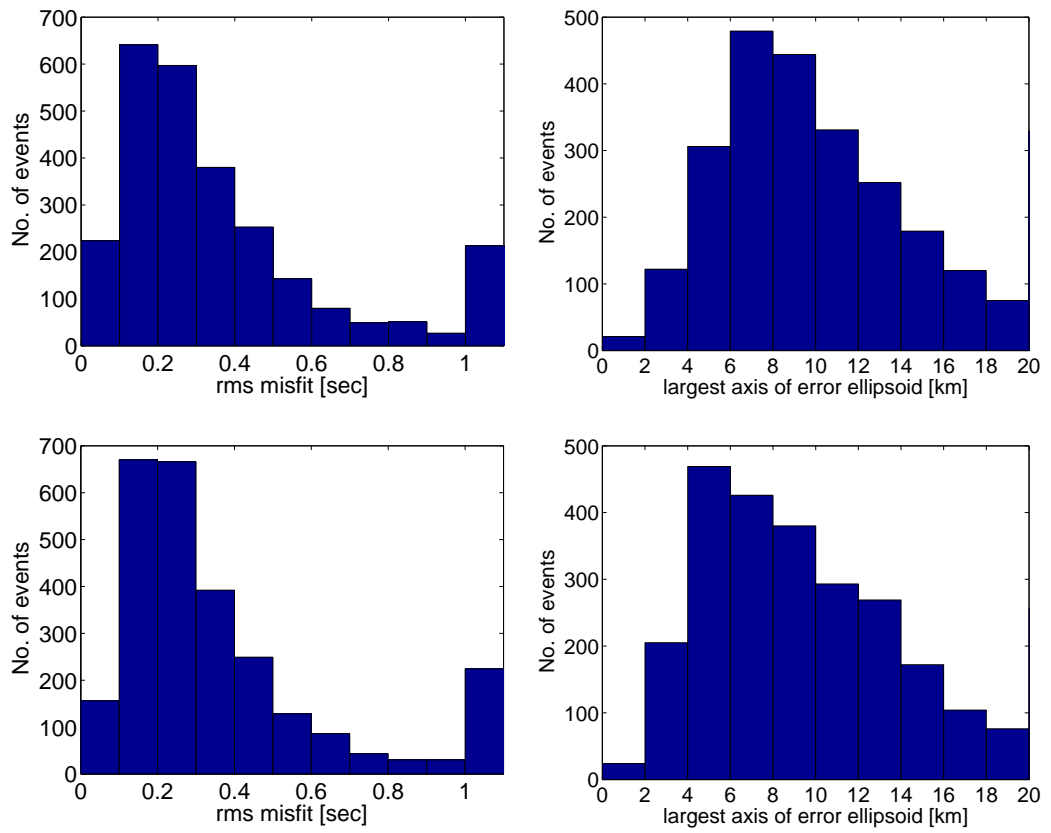
Figure 2.15: Comparison of rms misfits and maximum half axes of the error ellipsoid for 3-D velocity model (top) and the minimum 1-D velocity model (bottom).
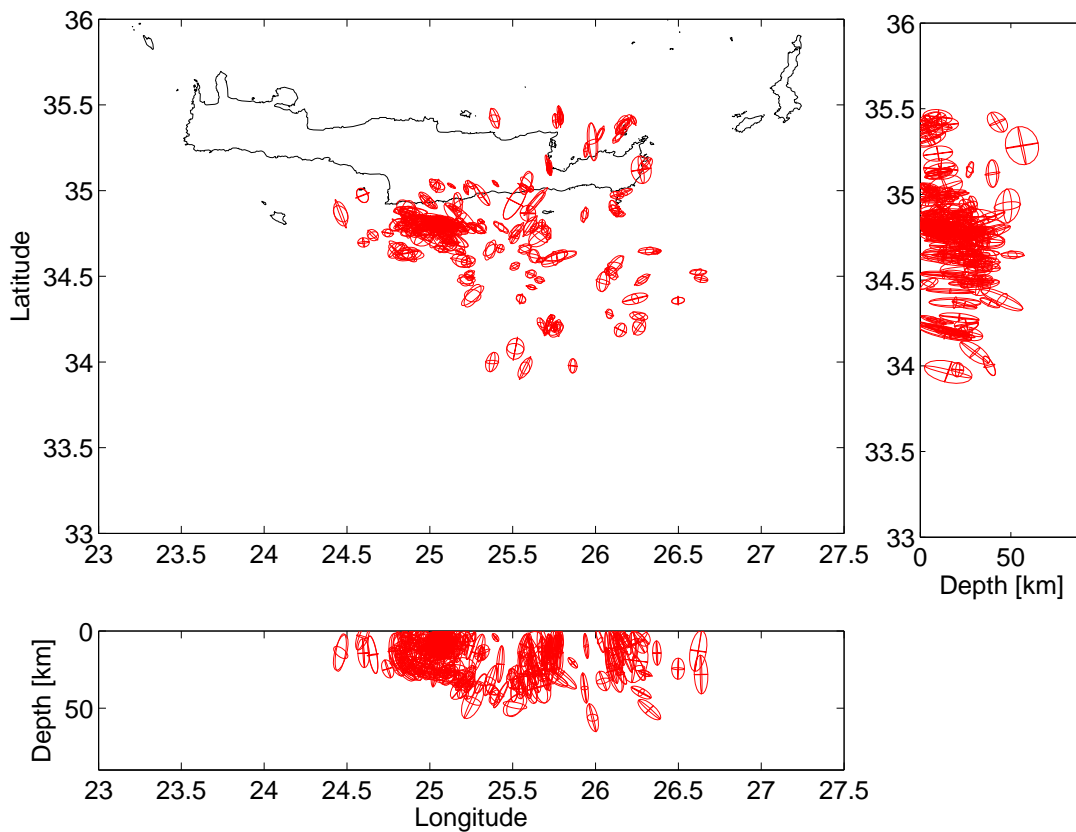
Figure 2.16: Example of error ellipsoids calculated with the minimum 1-D velocity model and the probabilistic location scheme of NonLinLoc. Plotted are all events with an rms misfit of less than 0.5 s and a maximum error ellipsoid half axis of no more than 15 km in the time interval 10/03/04 until 15/04/04.
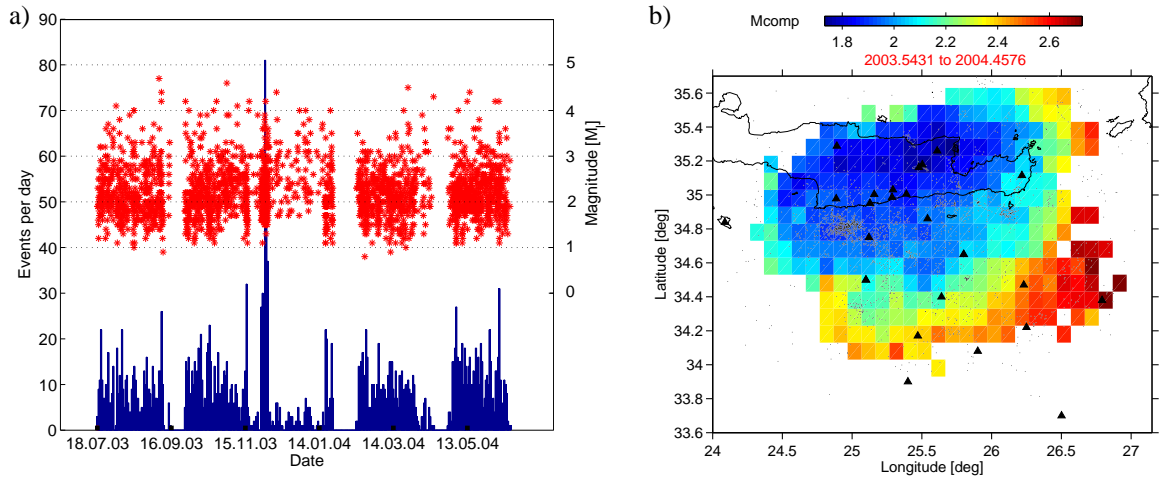
Figure 2.17: a) Magnitude over time plot for all located events during the five recording periods (red stars). Discontinuity of the dataset is caused by recovery and re-deployment of the OBS stations. Blue bars at the bottom indicate the number of events per day. b) Magnitude completeness map of the study region produced using the zmap software package (Wiemer, 2001) showing the increase in completeness magnitude with increasing distance from the island of Crete. White regions indicate areas with insuffiencent data for the calculation of the completeness magnitude.

sparse with only a few events located in the depth range between 40 and 80 km (Fig. 2.10).

2.6 Seismicity Statistics

The changing network geometry and consequently differing station spacings within the network as well as the different site characteristics caused by the variable station underground and coupling of the seismic signal lead to a spatially and temporally varying detection threshold. This variability must be addressed in order to properly assess the microseismicity patterns observed in the region and to quantify the microseismic energy release.

Fig. 2.17a shows a magnitude time plot of all located events. Magnitudes for LIBNET events were calculated as mean local Richter magnitudes averaged over all stations available for one event. Therefore, displacement waveforms were calculated from velocity proportional recordings taking the different seismometer characteristics into account.

Only stations with a hypocentral distance between 30 and 400 km were used in the magnitude calculation. Gaps in this magnitude time plot indicate the times of OBS recovery and redeployment. Towards the beginning and the end of the single observation phases gradual variations in the number of earthquakes per day (blue bars) are sometimes observed. This is caused by the fact that the deployment and recovery of the stations did not happen instantaneously but took several days. The high detection threshold in December and January obvious from this plot can be explained by maintenance problems of the on-shore short period network on Crete that was out of operation at this time. Therefore, the strong microseismic activity of the Ptolemy trench was recorded with a higher detection threshold. For any further interpretation of the seismic activity it is necessary to keep in mind that the existing earthquake catalogue is both incomplete and inhomogeneous.

This inhomogeneity is reflected in the spatial variability of the completeness magnitude calculated for 0.1 deg rectangles in the study region (Fig. 2.17b). The calculation was performed with the zmap software (Wiemer, 2001). White areas indicate regions of insufficient or inconclusive data. On the island of Crete and in the off-shore region up to the Ptolemy trench completeness magnitudes are between M_L 1.8 and 2.1 in general while they increase to values of M_L 2.5 and more further to the south and south-east. This trend is caused by the increasing interstation distances in this region and the inferior data quality observed at these stations. This means that the microseismic activity in the region of the Pliny and Strabo trenches can be as strong as the activity observed for the Ptolemy structure in agreement with ISC data for intermediate magnitude seismic activity in the forearc south of central and eastern Crete (Fig. 2.1).

In order to investigate the microseismic activity in the study region during the observation interval, a- and b- values and their spatial variability are estimated (Fig. 2.18). Most b-values are between 0.8 and 1.2 and thus in the normal range expected for this region from studies of instrumental seismicity (e.g. Papazachos, 1999; Manakou, 2000; Papaioannou and Papazachos, 2000). However, slightly higher values are observed for the region between the Pliny and Strabo trench in the south-east. In contrast, slightly lower than average values are found for areas with seismic activity that is predominantely associated with the plate contact. Estimating a-values for catalogues gives an idea of the absolute seismic activity in the study region. A-values calculated in this study indicate very strong microseismic activity between the Pliny and Strabo trenches in the south and also along the Ptolemy trench where most events located during the observation period.
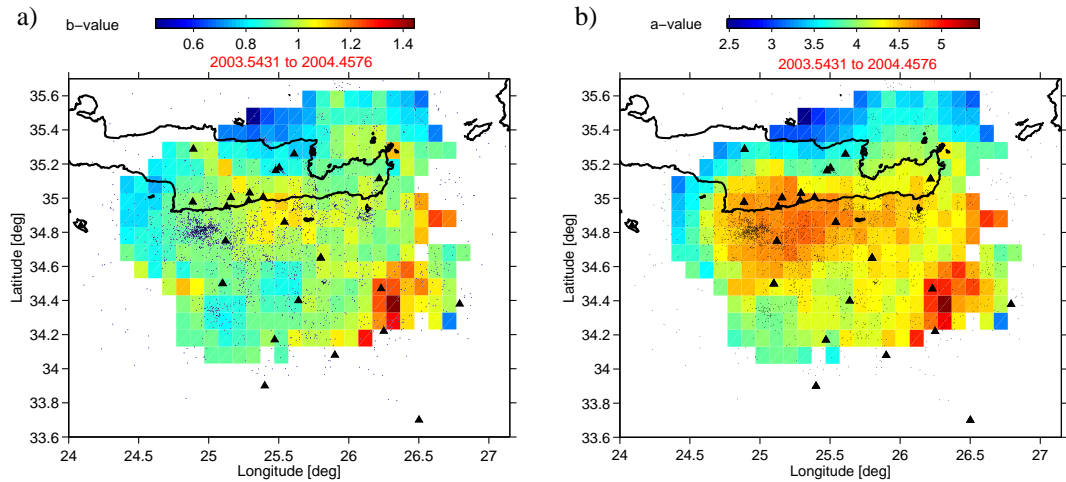
Figure 2.18: a) Calculated b-values for the LIBNET dataset in the study region. b) Calculated a-values for the LIBNET dataset in the study region.

2.7 Discussion and Conclusions

Microseismic activity in the forearc of the HSZ south of central and eastern Crete is studied by means of an amphibian network covering the entire transtensional trench system in that area. The OBS part of the network was operational between July 2003 and June 2004. In conjunction with the local short period network installed during the same time span at the south coast of central Crete and the permanent broadband stations in the region, the OBS network allowed us to study the microseismic activity in the transtensional trench system south of central and eastern Crete with unprecedented accuracy due to the low detection threshold and the good control of the hypocentre locations.

Different velocity models and location techniques were applied to the dataset. The general microseismicity distribution remains the same when comparing hypocentre locations obtained by (1) an initial velocity model derived in an earlier study (Meier et al., 2004a) (2) a minimum 1-D velocity model gained by simultaneous inversion for the velocity model and station corrections and (3) a simple 3-D velocity model used in conjunction with a probabilistic event location technique. Thus, the general trend of high seismic activity at the Ptolemy trench, the absence of crustal activity south of it, the crustal activity in the area of the Pliny and Strabo trench and the aseismic behaviour of the accretionary complex towards the south is not an artefact of the velocity model nor the location procedure. The influence of the slab on the seismicity distribution is small which can be expected because hardly any intermediate depth activity is observed and most of the seismicity is found

either within the crust or at the plate contact and is thus not very sensitive to the geometry of the subducting African lithosphere. This can be seen when comparing qualitatively the results for the 3-D velocity model (Fig. 2.12) with the minimum 1-D velocity model (Fig. 2.9) for the area north of the Pliny trench. Locations in this area are very similar for the 1-D and 3-D case. Towards the south however the influence of the low velocities and the high v_p/v_s ratios incorporated in the 3-D velocity model are clearly evident by the much shallower depths of the hypocentres in the 3-D case. This tendency towards shallower depths is also evident when comparing the minimum 1-D locations with the initial event locations. Also the large positive station residuals calculated in the inversion for stations in the south (Fig. 2.7d) hint at low velocities in that area and thus possibly shallower hypocentre depths. Despite the incorporation of low velocities and large v_p/v_s ratios in the southern area, the 3-D velocity does not perform better than the minimum 1-D velocity model with corresponding station corrections (Fig. 2.15). This might be due to the fact that the 3-D velocity model is too simple for the complicated geometry in this curved subduction zone with its transtensional structures. Furthermore the strong lateral velocity changes make the location procedure more sensitive to small changes in the hypocentral parameters. This effect can be seen in the larger scatter of the hypocentres when compared to the minimum 1-D solution and the fact that the maximum axis of the error ellipsoid tends to be larger than in the 1-D case (Fig. 2.15). Thus, the hypocentre solutions obtained with the 1-D model and corresponding station corrections are used to interpret the microseismicity distribution. However, it must be acknowledge that depths obtained for the region between Pliny and Strabo might be to deep.

The velocity model resulting from the VELEST inversion is generally slower than the initial model derived for the on-shore network by Meier et al. (2004a). This can be expected from the fact that the slower velocities in the upper layers in the southern off-shore region must somehow be incorporated in an average 1-D velocity model. Location uncertainties were estimated to be better than 5 km horizontally and slightly more than that in vertical direction for well resolved events.

Strong microseismic activity associated with the plate contact of the Aegean and African plate south of Crete as well as strong crustal activity within the Aegean plate in the area of the Ptolemy trench was observed throughout the whole observation campaign. This strong microseismic activity close to the southern coast of Crete and at the plate contact off-shore Crete was also found in earlier microseismic studies of the region (Delibasis et al., 1999; Meier et al., 2004a) which evaluated seismicity recorded with on-shore station networks. Combined with the instrumental observations of the ISC catalogue (Engdahl

et al., 1998) which also lists seismic activity in that area it can be said that the Ptolemy structure constitutes a seismically very active feature in the Aegean crust. Its microseismic activity was traced by this study up to the eastern shoreline of Crete (Fig. 2.10 Profile G-H) and possibly even further east towards the island of Karpathos (Fig. 2.9). Seismic activity in the Ptolemy trench is found throughout the study region from near surface depths down to the plate contact at approximately 40 km depth. These findings support the idea that the Ptolemy trench may form a sinistral strike-slip structure accomodating the effects of oblique subducting in the eastern Hellenic fore-arc (Kahle et al., 2000; Meier et al., 2004b; Bohnhoff et al., 2005) and representing a possible zone of crustal weakness allowing the ascend of fluids from the plate contact (Becker et al., 2006). While the crustal region between the Ptolemy and Pliny trench is nearly devoid of seismic activity the Pliny and Strabo trenches showed strong microseismic activity in this study. This agrees with studies indicating that the Strabo trench is not the termination of the Aegean lithosphere but an intra-crustal structure like the Ptolemy and Pliny trenches (Huguen et al., 2001). The observed seismicity distribution in the area of the Pliny and Strabo trenches is in agreement with current instrumental catalogues which also exhibit strong intermediate magnitude seismicity in that area (Fig. 2.1). Microseismic activity in this region might be as high as in the area of the Ptolemy trench as indicated by the calculated a- and b-values (Fig. 2.18). The lack of seismic activity in the region between the Ptolemy and the Pliny trench hints at a rigid block movement without significant internal deformation. This block can be interpreted as a forearc sliver seperated by the Ptolemy and Pliny trenches from the rest of the Aegean crust (Meier et al., 2004b).

Seismicity located in the area of the Ierapetra graben in the on-shore region of Crete can be correlated with the location of active quartenary normal faults (Angelier et al., 1982; Armijo et al., 1992). The activation of these north-east south-west trending normal faults is in agreement with the current stress field in eastern Crete (Bohnhoff et al., 2005).

The strong microseismic activity indicating the seismogenic part of the plate contact which has its southern termination in the area of the Strabo trench terminates abruptly below the south coast of Crete forming a seismogenic zone with a width of about 100 km. This interplate seismicity is rather evenly distributed and no locked zone indicating possible areas of stress accumulation were detected. Only very few seismic events were observed deeper than 40 km within the subducting African slab. These deeper events might be linked to processes within the slab like bending, dehydration and phase changes. The termination of the interplate seismicity roughly at the south coast of Crete indicates that the plate contact south of Crete is seismically coupled whereas it is decoupled below and north of

Crete. That means Crete is located above the updip limit of the decoupled plate interface and thus the uplift of Crete (e.g. Meulenkamp et al., 1994) hints at return flow above the slab in the region of the decoupled interface. Interestingly, seismicity within the Aegean lithosphere below Crete is low at depths below about 20 km pointing to rather ductile deformation of the overriding plate in contrast to brittle behaviour at shallower depths. These observations are in good agreement with numerical modellings of rheological properties of the plate contact in the forearc (e.g. Gerya et al. 2002; Gerya and Stöckhert, 2006). These modellings predict (1) rapid return flow of metamorphic rocks, including hydrated mantle material, along the hangingwall of the subducted slab that spread out beneath the forearc and (2) ductile behaviour of the plate contact and deeper parts of the overriding plate in the region of the forearc high.

Towards the south of the study region a thick sedimentary cover of up to 10 km which was found in refraction seismic studies of the region (Bohnhoff , 2001; Brönner, 2001) causes the low data quality of stations in the vicinity of the Strabo trench. The influence of this thick sediment package is evident in the large positive station corrections found in that region caused by low seismic velocities. Furthermore, the great variability of the velocities of the uppermost layers for different inversion runs can be explained by this strong lateral variation when comparing this area with the regions further north. Interestingly, intermediate depth seismicity originating in the subducting African slab further to the north with depths exceeding 100 km, exhibit high data quality at OBS stations close to Crete suggesting that the subducting slab acts as a waveguide as suggested by earlier studies on the attenuation of seismic signals and the distribution of macroseismic intensities in the region (Papazachos and Comninakis, 1971).

Furthermore, there was hardly any seismic activity recorded in the region south of the Strabo trench which can not solely be explained with the higher detection threshold in this region.

Higher b-values are calculated for the intra-plate seismicity of the Aegean plate when compared to those observed at the plate interface. This behaviour is interesting and possibly caused by the different faulting types dominating the inter- and intra-plate seismicity. Wiemer und Wyss (2002) generally found that normal-faulting events exhibit higher b-values than those found for thrust-type activity. Furthermore, it is often observed that higher b-values correlate with regions where large events are absent (Wyss, 2001), while low b-values tend to indicate locked fault patches or asperities (Schorlemmer and Wiemer, 2005). This might also explain the absence of historic seismicity with large magnitudes in the area of the Pliny and Strabo trenches which exhibit considerable current intermediate

seismicity (Fig. 2.1). Possibly, this region is accomodating the relative motions at the fault surfaces by numerous small and intermediate magnitude events, as indicated by the high a-values found in this study, but is not able to generate major seismic events. In contrast, the Ptolemy trench with its smaller b-values already showed its potential to generate large magnitude events.

In order to confirm and substantiate the observations of this study and to map possible spatio-temporal b-value changes, which might indicate regions of stress accumulation, a continuous (micro)seismicity monitoring of this part of the Hellenic forearc is desirable. Also GPS studies including the small island of Chrisi south of the Ptolemy trench would be helpful in identifying the character of this off-shore graben and quantify possible relative motions.

3 Spatio-temporal Microseismicity Clustering in the Cretan Region

3.1 Summary

Spatio-temporal clustering of microseismicity in the central forearc of the Hellenic Subduction Zone in the area of Crete is investigated. Data for this study were gathered by temporary short period networks which were installed on the islands of Crete and Gavdos between 1996 and 2004. The similarity of waveforms is quantified systematically to identify clusters of microseismicity. Waveform similarities are calculated using an adaptive time window containing both the P- and S-wave onsets. The cluster detection is performed by applying a single linkage approach. Clusters are found in the interplate seismicity as well as in the intraplate seismicity of the continental crust in the region of the transtensional Ptolemy structure. The majority of the clusters are off the southern coast of Crete, in a region of elevated intraplate microseismic activity within the Aegean plate. Clusters in the Gavdos region are located at depths compatible with the plate interface while cluster activity in the region of the Ptolemy trench is distributed along a nearly vertical structure throughout the crust extending down to the plate interface. Most clusters show swarm-like behaviour with seismic activity confined to only a few hours or days, without a dominant earthquake and with a power-law distribution of the inter-event times. For the largest cluster, precise relocations of the events using travel time differences of P- and S-waves derived from waveform cross correlations reveal migration of the hypocenters. This cluster is located in the region of the Ptolemy trench and migration occurs along the strike of the trench at 500 m/day. Relocated hypocenters as well as subtle differences in the waveforms suggest an offset between the hypocenters and thus the activation of distinct patches on the rupture surface. The observed microseismicity patterns may be related to fluids being transported along the plate interface and escaping towards the surface in zones of crustal weakness (Ptolemy structure), triggering swarm-like cluster activity along its way.

3.2 Introduction

3.2.1 Region

The Hellenic Subduction Zone is the most seismically active region in Europe. It currently shows a high level of intermediate magnitude activity but it has also generated events with magnitudes up to 8.3 in historic times (Papazachos et al., 2000; Stiros, 2001) (Fig. 3.1). The coupling of the subduction interface seems to be weak however with a large amount of slip being accomodated aseismically (e.g. North, 1974; Papadopoulos, 1989; Jenny et al., 2004; Becker et al., 2004). The general tectonic regime (McKenzie, 1970; LePichon et al., 1995) in the region is influenced by the extrusion and counterclockwise rotation of the Anatolian-Aegean region, the slow northward movement of Africa with respect to Eurasia (McClusky et al., 2000) and slab rollback caused by slab pull of the downgoing African slab. However, the thinned continental crust which constitutes the Southern Aegean north of Crete shows little internal deformation (McClusky et al., 2000; Kreemer and Chamot-Rooke, 2004). The relative movement between the southern Aegean and Eurasia is concentrated in the Northern Aegean Sea and along the Gulf of Corinth (McClusky et al. 2000). In the forearc, the Hellenic trench system consisting of the Ionian trench in the west and the Ptolemy, Pliny and Strabo trenches in the east, represent structures in the overriding Aegean lithosphere (Fig. 3.1). These transtensional features may be caused by sinistral movements of forearc slivers relative to the Aegean region due to increasingly oblique subduction towards the eastern forearc (ten Veen and Kleinspehn, 2003; Meier et al., 2004b). Seismic refraction profiles (Bohnhoff et al., 2001) show a 4 km deep, wedge-shaped sedimentary structure in the Ptolemy trench supporting this interpretation. Benioff zone seismicity in the east can be traced down to depths of about 160 km beneath Kos while seismicity in the shallower dipping western segment terminates at approximately 100 km below Milos. Large historic earthquakes are reported for the Cretan Sea north of Crete as well as for the plate interface south of the island (Fig. 3.1). Recent tectonic uplift of Crete with especially high rates in the western part of the island (Meulenkamp et al., 1994; Lambeck, 1995) is a further noteworthy point. Several studies have dealt with the microseismic activity in the Cretan region based on the evaluation of data from temporary dense seismic networks (e.g. de Chabalier et al., 1992; Hatzfeld et al., 1993; Delibasis et al., 1999; Becker, 2000; Meier et al., 2004a). These studies identified and mapped the plate contact between the African and Aegean plate as well as the currently active structures within the continental crust. They found abundant microseismic activity in the southern offshore region, especially in
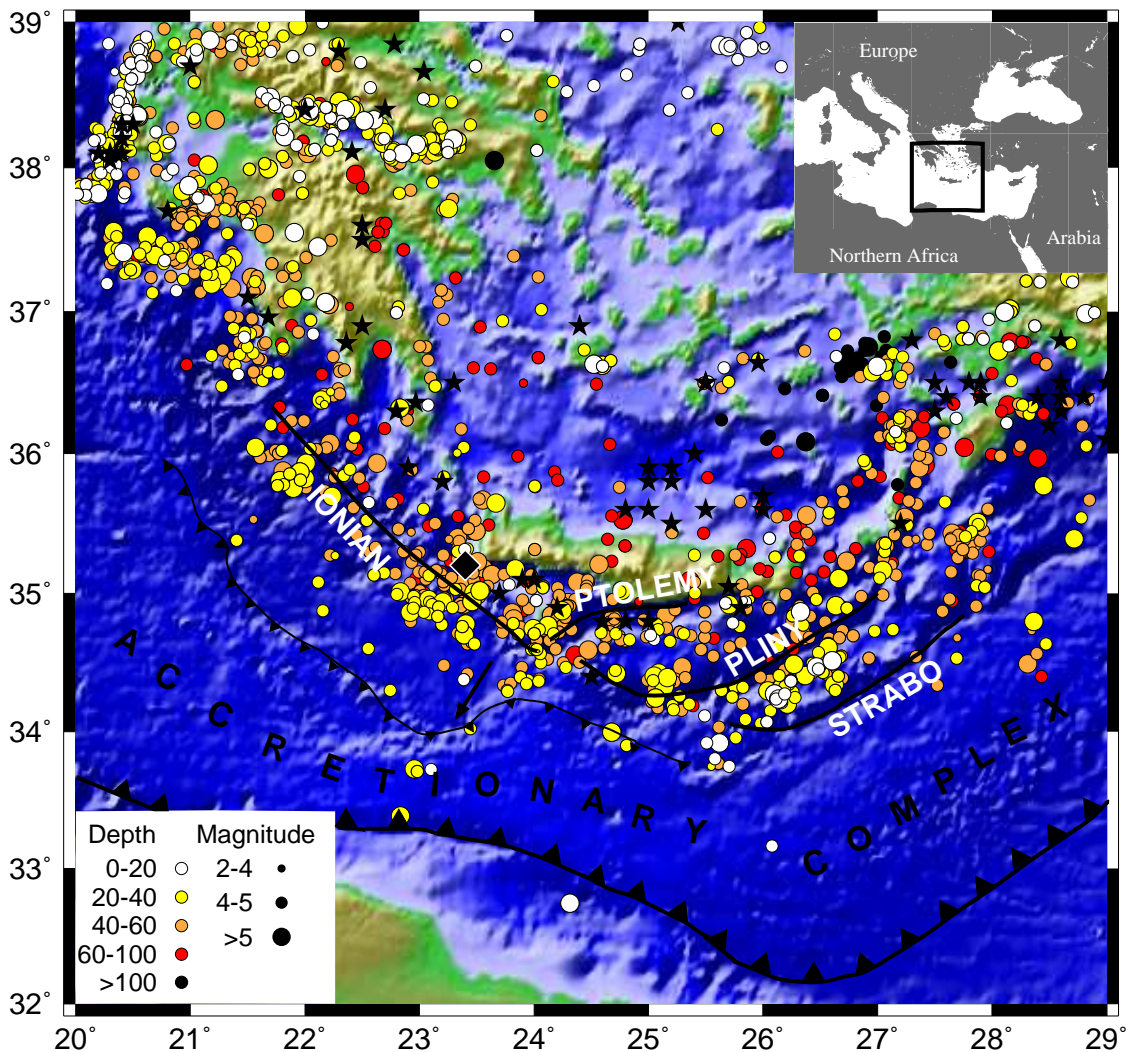
Figure 3.1: General tectonic setting of the research area. Solid black lines indicate the transtensional structures south-east of Crete (Ptolemy, Pliny, Strabo) and the western deep-sea trench (Ionian), respectively. Thick line with triangles indicates the southern border of the accretionary complex while the thin line with triangles indicates the border between the outer and inner unit of the accretionary complex which coincides with the presumed location of the crustal ocean-continent transformation. Filled circles indicate relocated ISC seismicity from 1964-1998 (Engdahl et al., 1998) while black stars indicate historic seismicity with $M_w \geq 7.0$ for the time period from 550 BC - 1999 AD (Papazachos et al., 2000). Diamond indicates location of $M_w = 8.3$ event in 365 AD.

the Ptolemy structure, as well as at the plate contact and within the top 20 km of the continental crust below Crete, while the microseismic activity in the depth range between 20 and 40 km below Crete and the Cretan Sea north of Crete is comparatively low (Meier et al., 2004a). In this study it is examined whether the microseismicity in the forearc of the central Hellenic Subduction Zone occurs in clusters. The aim is to detect and interpret zones of cluster activity within seismogenic structures of the forearc region.

3.2.2 Cluster

The occurrence of events with highly similar waveforms is well documented for regions with strike-slip regimes (e.g. Nadeau et al., 1995) and volcanic regions (e.g. Got et al., 1994). For the northeastern Japan subduction zone Igarashi et al. (2003) used similar events with magnitudes larger 3 to investigate the distribution of slip on the subducting surface.

Repeating events with nearly constant interevent time and an almost identical magnitude (Nadeau et al., 1995; Nadeau and Johnson, 1998; Igarashi et al., 2003) can be distinguished from a sequence of similar events occuring during swarm-like activity lasting hours or days. This swarm-like activity can either occur within the aftershock sequence of a larger event following the Omori law for aftershocks (Schaff and Beroza, 2004) or during the microseismic activity of an earthquake swarm without a major shock. Such swarm-like activity is generally linked to the presence of fluids (e.g. Yamashita, 1999; Parotidis et al., 2003; Kurz et al., 2004) while repeating events are usually attributed to the effect of tectonic loading (Nadeau and McEvilly, 1997).

The high waveform similarity of such events suggests a close spatial proximity of the seismic activity and makes them candidates for precise relative relocation techniques in order to delineate the structures activated. Shearer (2002) and Rubin et al. (1999) used this approach to locate streaks of similar events in California, while Got et al. (1994) inferred a dipping fault-plane below Kilauea volcano and Gillard et al. (1996) found narrow bands of seismicity below Kilauea volcano. In volcanic and hydrothermal regions the relocation technique has also been applied to image magma movement (Hayashi and Morita, 2003) and fluid migration (Spicak and Horalek, 2001) related to swarm activity.

In this study the characteristics of clusters found in the central Hellenic Subduction Zone are studied. Clusters are investigated with respect to migration of their hypocenters and the possible influence of fluids on their generation. Their spatio-temporal pattern is discussed.

3.3 Data

The data were collected during the operation of temporary short period networks by the Ruhr University Bochum on the islands of Crete and Gavdos. Details about the networks installed between 1996 and 2001 as well as an evaluation of the microseismic activity observed are described by Meier et al. (2004a). In this study also data gathered during a campaign in 2002 in the Rethymnon area is included. This network was intended to fill the gap in the observations between the networks on western Crete (1996) and in the Messara region (2000/1). From May 2003 until November 2004 the two south-eastern stations of the Messara network were reoccupied and three additional stations were installed at the southern shore of central Crete. The network's small aperture and its proximity to the Ptolemy structure were designed so that the previously detected cluster activity in this region could be mapped with higher resolution and with a lower detection threshold. The configurations of the various networks are shown in Fig. 3.2. The campaigns described by Meier et al. (2004a) as well as the Rethymnon data were evaluated using a routine data processing scheme. All events detected were processed manually by picking P- and S-phases whenever possible and were then located using the hypo71 location software (Lee and Lahr, 1972). Hypocenter locations and P- and S- arrival times for these events were thus readily available.

For the 2003/4 network the processing scheme was automatized. Events were detected by applying a STA/LTA trigger and subsequently requiring at least three simultaneously triggered stations. The results were then reviewed to exclude remote events and the catalogue was confined to events having S-P times of less than 8 seconds at at least one station. For the two main clusters in May and June 2003, however, all identifiable events were conventionally processed using hypo71. They were merged with the results from the routine processing for the years 1996 till 2002, resulting in a database containing 7299 hypocenters (see Fig. 3.2 for epicenter locations) and their corresponding P- and S-arrival times. This data set will be referred to as database A in the following. Furthermore, time series data from 4279 automatically processed events from the period May 2003 up to June 2004 with an S-P travel time of less than 8 seconds but without phase and hypocenter information were available for cross-correlation. This database will be referred to as database B in the following.
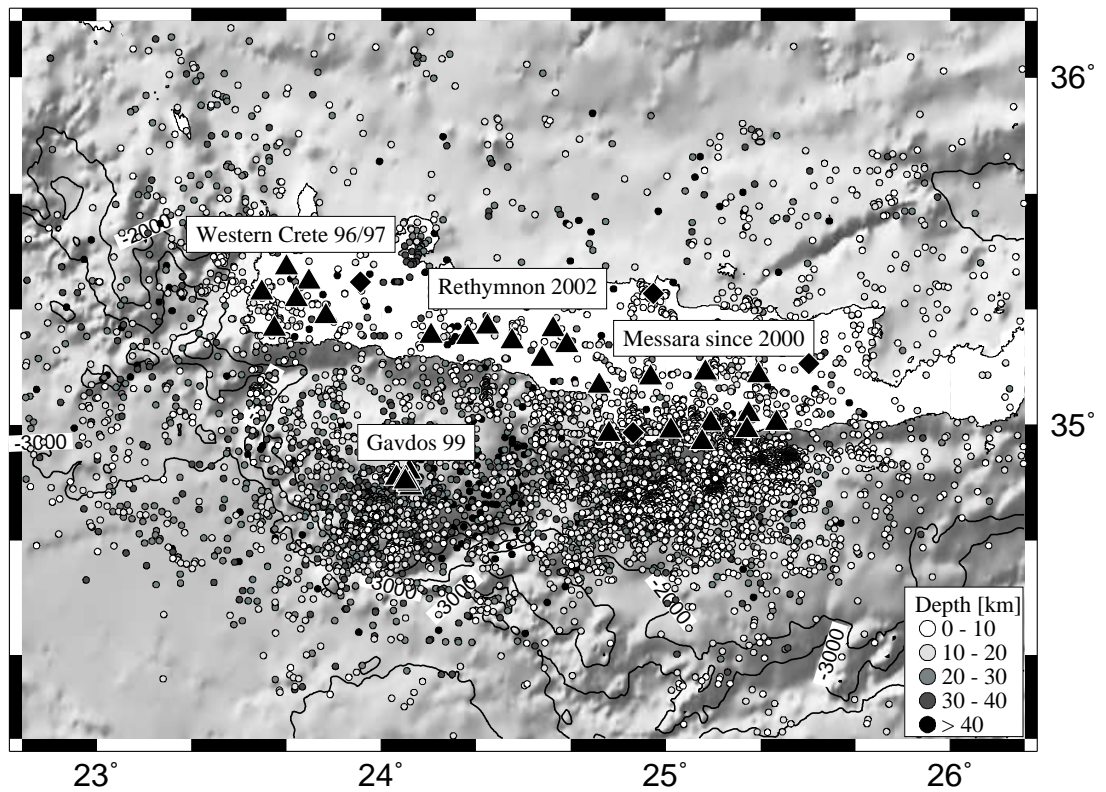
Figure 3.2: Seismic activity located with the short period networks on Crete and Gavdos from 1996-2003 constituting database A. Also indicated are the station locations (black triangles) of the different networks and the GEOFON broadband stations (Hanka et al., 1994) which were incorporated in the data analysis (black diamonds).
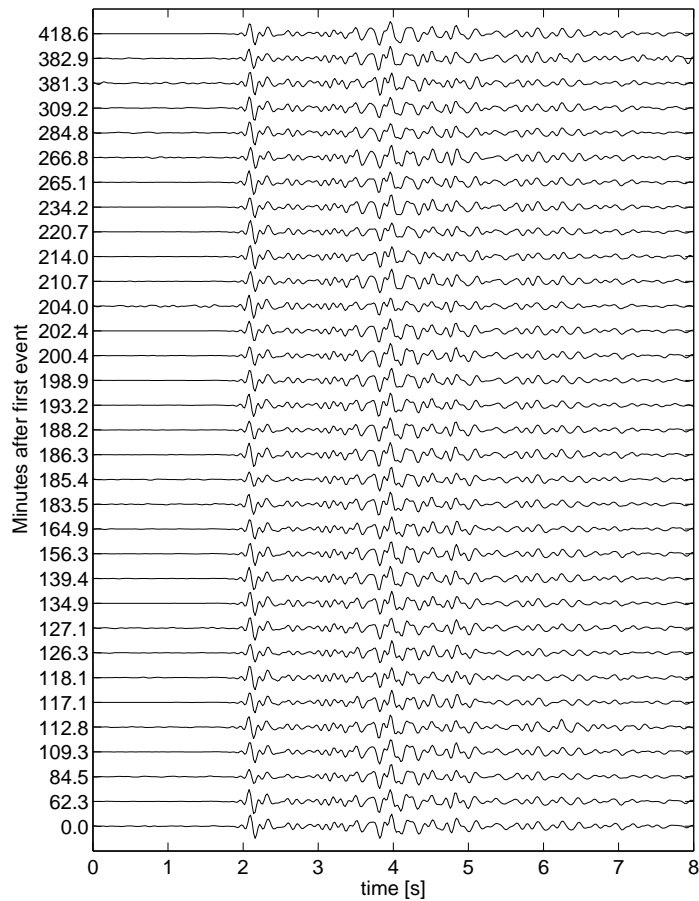
Figure 3.3: Waveform example of a cluster in 2000 at a station in the Messara network. The epicentral distance to the cluster which is located in the region of the southern shore line is approximately 12 km and the whole activity displayed here lasted for only 7 hours.

3.4 Cluster Analysis

3.4.1 Detection

In order to identify clusters of similar events waveform cross correlation was performed for each station. This was done for all events for which picked P- and S-phases from the respective station were present in database A. Because only data with identified P- and S-phases were considered, a high signal to noise ratio and a good data quality are assured for this dataset. Fig. 3.3 shows waveforms for a cluster consisiting of 33 events recorded at a station of the Messara 2000/1 network within an interval lasting 7 hours. Data filtered between 2 and 10 Hz and containing both P- and S-onset were used for all events in this database. The time window for cross-correlation started 1 second before the picked P-arrival and lasted until $T_p + 1.8 * (T_s - T_p)$ (where T_p is the time of the P arrival and T_s is the time of the S-arrival) thus constituting an adjustable window containing both the P- and S-arrivals. Correlating waveforms which contain information about the S-P time as well as the P- and S-wave ratios ensures close spatial proximity and similarity of source mechanism resulting in high correlation coefficients. See Fig. 3.3 for an example of similar waveforms found in this study.

Fig. 3.4 shows an example of a similarity matrix for events in southern central Crete and the adjacent off-shore region recorded in 2000 at station M005 of the Messara network (Fig. 3.5b). This symmetric matrix contains the correlation coefficients of all possible event combinations at a single station. The matrix shows correlation coefficients for the chronologically ordered events shown in Fig. 3.5b. Clusters of similar events are detected which belong to episodal swarm-like activity (Fig. 3.5a) in distinct areas (Fig. 3.5b). These are typical of the cluster activity south of Crete. In a further processing step all available cross correlation coefficients for a specific event pair were stacked and for all pairs with at least 3 observations (i.e. at least three stations for which cross correlation coefficients were determined) average correlation coefficients were calculated. Only these events were considered in the further analysis of events present in database A.

The final association of an event to a specific cluster can be achieved either by a single, a complete or some intermediate linkage approach (Everitt, 1993; Aster and Scott, 1993). In these clustering schemes each event is initially regarded as a separate cluster. In the single linkage approach two clusters are always merged to form a new cluster when any two members of the different clusters exhibit a correlation coefficient larger than a threshold value. The complete linkage approach demands that this constraint is met by all possible
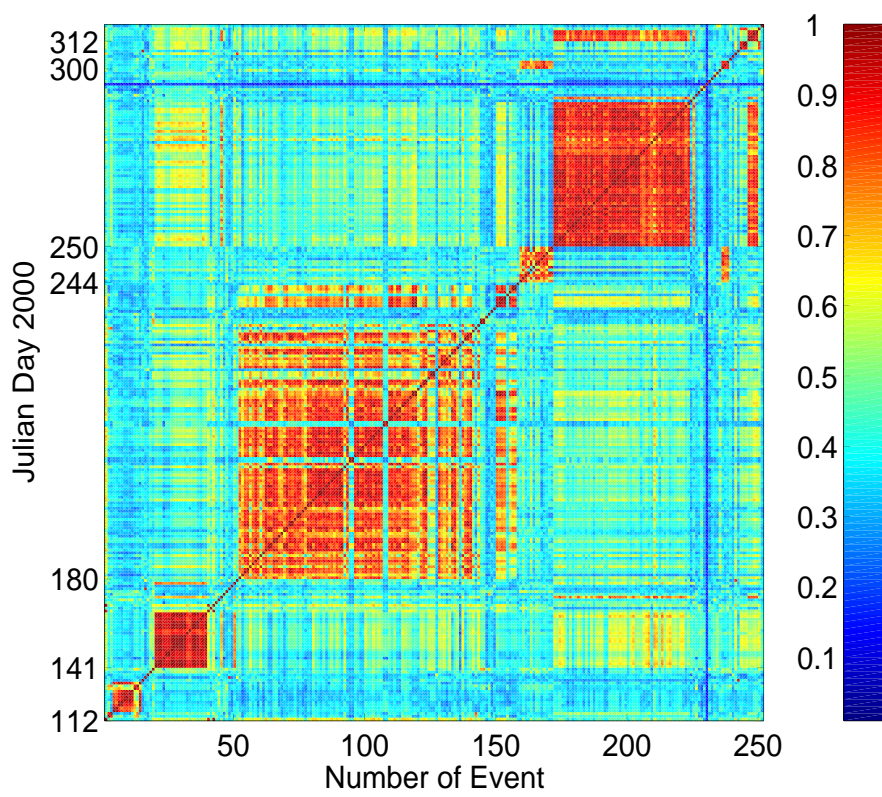
Figure 3.4: Cross correlation matrix for the events shown in Fig. 3.5.

event combinations. An intermediate approach may ask that a certain similarity threshold is met with respect to the mean correlation coefficient for all possible event pairs (Everitt, 1993). By definition a single linkage approach creates larger clusters than a complete linkage approach which on the other hand tends to create more but smaller clusters of highly similar events for the same threshold value. In this study a single linkage approach was used (Everitt, 1993; Aster and Scott, 1993) after initial trials with a complete linkage algorithm showed that many small, closely spaced clusters with highly similar waveforms active during the same time period were artificially separated by the clustering algorithm. The threshold of the cross correlation value was set to 0.9 after visual inspection of the cross correlation matrices and the waveforms belonging to the same cluster. By applying these processing steps to the data contained within database A we were able to identify a total of 315 multiplets with 1066 events. Most of the multiplets (210) consist of only 2 events (doublets) but 46 clusters have 5 or more members. The largest clusters consist of 33, 26 and 24 members, respectively.

The events in database B were analysed using a different approach due to the lack of P- and S- arrival times for them. Data for time windows of 50 seconds length were stored and in the first step the time lag for the highest cross correlation coefficient between two windows was determined. In a second step the time windows were shifted with respect to each other by this time lag and the maximum cross correlation coefficient of a time window lasting 10 seconds was calculated. As no adaptive windowing was used and no emphasis was put on data quality, correlation coefficients are generally lower than for data from database A. Nevertheless, this approach proved to be robust enough to identify clearly distinct clusters during the subsequent processing steps.

For the events in database B the station showing the best overall signal to noise ratio (SNR) was chosen as the reference station for which the cluster analysis was performed. For this station a cross correlation matrix was constructed containing all available events and the clustering algorithm was performed with a threshold value of 0.7. The cross correlation scheme was extended to this value lower than that used for events in database A, and the data processing automized as described in order to include events with lower SNR. In this way clusters consisting of weaker events could be detected by lowering the detection threshold. Although this increased the chance of misassociating individual events and thus merging actually distinct clusters, the procedure proved to be robust. Visual inspection of all clusters with at least ten members showed that only one of them was created by incorrect linkage of actually distinct events. This cluster was subsequently broken into 2 smaller clusters and the misassociated events removed. This led to a total of 31 clusters
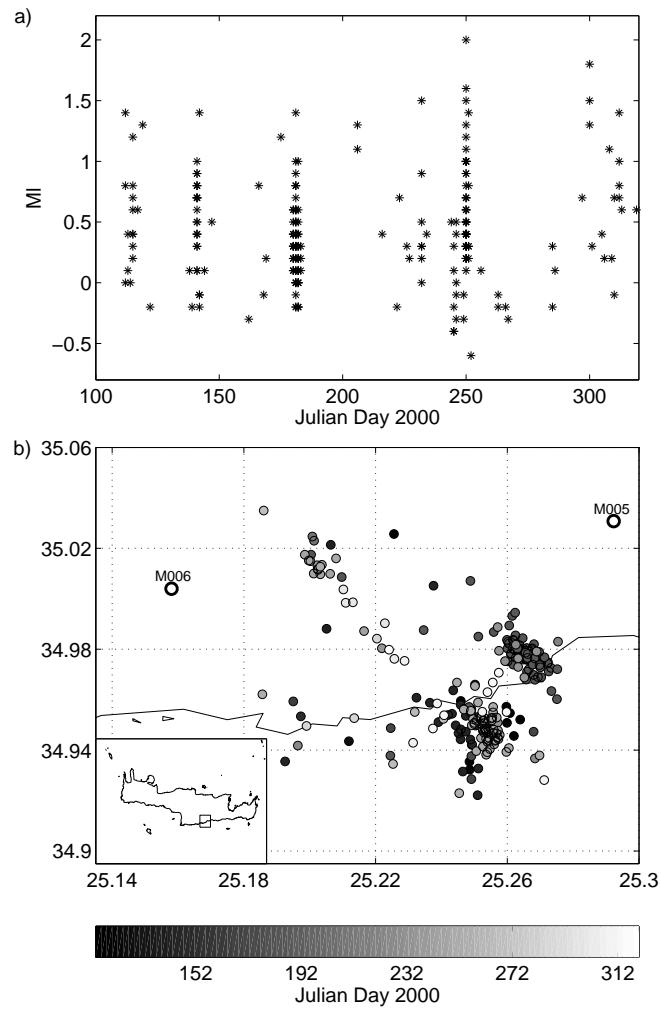
Figure 3.5: Microseismic activity recorded in 2000 in the region of the southern Cretan shore. a) Magnitude-Time plot of the events. b) Locations of the microseismic activity. Gray shading with respect to time of occurrence.

each with at least 10 events for database B. For each cluster the event with the best SNR at the reference station was taken to be the master event. This event was located using waveforms from the stations of the Messara 2003/4 network.

3.4.2 Location

Locations of cluster centroids from database A are indicated in Fig. 3.6 by filled circles scaled to the number of members within each cluster. Obviously, the clusters are located throughout the study region with depths ranging from near the surface to more than 40 km. A major accumulation of clusters is evident off the southern shore of central Crete in the area of the Ptolemy trench. Of course this picture is enhanced by the fact that this region is part of the area with the longest observation period. The greatest cluster activity in this region is associated with a nearly vertically dipping structure in the region of the Ptolemy trench described by Meier et al. (2004a). Most of the activity in this region is located at crustal depths pointing to processes within the continental Aeagean crust. In contrast, cluster activity below the island of Gavdos is deeper and considered to be part of the interplate seismicity between the subducting African lithosphere and the Aegean plate. Further activity is observed in the onshore region of central Crete as well as the south-western offshore region; for the latter the control on the hypocenter locations is lower due to the fact that these events are far outside the networks.

Results for database B are depicted in Fig. 3.6 by inverted triangles. The cluster activity is restricted to the region of the Ptolemy trench in the south, to a small area at the northern coast of Crete and to one spot in the Messara region where there are also clusters from database A. The distribution of clusters in the region of the Ptolemy trench supports the results from database A. This trench exhibits cluster activity along almost its entire length towards its north-eastern landward termination. While this activity is detected throughout the entire observation period at distinct locations, activity in the north is confined to a few days in 2003.

3.4.3 Characteristics

Clusters detected in this study generally exhibit swarm-like microseismic activity lasting for only a few hours or days (Fig. 3.5). The magnitude time plot for events close to the southern shore in central Crete (Fig. 3.5a) shows that the seismic sequences are not domi-
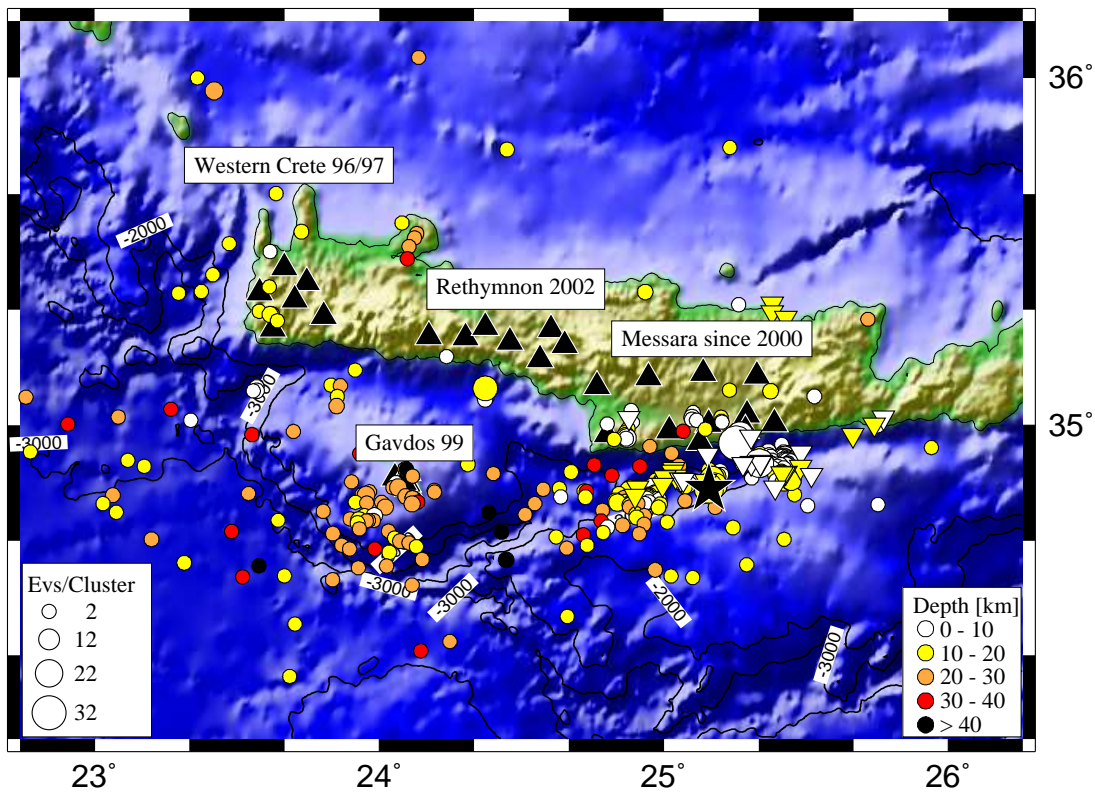
Figure 3.6: Locations of all cluster centroids determined in this study. Circles donate centroids for clusters of database A while triangles donate those of database B. Star marks the location of the relocated cluster in Fig. 3.8.

nated by a major event but in fact exhibit swarm-like behaviour which can be attributed to spatially distinct microseismic activity (Fig. 3.5b). The absence of larger events in clusters is also apparent in Fig. 3.7a. The histogram shows the magnitude frequency distribution for the largest events belonging to each cluster identified using data from the Messara 2000/1 campaign and thus constituting a data subset from database A. This observation also holds when considering all seismicity within a cluster region and not only the similar events of a single cluster.

Although occasinally a cluster may reactivate such behaviour is not characteristic for the clusters studied within the period of observations. Subtle differences in color for event pairs belonging to the same cluster in in the similarity matrix of Fig. 3.4 hint at corresonding changes in their waveforms. These waveform differences may be attributed to a small change in hypocenter position or source characteristic and thus support the idea that we are not dealing with repeating events but an activity spanning a spacial extent of up to several hundreds of meters.

Fig. 3.7b shows the distribution of interevent times for events belonging to the same cluster. The double logarithmic plot is created by deviding the time axis into logarithmically scaled intervals, counting the number of inter-event times between two successive events belonging to the same cluster within each interval and subsequently normalizing the number contained within each interval to one day. Squares in Fig. 3.7b are for successive inter-event times of the largest cluster (Fig. 3.8) while triangles indicate the results for all clusters in database A and B. The distribution follows a power law with different slopes for events belonging to the largest cluster and all identified clusters combined. For events of the largest cluster a power law $t^{-1.55}$ exists while the result for all cluster events combined suggests a power law $t^{-1.1}$.

 The well known Omori law (e.g. Utsu et al., 1995) which predicts an exponential decay in the number of aftershocks of major events with time shows a power law behaviour. Assuming that an aftershock sequence can be represented by a non-stationary Poisson process, Senshu (1959) showed that the inter-event time distribution of the aftershock sequence also follows a power law behaviour. Recently, Hainzl (2004) observed this power law behaviour of inter-event times in seismic swarms in the Vogtland region (Hainzl, 2004). Seismic swarm activity in that region is generally linked to fluid intrusions (Spicak and Horalek, 2001; Hainzl, 2004). He was able to model the observed power law $t^{-1.5}$ in a numerical simulation incoporating fluid diffusion and postseismic creep (Hainzl, 2004). The findings of this study for the Hellenic Subduction Zone support the idea of a power law behaviour of inter-event times in seismic swarms.
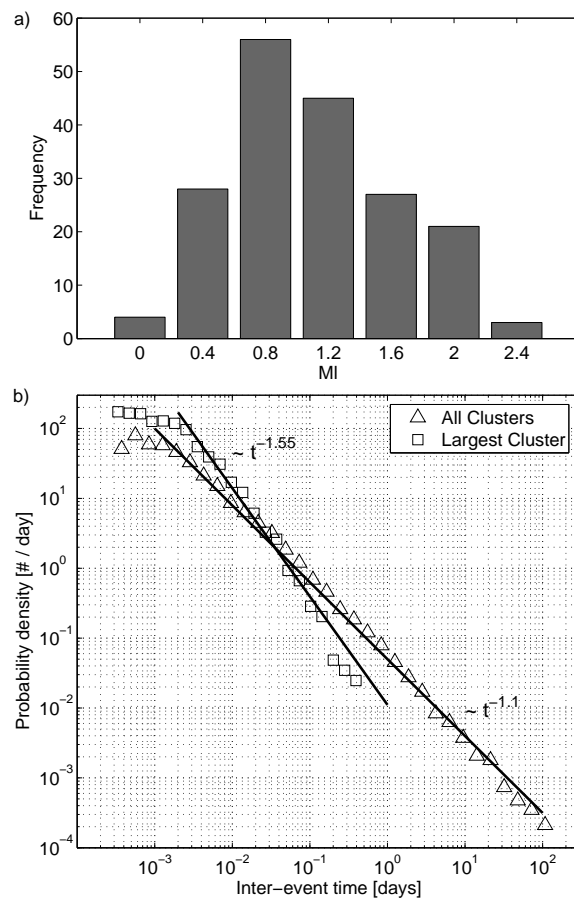
Figure 3.7: a) Magnitude of the largest event within each cluster for the 2000/1 Messara campaign. b) Inter-event time probability distribution for all events belonging to the largest cluster (stars) and all events in database A and B (triangles).

3.5 Relative cluster relocation

The cluster analysis has revealed that adjacent clusters often exhibited seismic activity within the same time period. One possible explanation for this is a migration of the seismic activity between them. This can be tested by precise relative relocation of the hypocenters of the cluster events. To jointly investigate the behaviour of such closely spaced clusters, the correlation threshold was decreased to 0.7 while maintaining the requirement that the events be recorded by a minimum of three stations. Applying this approach to the data in database A merged previously distinct clusters to considerably larger entities and also created clusters which did not exist previously. The most prominent feature is a cluster containing more than 250 members in the Ptolemy region (star in Fig. 3.6). Further clusters with 30 to 160 members were also created by this approach and predominantly located in the same area.

For the relative relocation the program hypoDD (Waldhauser and Ellsworth, 2000) was used. While catalogue times were taken directly from the routine processing, cross correlation times were calculated for the 30 nearest neighbours of each event. This was done in the time domain by resampling 50 Hz data to 1000 Hz and than finding the time lag for the highest cross correlation coefficient. This approach was performed for P- and S- arrivals separately with time windows of 1 second cut out from data bandpass filtered between 2 and 10 Hz. Only times with cross correlation coefficients larger than 0.65 were retained and the times were weighted according to their cross correlation coefficient.

Fig. 3.8 shows the result for the largest cluster. The activity began to the east of the cluster centroid and initially migrated toward the east and then toward the west. Later activity however was only recorded at the western end of the cluster. The cluster extends approximately 3 km in EW direction. The distance of 2 km from its point of initiation to its western termination was covered in a little less than 4 days suggesting a migration velocity of about 0.5 km per day.

In order to address the uncertainties in the locations of the relocated events, synthetic tests were performed. Exact travel times from the cluster centroid to the recording stations were perturbed with a realistic, normally distributed random error. Fig. 3.9 compares the results for 64 synthetic events initially located at the centroid of the largest cluster (black triangles) to locations of the 75 best constrained events (at least 10 cross correlation and catalog times per event pair) of this cluster (filled circles). The ENE-WSW elongation of the cluster which follows the trend of the Ptolemy trench in this region is in sharp contrast to the structure dipping from south to north obtained from the sythetic tests.
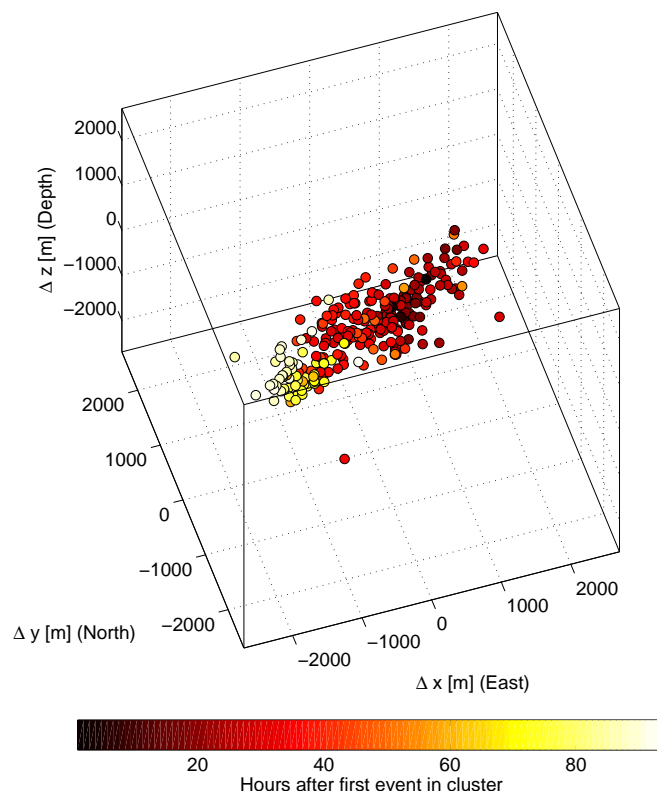
Figure 3.8: Perspective view of relocated hypocenters belonging to the largest cluster depicted as star in Fig. 3.6 and showing a migration of the hypocenters.
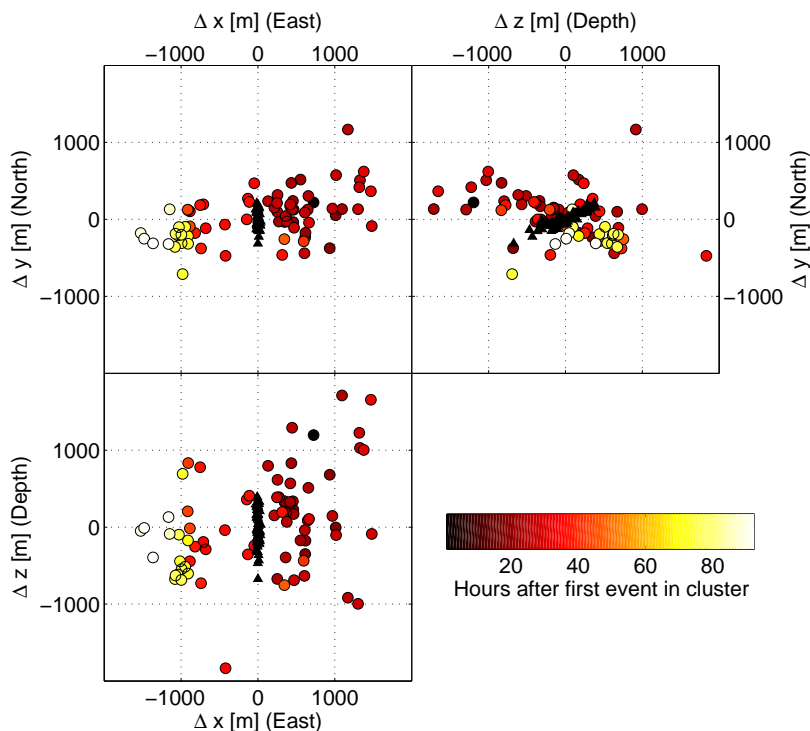
Figure 3.9: Comparison of best constrained hypocenters of the cluster in Fig. 3.8 (color coded circles) with the locations of hypocenters derived from exact traveltimes perturbed with a realistic random error (small black triangles).

This apparent structure clearly reflects the influence of the network configuration on the hypocenter distribution. The north-south vertical section in Fig. 3.9 hints at a fault-plane dipping steeply to the south which contrasts with the northward dipping structure created by the incorporation of random errors. Error estimates for the catalog locations in database A can be found in Meier et al. (2004a) and are of the order of 5-10 km. However the maximum relative error for the relocated hypocenters infered from the synthetic tests is in the range of 500 m for the least constrained axis of the error ellipsoid (Fig. 3.9).

Fig. 3.10a shows the magnitude-time plot for this cluster indicating embedded swarm activity consistent with the subclustering observed in the cluster analysis. It is also evident that the subclusters also behave like swarms without a dominant event. Fig. 3.10b displays a histogram of all possible event combinations for the cluster with the bins determined both by interevent distance and interevent time. The majority of event combinations plots just above the origin thus indicating events with a very short interevent time and a small offset in position. Repeating events would plot in the lowest row of Fig. 3.10b which repre-

sents an interevent distance of less than 100 meters. This offset in the interevent distance increases with increasing interevent time. Furthermore, it is also possible to infer a feature with positive slope in this plot. It is especially pronounced in the interevent time range from 40 to 70 hours representing the interval between the beginning of strong activity and the last two sub-swarms of Fig. 3.10a. The slope can be interpreted as the migration velocity of the hypocenters and is of the order of 500 m/day.

Migration of the microseismic activity over time was also observed to a lesser degree for two other clusters with much smaller spatial extents.

3.6 Discussion and Conclusions

This study was aimed at finding clusters of events displaying a high degree of waveform similarity and obtaining quantitative measures for the event sequences forming these clusters. Because the results of the cluster analysis depend on the choice of the threshold value for the cross correlation coefficient and the minimum number of stations required to meet this threshold value, changing these values will also change the results. The different threshold values and required numbers of stations meeting this value for database A and B, however, produced very similar results with respect to the spatio-temporal behaviour of the identified clusters. Thus, a careful analysis of the similarity matrices to find the appropriate cross correlation threshold value seems to be a viable approach.

The event sequences making up these clusters belong to the swarm type because most of the activity for a given cluster is limited to a short time interval and has no major events (Fig. 3.5). Although a seismic reactivation was observed for several regions, the events did not meet the necessary cluster criteria. The spatial and temporal extent of the different clusters varies. While most clusters show microseismic activity confined to only a few hours and a spatial extent confined to hundreds of meters, occasionally a cluster occurs in which activity lasts for several days and the hypocenters tend to migrate from one center of activity to another (Fig. 3.8) covering distances of several kilometers. This behaviour is also observed in other regions with swarm-like activity and is related to the triggering effect of fluids (Parotidis et al., 2003).

The absence of repeating earthquake sequences in this analysis does not exclude the possibility of their occurrence in the study area. It merely shows the limitation of the data used in this analysis with its short recording periods of generally only a few months. This recording period may be to short to include the repeated occurrence of events forming a
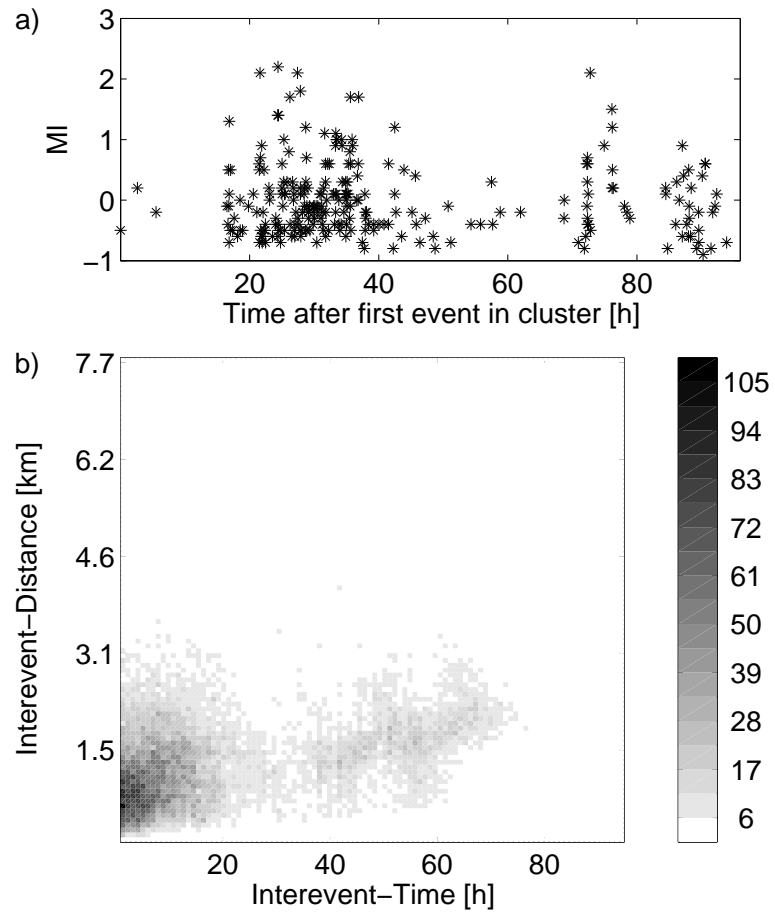
Figure 3.10: a) Magnitude-time plot for the events frroming the cluster of Fig. 3.8. b) Plot of cumulative interevent distance versus interevent time for all possible event combinations of the cluster in Fig. 3.8. The shading shows to the number of event pairs that belong to the same bin.

series of repeating events which generally show recurrence intervals of several months or years (Nadeau and McEvilly, 1997).

The presence of spatially and temporally distinct subclusters with higher correlation coefficients within larger clusters suggests the activation of different fault patches caused by a driving force which migrates. This pattern hints at a highly heterogeneous rupture surface. The possibility that distinct focal mechanisms due to the activation of differently oriented fault planes create the subclustering is not supported by the distribution of the hypocenters for the largest cluster (Fig. 3.8) which seem to belong to the same fault-plane. The decay in activity within a single cluster or subcluster follows an Omori law (Fig. 3.7)(Utsu et al., 1995) and may thus be linked to a stress triggering mechanism within the single cluster as it is evident for aftershock sequences (Stein, 1999). Such behaviour has also been observed and modelled for other regions with swarm activity triggered by fluids (Hainzl, 2004). The slight offset in interevent distances observable in Fig. 3.10b as well as subtle differences in the waveforms of events belonging to the same cluster suggest the activation of adjacent patches of the rupture surface. This contrasts with the idea of repeating events and can be explained with a decrease in shear stress at the ruptured fault patch making this now relaxed portion of the rupture surface less likely to break again. Such behaviour is reported in other studies (e.g. Rubin et al., 1999) as well, although cases of repeating events within aftershock sequences (Schaff and Beroza, 2004) have been observed as well.

The spatial distribution of clusters is not random but generally follows the observed distribution of microseismicity in the study area (Meier et al., 2004a). The accretionary prism of the Hellenic Subduction Zone to the south exhibits aseismic deformation and compaction of the sediments with related mud volcanoes (Cifci et al., 1997; Kopf, 2002). The plate contact south of Crete shows strong microseismic activity between about 20 and 40 km depth (Meier et al., 2004a) as well as intermediate magnitude activity (Engdahl et al., 1998) and may also have the potential to create major events (Papazachos et al., 2000). Cluster activity at depths compatible with the plate interface was located in the central forearc region of the Hellenic Subduction Zone, especially in the region of the island of Gavdos and the western part of the Ptolemy trench. Here depths up to more than 40 km indicate low seismic coupling in this depth range.

The eastern part of the Hellenic forearc consists of forearc slivers separated by the Ptolemy, Pliny and Strabo trenches which were identified as deep-sea depressions with wedge-shaped sedimentary basins of up to 4km thickness (Bohnhoff et al., 2001) that developed in a regime of sinistral transtension active in the region for the last approximately 3 Ma (ten

Veen and Kleinspehn, 2003). Microseismic studies (Meier et al., 2004a; see Section 4) identified a nearly vertical, seismically active structure reaching from the plate interface to near surface depths within the Ptolemy trench that may represent the contact between the forearc sliver and the Aegean lithosphere beneath Crete. This observation correlates with seismic studies which identified fault zones down to the mid-crustal reflector in that region (Bohnhoff et al., 2001). The cluster analysis identifies the Ptolemy trench as being very active, with nearly continuous cluster activity spanning its entire length and presumably also its entire depth from the lower continental crust to the surface (Fig. 3.6). Relocation of the largest cluster revealed a hypocenter migration following the strike of the Ptolemy trench. As the campaigns were limited to land-based stations, the question whether the Pliny and Strabo trenches show a similar behaviour can not be addressed. The detection threshold is too high to quantify possible cluster activity at those distances. Following the subduction to greater depths in the north, microseismic and cluster activity ceases and we enter a domain of aseismic deformation. This might be explained by the serpentinization of the Aegean mantle due to the dehydration of the subducting African crust as suggested by receiver function studies in the region (Li et al., 2003).

The distribution of observed clusters might be linked to fluid circulation in the forearc of the Hellenic Subduction Zone. A model for such a circulation system is schematically sketched in Fig. 3.11. Some of the water contained within the thick sediment cover of the Libyan Sea is expelled in mud volcanoes of the accretionary prism (Cifci et al., 1997; Kopf, 2002) without detectable microseismic activity. Another portion of the water contained as pore fluids within the sediments or in the form of hydrated rock within the upper part of the oceanic crust is subducted. Increased pore pressure may cause the observed microseismic activity. Finally the transtensional Ptolemy structure may form a region of crustal weakness where the fluid ascends towards the surface triggering clusters of seismic events along its way. Detailed studies of the seafloor in the region of the Ptolemy trench could reveal the surfacial expressions of such fluid circulation. Below 40 km cluster activity and microseismicity cease, pointing to a change in the properties of the plate contact and a seismic decoupling of the plates at greater depth.
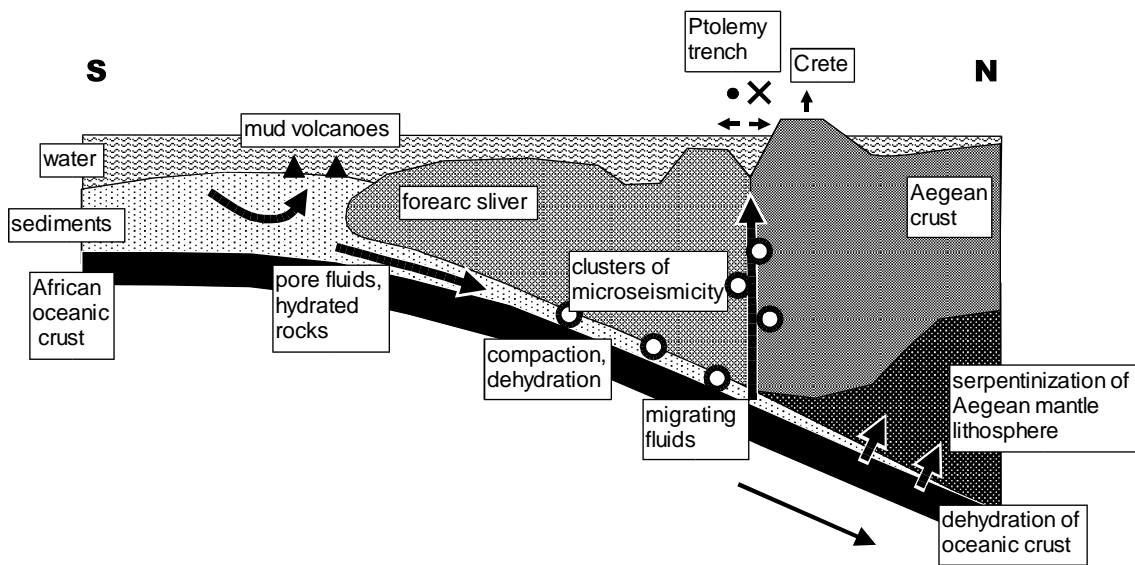
Figure 3.11: Sketch of possible fluid circulation in the Hellenic forearc region and associ-
ated cluster activity. Fluids contained within the sediments of the Libyan
sea are either expelled at mud volcanoes in the Mediterranean Ridge or
subducted. The subsequent compaction of sediments or dehydration of the
oceanic crust may trigger microseismic cluster activity at the plate interface
while ascending fluids in the Ptolemy structure are responsible for its strong
cluster activity.

4 Seismic Slip Coupling in the western HSZ

4.1 Summary

A formula for the estimation of the maximum cumulative seismic slip on a given rupture surface using events listed in a catalogue of historic or instrumental seismicity is given. The formula utilizes empirical relationships linking rupture area and average slip of an event to its moment magnitude (M_w). To estimate the contribution of events with magnitudes below the completeness of the catalogue, the magnitude frequency distribution (MFD) is extrapolated using the Gutenberg-Richter-Relation. The resulting maximum cumulative seismic slip can be compared to the total slip estimated by geodetic or tectonic studies to obtain the seismic coupling of the active rupture surface.

The maximum cumulative seismic slip along the shallow plate contact of the Hellenic Subduction Zone (HSZ) south-west of Crete in the vicinity of the presumed rupture area of the largest known earthquake in the HSZ, the Crete 365 AD M_w8.3 event, is estimated for the last 2000, 500 years and for the time interval between 1964 and 1998 using catalogues by Papazachos et al. (2000) and Engdahl et al. (1998). Estimates of the maximum cumulative seismic slip amount to about 22 m, 2 m and 11 cm, respectively. Assuming a constant relative plate motion of about 4 cm/a for the last 2000 a, the seismic coupling is about 0.25, 0.1 and less than 0.1, respectively. Even for a conservative parameter estimation of the b-value, the seismic coupling is low and a substantial part of the total slip is accomodated aseismically in the region under consideration.

The shallow plate contact of the HSZ south-west of Crete seems to be recently weakly coupled, shows high seismic activity up to magnitudes of about 6, but exhibits the potential to generate larger earthquakes. The behaviour of the plate contact south-west of Crete may be described as conditionally stable.

4.2 Introduction

The HSZ where African oceanic lithosphere is subducting beneath the continental Anatolian-Aegean plate is the seismically most active region in Europe. Apart from a high level of intermediate magnitude activity, destructive events with magnitudes up to $M_w 8.3$ occurred at shallower depths in historic times (Papazachos et al., 2000; Stiros, 2001)(Fig. 4.1). A thrust type source mechanism is assumed for the $M_w 8.3$ event south of Western Crete in 365 AD (Taymaz et al., 1990; Papazachos et al., 1991). Fault-plane solutions for current intermediate magnitude events within the Aegean plate in the area of western Crete are of the normal faulting type and indicative of along arc extension while interplate seismicity in this area shows predominantly thrust-type activity and a P-axis in agreement with relative GPS velocities between the plates (Bohnhoff et al., 2005).

In order to estimate the seismic hazard caused by this major interplate seismicity, it is necessary to quantify the amount of relative slip between the African and Aegean plates that is accomodated seismically. Furthermore, the temporal and spatial variability of this seismic slip as well as of the total slip needs to be addressed to understand the seismic behaviour of the plate contact. Information about the interplate seismicity may be gained from palaeoseismological studies, macroseismic studies using historical sources, and older as well as modern instrumental seismicity studies. These studies cover successively smaller time spans and are characterized by an increasingly lower detection threshold from about $M_w 8.0$ for the oldest historical sources to about $M_w 3$ for modern instrumental catalogues and can be continued to magnitudes of about $M_w 0$ by microseismicity studies covering time spans of several months.

In this study, a formula is derived that allows to estimate the maximum cumulative seismic slip on a seismically active fault from a seismicity catalogue using empirical relations between the average displacement, the rupture area, and the moment magnitude. To apply this approach to the western HSZ, a historical catalogue covering more than 2500 years (Papazachos et al., 2000) is evaluated for the last 2000 and 500 years, respectively. The instrumental ISC catalogue (Engdahl et al., 1998) is investigated for comparison using a time interval of 34 years. The catalogues are extrapolated towards smaller magnitudes using information about the b values in the region derived from the catalogues and studies of microseismicity in the region.

Information about the total slip between plates can be gained from different sources covering different time scales. GPS studies covering the last approximately two decades give information on the current plate velocities. Geological and archaeological information on
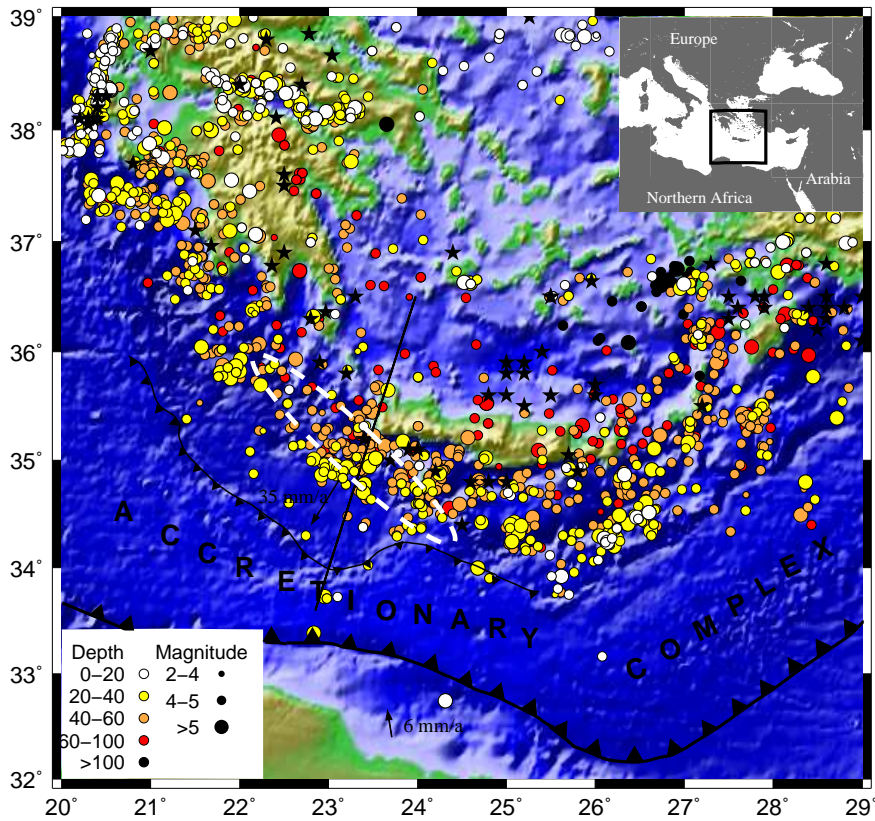
Figure 4.1: General tectonic setting of the research area. Thick line with triangles indicates the southern border of the accretionary complex while the thin line with triangles indicates the border between the outer and inner unit of the accretionary complex which coincides with the presumed location of the crustal ocean-continent transformation. Filled circles indicate relocated ISC seismicity from 1964-1998 (Engdahl et al., 1998) while black stars indicate historic seismicity with $M_w \geq 7.0$ for the time period from 550 BC - 1999 AD (Papazachos et al., 2000). Dashed white line indicates surface projection of the presumed rupture area of the 365 AD event. Black arrows indicate motion of Aegean and African plate with respect to stable Eurasia.

uplift rates and relative offsets at fault lines and plate contacts give insight into the kinematics of the last thousands of years or longer while tectonic reconstructions model the plate motions over millions of years. These reconstructions can be compared with recent GPS measurements and geological and archaeological evidence to identify changes in the relative plate velocities.

The total slip at the plate interface is compared with the estimated seismic slip to quantify the amount of seismic coupling at the plate interface. This seismic coupling is often linked to asperities at the plate contact (e.g. Ruff and Kanamori, 1980) with a large area of asperity contact indicative of high seismic coupling and a small area of asperity contact indicative of lower coupling. At a subduction zone plate contact, seismic coupling was devided by Scholz (1988) into three different categories. (1) Unstable asperities which show complete seismic coupling and form the nucleation points for most large earthquakes. (2) 'Weak zones' which slip aseismically in interseismic periods but rupture coseismically. These zones are conditionally stable and break in dynamic loading but slip aseismically in static loading. (3) Stable regions which always slip aseismically and have zero seismic coupling. Pacheco et al. (1993) used these ideas to develop a model for the seismic coupling in subduction zones in which they link the seismic coupling to the frictional behaviour of material at the plate boundary. In this study, the seismic activity in the vicinity of the presumed rupture area of the Crete 365 AD $M_w 8.3$ event is investigated to find indications for the presence of asperities, aseismic patches or regions which may exhibit conditionally stable behaviour.

4.2.1 The plate contact of the HSZ in the area of Crete

The seismogenic part of the HSZ in the area southwest of Crete was mapped by microseismicity studies (e.g. Meier et al., 2004a) and is also clearly evident in the global ISC catalogue (Engdahl et al., 1998, Fig. 4.3). The width of the interplate seimogenic zone from updip to downdip limit is on the order of 100 km and ranges in depth from 20 km in the Libyan Sea to approximately 40 km at the south coast of Crete (Meier et al., 2004a). The relative motion at the plate contact can be estimated from the velocities of the Aegean and African plates with respect to stable Europe. GPS measurements (Kahle et al., 2000; McClusky et al., 2000) calculated a velocity of 35 mm/a in roughly SSW direction with respect to stable Eurasia for the Aegean plate while the velocity of the African plate was determined with 6 mm/a in north-westward direction resulting in about 40 mm/a of relative movement between the plates. The higher velocities for the southern tip of the
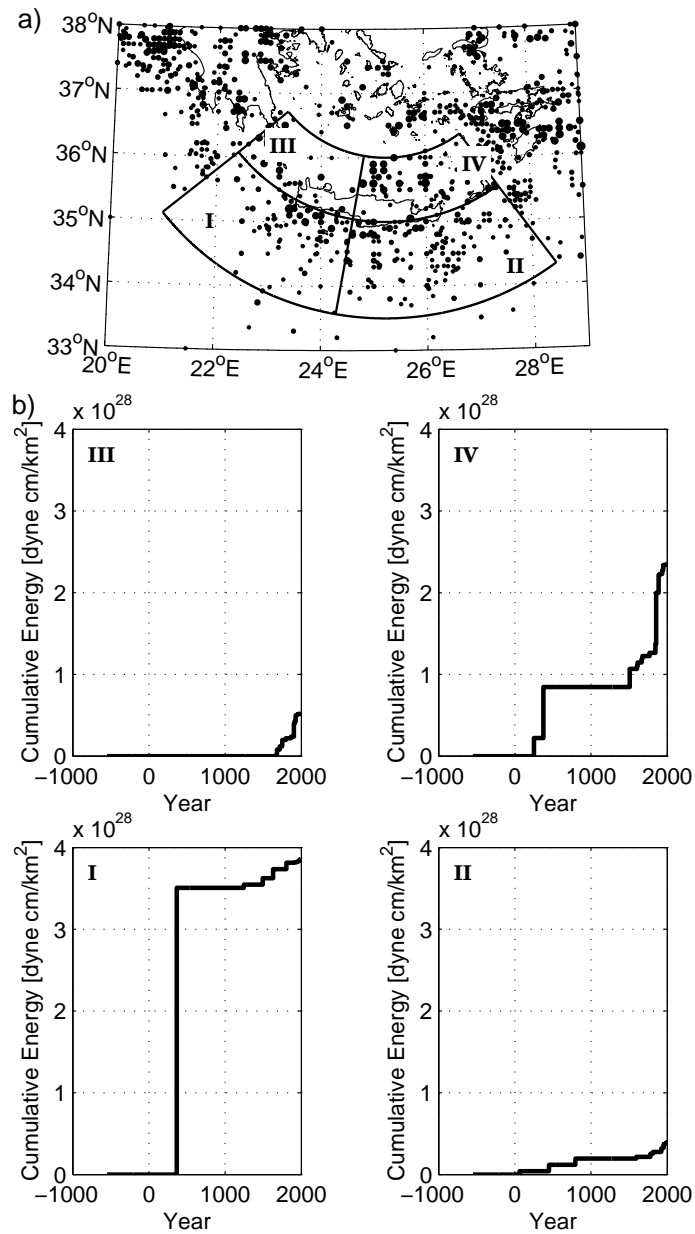
Figure 4.2: a) Mapview of historical and instrumental seismicity with $M_w \geq 5.0$ spanning the time period 550 BC - 1999 AD as given by Papazachos (2000). b) Cumulative energy release normalized to $1km^2$ for the different sectors indicated in a).
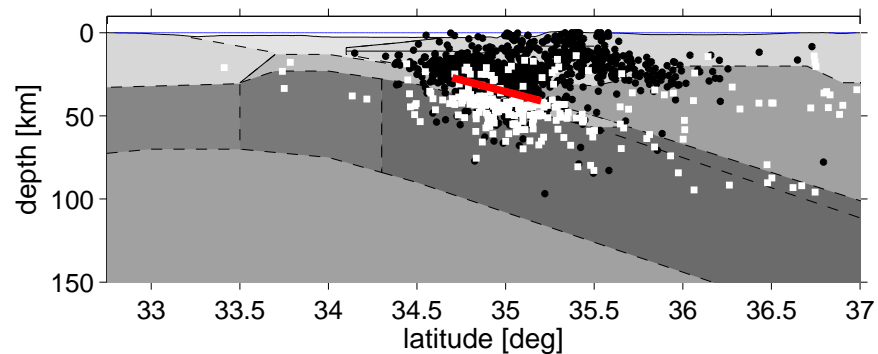
Figure 4.3: Cross-section along the line indicated in Fig. 4.1. Thick red line indicates the assumed width of the 365 AD rupture, white squares indicate ISC seismicity from 1964-1998 while black dots are results from microseismicity campaigns on western Crete in the years 1996/7 (Meier et al., 2004a). Geometry of slab and continental crust is based on results from seismological (Endrun et al., 2004) and refraction seismic studies (Bohnhoff et al., 2001).

Aeagean plate when compared to the motion further north in the Aegean trough is often explained by slab rollback initiated by the slab pull of the downgoing African lithosphere (e.g. Meijer and Wortel, 1996) causing the thinning of the Aeagen crust (e.g. LePichon et al., 1995) which is evident e.g. in refraction seismic studies (Bohnhoff et al., 2001).

4.2.2 Seismic slip and coupling in the HSZ

Despite the high seismic activity in the HSZ many studies dealing with the total energy release of the seismogenic volume in the region of the forearc (e.g. North, 1974; Papadopoulos, 1989; Papazachos et al., 1992, Jenny et al., 2004) found a rather low contribution of seismicity to the total convergence in the southern Aegean. North (1974) compared moment rates computed from earthquakes in the time period 1910-1970 with rates calculated for plate tectonic models and found a large deficit for the seismic moment rate which he linked to visco-elastic processes such as creep. The same method was applied to a more complete catalogue covering the period 1800-1986 which is complete for events with $M_s \geq 6.5$ and also includes magnitudes as small as 3.0 by Papadopoulos (1989). By combining all available historic data with information about the dominant focal mechanism in the seismogenic zones Papazachos et al. (1992) estimated the amount of seismic crustal deformation in the Aegean. For the HSZ they found a significant deficit. Jenny et al. (2004)

determined a long-term seismic moment rate from estimated earthquake recurrence parameters and found a high amount of aseismic deformation for the Hellenic Arc. They explained the low seismic coupling in the area of western Crete by a reduction of the compressive normal stress acting on the seismogenic interface. This idea was introduced by Scholz und Campos (1995) for subduction zones with back-arc spreading or retreating slabs. Laigle et al. (2004) explain this reduction with slab pull caused by the slab that is still attached to the continental African plate in the region of the Libyan Sea while it might be detached in the region of Peloponese further to the north-west in the subduction zone. However, source mechanisms indicate compressive normal stress on the plate interface in the western forearc of the HSZ (Lyon-Caen et al. 1988, Bohnhoff et al. 2005).

The low seismic coupling along the Hellenic Arc contrasts with results for the strike-slip zones in the region (Kephalonia Fault and North Anatolian Fault Zone) which show a nearly total seismic coupling (e.g. Jenny et al., 2004). Ambraseys (2006) found in a study of long-term seismicity data for the Gulf of Corinth, the Marmara Sea and the Dead Sea Fault Zone a good agreement with present day GPS rates which indicates only a small amount of aseismic slip in these regions. Fig. 4.2 shows the temporal evolution of the released seismic energy normalised to one km^2 for four different segments in the Hellenic forearc. As can be seen from this figure the Crete 365 AD $M_w8.3$ event dominates the seismic energy release in the south western segment which is otherwise comparable to the south eastern part of the HSZ. Apart from the Crete 365 AD event the two southern segments exhibit a significantly lower energy release than the north eastern segment which contains some strong intermediate depth events but no interplate seismicity. In a study of earthquakes with magnitudes larger than 4.9 spanning the period 1950-1978 Wyss and Baer (1981) observerd an 80 % decrease in the seismicity rate of the westernmost part of the HSZ in the time period 1962-1980 when compared to the 1950-1961 activity in the same area while they observed rather constant rates in the central and eastern portions of the HSZ.

In this study, the interplate seismicity south of western Crete in the source region of the $M_w8.3$ 365 AD event is investigated. The ratio between seismic and aseismic slip is estimated for different time intervals using available catalogues.

4.3 Estimation of maximum cumulative seismic slip on an active rupture surface

Moment summation methods to calculate the deformation rate in a given region (e.g. Molnar, 1979; Jackson and McKenzie, 1988; Papazachos et al., 1992) from seismic data are well established. These formulations incorporate information about the expected maximum magnitude in the region, a- and b-values of the MFD (Gutenberg and Richter, 1944) and the dominant focal mechanism to calculate a scalar moment rate (Molnar, 1979) for the seismogenic volume under consideration.

In this section a formula to calculate the cumulative seismic slip on a single rupture surface for a given time interval is derived by incorporating empirical formulas relating average slip during an event and rupture area to the moment magnitude. This cumulative seismic slip can then be related to the cumulative total slip to obtain the seismic coupling. Because the slip formulation incorporates moment magnitudes and not moment tensors the database can be extended to historic events for which no moment tensors are available.

The slip rate on a fault as a function of time is $d(t, x, y)$, where (x, y) denotes the considered point on the fault. The spatially averaged slip rate on the considered fault area A as a function of time is

$$d(t) = \frac{1}{A} \int_A d(t, x, y) dx dy \tag{4.1}$$

and the cumulative slip on the considered area in the time interval (t_1, t_2) is

$$D(t_1, t_2) = \int_{t_1}^{t_2} d(t) dt. \tag{4.2}$$

The slip rate averaged over the time interval (t_1, t_2) is $\bar{v}(t_1, t_2) = \frac{D(t_1, t_2)}{t_2 - t_1}$. $D_{total}(t_1, t_2)$ denotes the cumulative total slip that might be estimated from observations in the field or from GPS measurements. If the average total slip rate on the fault in the time interval (t_3, t_4), $\bar{v}_{total}(t_3, t_4)$, is known, the cumulative total slip in the time interval (t_1, t_2) might be estimated according to $\bar{v}_{total}(t_3, t_4) \times (t_2 - t_1)$ assuming a constant slip rate. $D_{seis}(t_1, t_2)$ denotes the cumulative seismic slip on the considered fault area. The cumulative total slip is the sum of the cumulative seismic and the cumulative aseismic slip: $D_{total}(t_1, t_2) = D_{seismic}(t_1, t_2) + D_{aseismic}(t_1, t_2)$. Given $D_{total}(t_1, t_2)$ and $D_{seis}(t_1, t_2)$, the seismic coupling

of the fault in the time interval (t_1, t_2) is

$$\nu(t_1, t_2) = \frac{D_{seis}(t_1, t_2)}{D_{total}(t_1, t_2)}. \tag{4.3}$$

In order to estimate $D_{seis}(t_1, t_2)$ at first the contribution of a single event with moment magnitude M_w that occurs on the respective fault area must be considered: $\frac{a(M_w)}{A} D(M_w)$, where $a(M_w)$ denotes the rupture area of the event and $D(M_w)$ the average slip during the event. The rupture area might be expressed by $A = N_0(M_w) a(M_w)$, where $N_0(M_w)$ is the number of events with magnitude M_w necessary to rupture the entire considered fault area. Therefore, the contribution of a single event to $D_{seis}(t_1, t_2)$ is $D(M_w)/N_0(M_w)$. Multiplication by the number of events with magnitude M_w that occurred on the fault in the considered time interval, $n(M_w, t_1, t_2)$, and integration over all magnitudes yields

$$D_{seis}(t_1, t_2) = \int \frac{n(M_w, t_1, t_2)}{N_0(M_w)} D(M_w) dM_w. \tag{4.4}$$

The values $n(M_w, t_1, t_2)$, $N_0(M_w)$ and $D(M_w)$ can be estimated using empirical relations like the Gutenberg-Richter relation and empirical relations between magnitude, source area and average slip (e.g. Wells and Coppersmith, 1994). This estimate of $D_{seis}(t_1, t_2)$ using eq. (4.4) represents an upper bound for the cumulative seismic slip because not all events listed in a catalogue for a given fault occur directly on the fault and the source mechanisms of the individual events are very likely to vary. That means the contribution of a single event to the cumulative seismic slip might be smaller than $\frac{a(M_w)}{A} D(M_w)$.

In the following an expression for $D_{seis}(t_1, t_2)$ is given using (1) magnitudes of events listed in a catalogue, (2) an estimate of the b-value of the MFD and (3) empirical relations relating rupture area and average slip of an event to its magnitude. The value of $n(M_w, t_1, t_2)$ can be estimated from the Gutenberg-Richter relation which is a measure for the cumulative number of events that can be expected above a certain magnitude M_w in a given region and time:

$$logN(M_w, t_1, t_2) = a - bM_w. \tag{4.5}$$

where M_w is the moment magnitude and N is the number of events larger or equal M_w. If a constant b-value is assumed for the entire magnitude range, i.e. a rupture surface in critical condition (Main, 1987), and a maximum moment magnitude M_{wmax} for the considered seismogenic contact given by the extent of the largest fault area that can be ruptured in a single event eq. (4.5) can be rewritten in terms of the largest observed event, i.e. $logN(M_w, t_1, t_2) = 0$ for $M_w = M_{wmax}$:

$$logN(M_w, t_1, t_2) = b(M_{wmax} - M_w). \tag{4.6}$$

Eq. (4.6) can also easily be adjusted to account for a completeness threshold in a given seismicity catalogue. In this case $logN(M_{wc}, t_1, t_2) = logN_c(t_1, t_2)$ for $M_w = M_{wc}$, with M_{wc} the magnitude of completeness for the seismicity catalogue in the time interval (t_1, t_2) and $N_c(t_1, t_2)$ the number of events with magnitudes equal or larger than M_{wc}. For events smaller than M_{wc} this leads to the equation:

$$logN(M_w, t_1, t_2) = logN_c(t_1, t_2) + b(M_{wc} - M_w). \qquad (4.7)$$

Contributions by events with magnitudes equal or larger than M_{wc} are then expressed by summation over these events.

The absolute number of events within a magnitude range dM_w and time interval (t_1, t_2), $N(M_w, M_w + dM_w, t_1, t_2)$, is given by $-N(M_w + dM_w, t_1, t_2) + N(M_w, t_1, t_2)$. If the cumulative number of earthquakes is regarded as a continuous variable, its density function $n(M_w, t_1, t_2)$ is given as the negative derivative of the cumulative distribution $N(M_w, t_1, t_2)$ in eqs. (4.6) or (4.7) where the minus sign is due to the negative slope of the cumulative distribution:

$$n(M_w, t_1, t_2) = -\frac{dN(M_w, t_1, t_2)}{dM_w}. \qquad (4.8)$$

This density function can be obtained by differentiating the expression for $N(M_w, t_1, t_2)$ given in (4.6). If this function is scaled with respect to the considered area of the fault A and the desired duration of the time interval (t_1, t_2) for which we want to estimate the cumulative slip we get:

$$n(M_w, t_1, t_2) = \frac{b \ ln(10) \ 10^{b(M_{wmax} - M_w)}A \ (t_2 - t_1)}{A' \ (t_4 - t_3)}. \qquad (4.9)$$

In this equation A' and the time interval (t_3, t_4) indicate the area and the time interval spanned by the catalogue. Because the study region in the following is given by the extent of the rupture area A of the largest event, A' equals A. If the catalogue covers the time interval (t_1, t_2), t_3 and t_4 are equal to t_1 and t_2, respectively. In case of an earthquake catalogue with known completeness magnitude, the event density function for events below this completeness magnitude M_{wc} can be obtained from eq. (4.7) assuming a constant b-value as:

$$n(M_w, t_1, t_2) = \frac{b \ ln(10) \ 10^{log(N_c(t_3, t_4)) + b(M_{wc} - M_w)}A \ (t_2 - t_1)}{A' \ (t_4 - t_3)}. \qquad (4.10)$$

The last two eqs. assume a b-value that is constant over the whole magnitude range and that does not change in time. While this assumption is used for the rest of this study it is possible to account for a temporally varying b-value by splitting the catalogue into smaller subsections with constant b-values and then summing over these subsections. A

change in the b-value between different magnitude ranges can be accounted for by a piecewise integration of eq. (4.4) using the linear parts of the MFD utilizing eq. (4.10) with appropriate values of $log(N_c)$.

The contribution of all these events to the seismic slip $D_{seis}(t_1, t_2)$ is magnitude dependent and given by empirical relations for $D(M_w)$ and $a(M_w)$. Those empirical relations were derived by Wells and Coppersmith (1994) by applying a linear regression to events of different faulting type (normal, reverse, strike-slip). For reverse faulting events the formula connecting the rupture area $a(M_w)$ of an event to its moment magnitude M_w is given by

$$log(a(M_w)) = -3.99 + 0.98 \, M_w. \tag{4.11}$$

However, they had only insufficient data to derive also the regression coefficients for the slip - magnitude relationship with sufficient accuracy. A slip - magnitude relationship can be estimated by combining the formula for the scalar seismic moment M_0 (Kostrov, 1974)

$$M_0 = \mu \, a(M_w) \, D(M_w), \tag{4.12}$$

where μ is the shear modulus at the rupture surface and $a(M_w)$ given by (4.11) with the definition of the moment magnitude as derived by Kanamori (1977):

$$M_w = \left(\frac{logM_0}{1.5} \right) - 10.73 \, . \tag{4.13}$$

By replacing M_0 in (4.12) with the expression for M_0 from (4.13) and $a(M_w)$ with the corresponding expression in (4.11) we obtain a function relating the average displacement $D(M_w)$ to the moment magnitude M_w:

$$logD(M_w) = 0.52M_w - log(\mu) + 10.09 \, . \tag{4.14}$$

This result which gives the average displacement in cm when the shear modulus μ is given in $dyne/cm^2$ as well as the relationship combining moment magnitude and rupture area is plotted in Fig. 4.4. For the shear modulus a value of $3.3 * 10^{11} dyne/cm^2$ is assumed throughout this study. Also shown are results derived by Papazachos (1989) for 14 events in the Aegean region.

After deriving the relation for $D(M_w)$ we have everything in place to estimate the seismic slip according to eq. (4.4). Substituting A in eq. (4.9) by $N_0(M_w)a(M_w)$, the number of events with magnitude M_w needed to rupture the considered fault area A, and using this new expression for $n(M_w)$ in eq. (4.4) yields:

$$D_{seis}(t_1, t_2) = \int\limits_{M_{wmin}}^{M_{wmax}} D(M_w) \frac{b \, ln(10) \, 10^{b(M_{wmax} - M_w)}(t_2 - t_1) \, a(M_w)}{A'(t_4 - t_3)} dM_w. \tag{4.15}$$
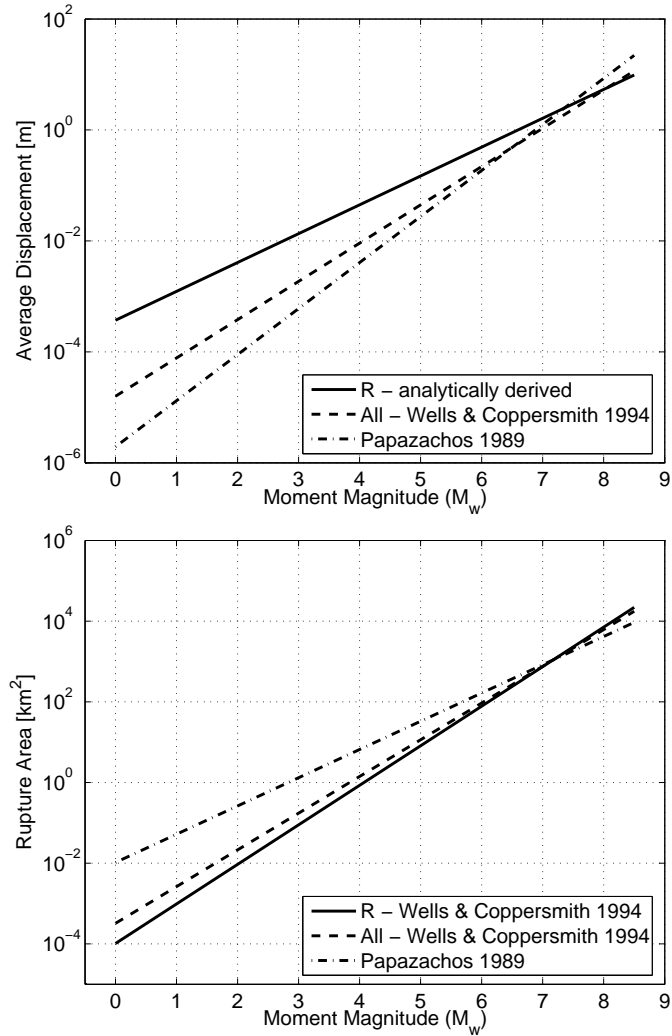
Figure 4.4: Relationships linking the moment magnitude of a seismic event M_w with the average displacement on the rupture surface (top) and the rupture area of the event (bottom), respectively. 'R' indicates that the parameters of the relationships were derived exclusively from reverse faulting events. 'All' indicates that also normal faulting and strike-slip events were used. The relations obtained by Papazachos also include events of all faulting types.

For a seismicity catalogue with known magnitude of completeness the maximum cumulative seismic slip $D_{seis}(t_1, t_2)$ can be calculated by a summation over all events equal or greater than M_{wc}, the completeness magnitude, and an integration over smaller events by extrapolating the MFD towards smaller magnitudes:

$$D_{seis}(t_1, t_2) = \sum_{i=1}^{N_c(t_3, t_4)} \frac{D(M_w) a(M_w)(t_2 - t_1)}{A'(t_4 - t_3)} +$$

$$\int_{M_{wmin}}^{M_{wc}} D(M_w) \frac{b \, ln(10) 10^{log(N_c(t_3, t_4)) + b(M_{wc} - M_w)}(t_2 - t_1) \, a(M_w)}{A'(t_4 - t_3)} dM_w. \quad (4.16)$$

It is often observed that large events are more scarce than expected from the extrapolation of MFDs obtained for medium sized events to large events (e.g. Ambraseys, 2006; Main, 1995). This can be explained by the fact that a finite maximum magnitude introduces a roll-off towards the largest magnitudes when considering the cumulative frequency magnitude distribution (Main, 1995). An apparent lack of large magnitudes is also observed in the frequency-magnitude distribution when this distribution was obtained by summing over multiple seismogenic sources each with a different maximum magnitude given by the geometrical constraints of that source (e.g. Papazachos, 1999). This may lead to an underestimation of the maximum cumulative seismic slip when eq. (4.15) is applied to a catalogue time span longer than the return period of the maximum event as determined from the linear part of the frequency-magnitude distribution. This underestimation is avoided by using eq. (4.16) when M_{wc} is lower than the magnitude were the roll-off in the cumulative frequency-magnitude distribution occurs.

Throughout this study a value of $M_{wmin} = -1$ for the lower limit of integration is adopted because for smaller values of M_w the distinction between seismic and aseismic slip is no longer possible. Furthermore, $M_w = -1$ is often of the order of the smallest events observed in microseismicity studies. Everything below this value is treated as aseismic slip. Eqs. (4.15,4.16) can be used in eq. (4.3) to calculate the maximum seismic coupling $\nu(t_1, t_2)$ provided that an estimate for $D_{total}(t_1, t_2)$ is given. In the following, the maximum cumulative slip of the plate contact in the source region of the 365 AD event south of western Crete is estimated. However, eqs. (4.15) and (4.16) may also be applied to well defined transform or strike slip faults.

4.3.1 Sensitivity of the maximum cumulative slip on the parameter choice

Figs. 4.5 and 4.6 show how the seismic coupling calculated with eq. (4.15) for the rupture area of the Crete 365 AD event depends on the b-value for different maximum moment magnitudes and different observation periods assuming a constant b-value over the whole magnitude range and observation period. The cumulative seismic slip was calculated using the relationships shown in Fig. 4.4 for reverse faulting events from Wells and Coppersmith (1994) and the relationships derived by Papazachos (1989), respectively. The different scaling factors of the slip-magnitude and rupture area- magnitude relations produce considerably different results especially when considering different maximum magnitudes because the scaling laws derived by Papazachos (1989) have very large average displacements and rather small rupture areas when extrapolated to large magnitudes (Fig. 4.4). Thus the relationship by Wells and Coppersmith between rupture area and moment magnitude which was derived for large reverse faulting events and the relationship between average displacement and moment magnitude derived above by incorporting empirical formulae seem to produce better results for large thrust events.

For b-values smaller than 1 the ratio increases only modestly with b while for larger values of b we observe a strong increase in the seismic coupling. At a b-value of 1.5 the contribution of all magnitudes to the total slip would be equal while for smaller b values the contribution of large magnitudes is dominant and for b-values larger than 1.5 the contribution of small events dominates because the integrand in eqs. (4.15, 4.16) goes to infinity for a b-value larger than 1.5 when $M_w \rightarrow -\infty$ while the integrand is independent of M_w for $b = 1.5$. The quantitative behaviour of the integrand of eq. (4.15) is depicted in Fig. 4.7 for different values of b. However, b-values equal or larger than 1.5 are not physically feasible for the complete magnitude range because they would allow an infinite accumulation of slip for small magnitudes (Molnar, 1979). There are several studies dealing with the determination of the b-value in the area of western Crete and the western Hellenic Arc (e.g. Hatzidimitriou et al., 1985; Papazachos, 1999; Manakou and Tsapanos, 2000; Papaioannou and Papazachos, 2000) based on a combination of historic and instrumental data. When smoothed over the whole rupture area these values vary between 0.9 and 1.1 with peak values of more than 1.2 in smaller subregions (Manakou and Tsapanos, 2000). B-values towards central and eastern Crete (Papazachos, 1999; Manakou and Tsapanos, 2000) generally tend to be slightly higher than in the west. Taking a b-value of 1.1 or, more conservatively, 1.2 as upper bound seems to be a good choice to calculate the maximum cumulative seismic slip.

Figure 4.5: Top: Seismic slip ratio calculated for different observation intervals assuming a maximum event of $M_w = 8.3$ and a relative plate motion of $4 \, \text{cm/a}$ using the relationship for the average displacement derived above and the Wells and Coppersmith relationship for rupture area and moment magnitude. Bottom: Seismic slip ratio calculated for maximum events between $M_w = 8.1$ and $M_w = 8.5$ assuming an observation period of $2000 \, \text{years}$ during which one maximum event occurred and a relative plate motion of $4 \, \text{cm/a}$ using using the same relationships as in the upper figure.
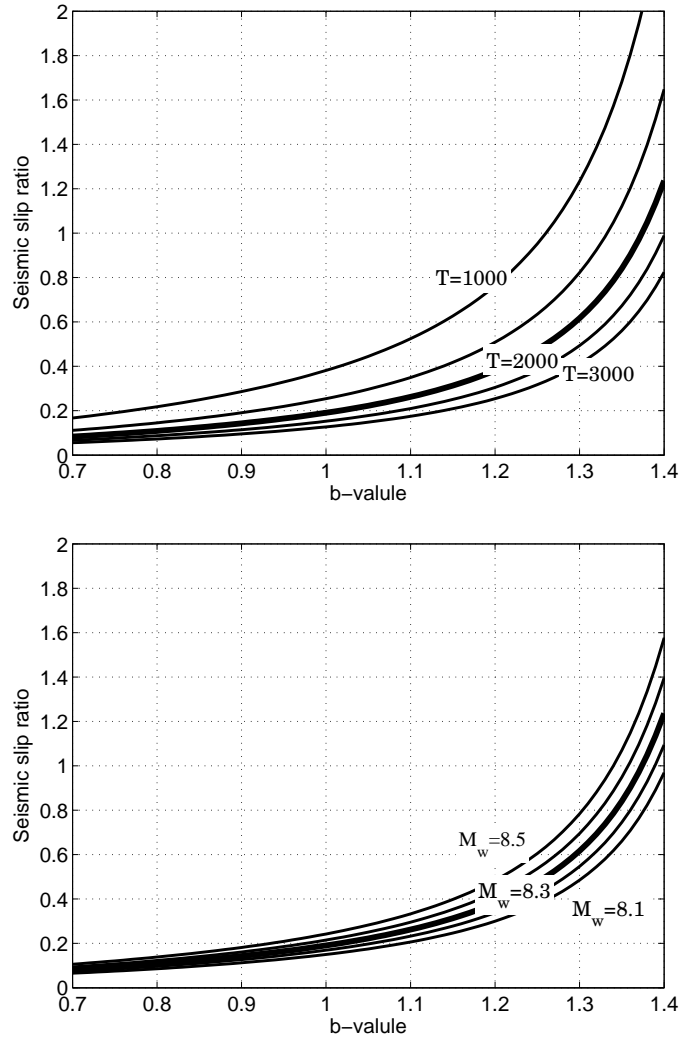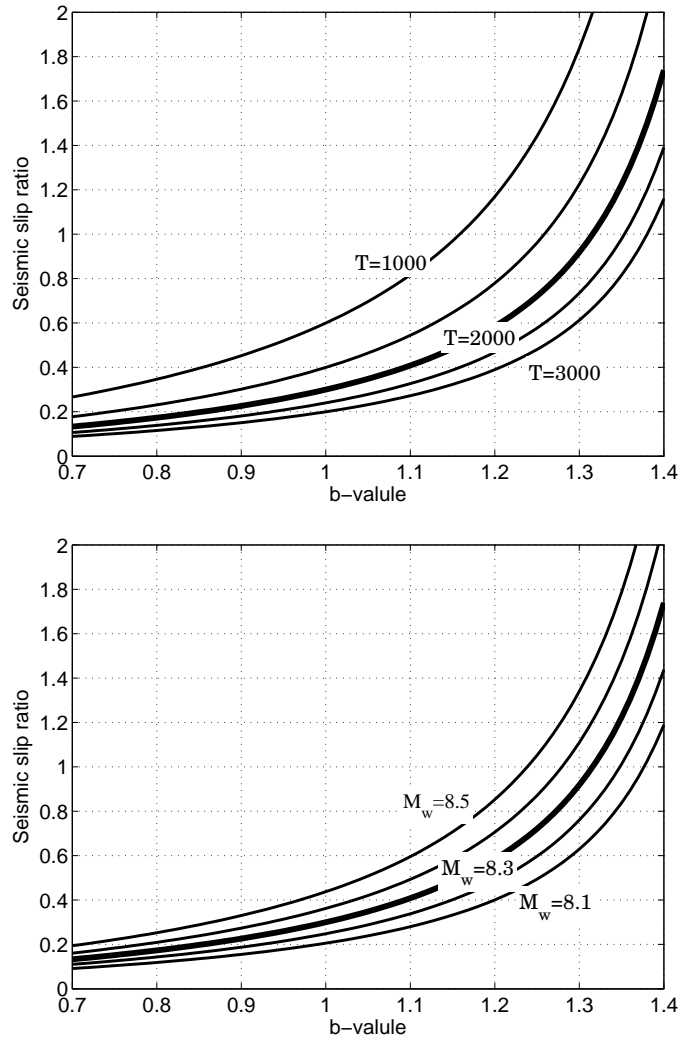
Figure 4.6: Top: Seismic slip ratio calculated for different observation intervals assuming a maximum event of $M_w = 8.3$ and a relative plate motion of $4\,\text{cm/a}$ using the empirically derived relationships between average displacement and moment magnitude and rupture area and moment magnitude, respectively, as given by Papazachos (1989). Bottom: Seismic slip ratio calculated for maximum events between $M_w = 8.1$ and $M_w = 8.5$ assuming an observation period of $2000\,\text{years}$ during which one maximum event occurred and a relative plate motion of $4\,\text{cm/a}$ using using the same relationships as in the upper figure.
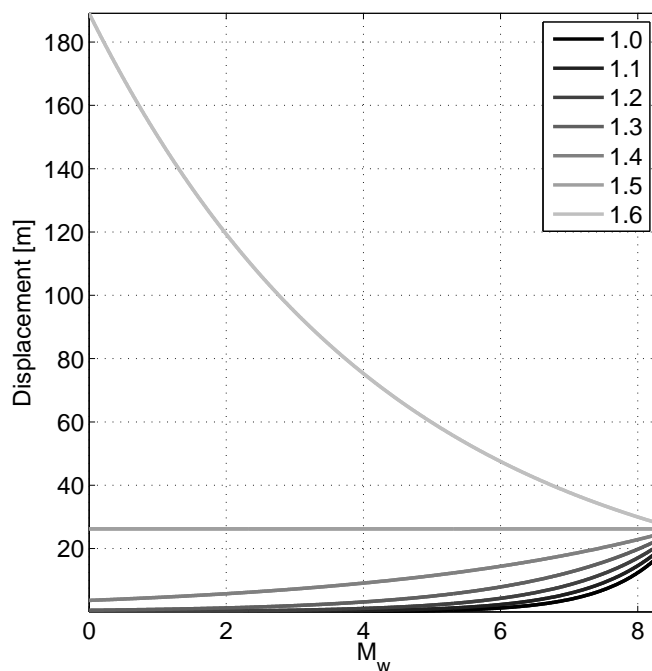
Figure 4.7: Dependance of the integrand in eq. (14) on the b-value. For a b-value of 1.5 all magnitudes contribute equally to the cumulative seismic slip while for smaller b-values the influence of larger events dominates and for b-values larger than 1.5 small events dominate the cumulative seismic slip budget. The example is calculated for an $M_w = 8.3$ event and an observation interval of 2000 years.

In this study a constant b-value for the whole magnitude spectrum and observation time is assumed. Although it is well known that small scale spatial changes of the b-value exist which may help in locating the nucleation point of future major events (e.g. Wyss and Stefansson, 2006; Wiemer and Wyss, 2002) it was shown for the Parkfield region that these b-values are generally constant in time (Schorlemmer et al., 2004). B-values calculated for the western part of the HSZ using different time intervals also show similar values (e.g. Papazachos, 1999; Manakou and Tsapanos, 2000; Papaioannou and Papazachos, 2000Papaioannou und Papazachos (2000); Koravos et al., 2003) between 0.9 and 1.1. Also the b-values for the time spans 1910-1999 and 1964-1998 calculated in this study (Figs. 4.9 and 4.10) show similar values and thus support the idea of a temporally constant b-value. A b-value change below the completeness threshold of the used catalogue (either historic or instrumental) can not be ruled out. However, Abercombie and Brune (1994) compared microseismicity catalogues in California which are complete above $M0$ with network cat-

alogues covering the magnitude range $M3 - 6$ and found a constant b-value for the whole magnitude range above $M0$. Because large b-values for small magnitudes have the potential to compensate for a seismic slip deficit found when only considering major events, the b-value on the plate contact south-west of Crete is calculated from microseismicity data. Fig. 4.8 shows results from a microseismicity survey conducted on the island of Gavdos during May 1999 - August 1999. As can be seen in Fig. 4.8b, most of the seismicity locates close to the plate contact. The b-value for events with $M0.3 - 3.5$ is 0.92 and thus not significantly different from those found for the instrumental seismicity with magnitudes up to $M_w6.5$ (Fig. 4.9). Although this data only spans a few months and covers only a portion of the seismically active plate contact it further supports the results obtained from historic and instrumental catalogues.

4.4 Estimation of the maximum cumulative seismic slip in the source region of the 365 AD event

4.4.1 The 365 AD event and relative motion at the plate contact

The largest seismic event in the HSZ in historic times is the Crete 365 AD event (Papazachos et al., 2000; Stiros, 2001). This event presumably ruptured the shallow plate interface between the Aegean-Anatolian and African plate south-west of Crete (Papazachos, 1996). The moment magnitude of this event was determined by Papazachos and Papazachou (1997) as 8.2 from macroseismic intensity data in the city of Gortyn on Crete (Vita, 1996). When calculating the moment magnitude incorporating information about the presumed fault length of $300\,\text{km}$, Papazachos (1996) proposed a magnitude of 8.5. Consequently, the adopted value for this event is $M_w = 8.3 \pm 0.2$. The 365 AD event is an order of magnitude larger than the second largest event observed in the shallow seismicity in that region ($M_w7.3$ event in March 1630 at 35.0°N - 23.7°E; Papazachos et al., 2000) dominating the energy release over the last 2000 years in the whole southern Aegean (see Fig. 4.2). This shows that the $M_w8.3$ event of 365 AD is an exceptional event for the whole region. Studies of ancient shorelines (Pirazzoli et al., 1982; Pirazzoli et al., 1996; Stiros and Jones, 1996) on the islands of Crete and Antikythira show an uplift of up to $9\,\text{m}$ on western Crete which is linked to the 365 AD event. However, it is not possible to determine whether the whole slip was accomodated as seismic slip during the event or whether a portion of it was accomodated aseismically, either coseismically or as afterslip.
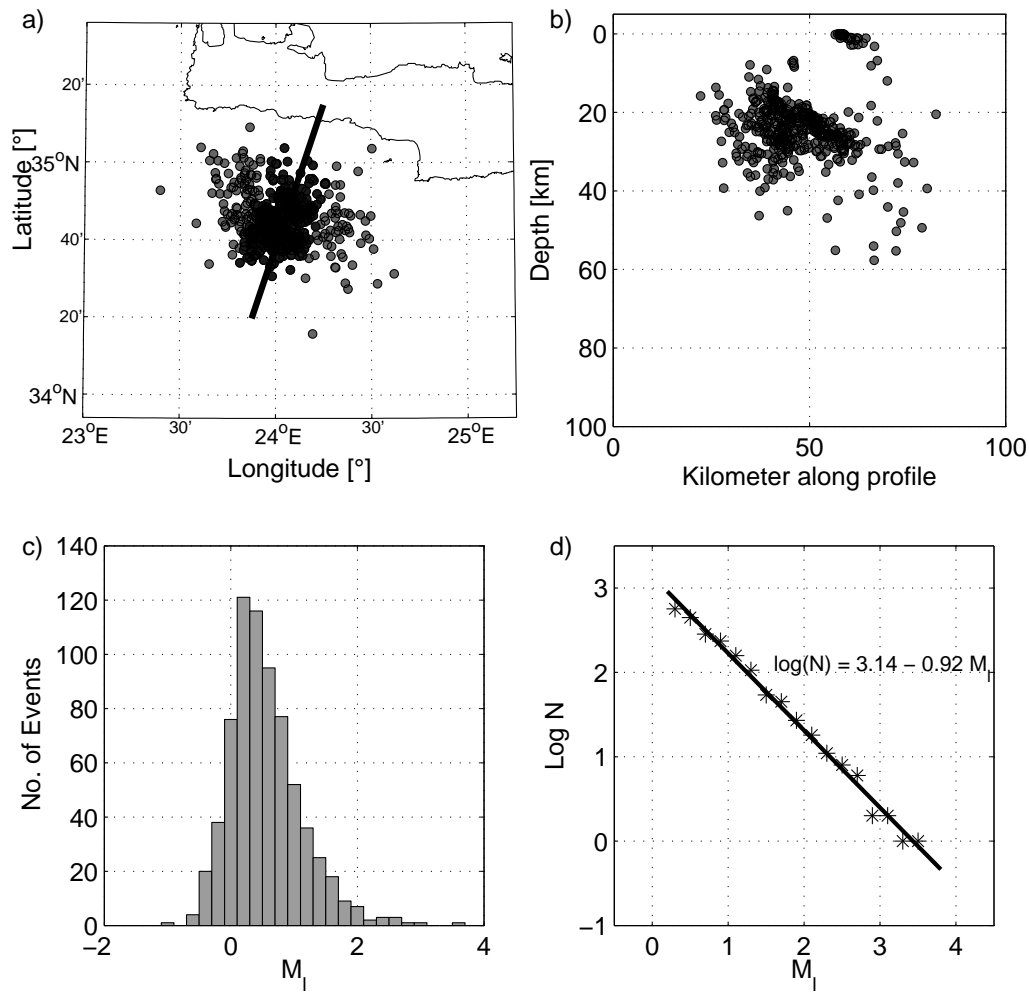
Figure 4.8: Microseismicity observed in the vicinity of the island of Gavdos during May 1999 - August 1999. a) Mapview of the located seismicity. b) Cross-section along the profile indicated in a) by the solid line. c) Histogram of the magnitude distribution. d) Fit of the Gutenberg-Richter relation to the data.

Furthermore, besides the plate contact normal faults along the southern and western coast of Crete may have been seismically active during the 365 AD event.

Following the ancient shorelines further into the past a stepwise subsidence of these marine marks in the time 4000-1700 BP reaching a cumulative value of approximately 1.5 m was observed (Pirazzoli et al., 1982Pirazzoli et al. (1982); Pirazzoli et al., 1996). This behaviour might be explained by a locked plate contact dragging down the continental Aegean-Anatolian plate. The absence of large events with $M_w \geq 7.0$ during the last 200 years, especially when compared with the increased seismic energy release in the years 1600-1800 (Fig. 4.9) is a further indication for a temporal variability of the seismic energy release.

The relative motion at the plate contact can be estimated from recent GPS measurements in the Eastern Mediterranean. In the southern Aegean region, average GPS velocities for the time interval 1988-1998 agree reasonably well with tectonic deformation rates inferred from geology (e.g. Ward, 1990; DeMets et al., 1994; Argus and Heflin, 1995). The current south-westward motion of 35 mm/a obtained for the Aegean-Anatolian plate from GPS measurements (e.g. Cocard et al., 1999; Kahle et al., 2000; McClusky et al., 2000) correlates well with the 350-500 km of south-westward motion of the island over the last approximately 10 Ma as obtained from tectonic reconstructions (tenVeen and Kleinspehn, 2003). Thus, it seems reasonable to use this GPS plate velocity determined during a rather short time period of several years as the average plate velocity for much longer time periods of thousands of years. Data for the African plate which are much more scarce when compared to the Aegean-Anatolian plate indicate a roughly north-north-westward motion of 6 mm/a which is in agreement with plate tectonic models (e.g. Argus et al., 1998) for the region predicting a couterclockwise rotation of Africa around a Euler pole at 21.4°N, 20.5°W with an angular velocity of $0.104° Myr^{-1}$. The movement of the Aegean plate on the other hand can be described by a counterclockwise rotation around an Euler pole located in northern Egypt with an angular velocity of $2.4° Myr^{-1}$ (LePichon et al., 1995; Reilinger et al., 1997). Thus $\bar{v}_{total}(t_1, t_2)$ (the average relative velocity between the plates at the interface) is taken to be on the order of 4 cm/a.

The rupture surface A is given by the rupture area of the assumed maximum event and is estimated by eq. (4.11) or the equivalent formula from Papazachos (1989). For a presumed fault length of 300 km this requires a rupture width of approximately 50 km. The arc-normal width of the seismogenic zone at the plate contact as given by global seismicity observations and local microseismicity studies, however, for this region (Fig. 4.3) is roughly twice that value.

4.4.2 Maximum seismic slip obtained from 2000 years of historic seismicity

The most complete historic catalogue for the Aegean region was compiled by Papazachos et. al (2000) for the period 550 BC until 1999 AD. The completeness magnitude of this catalogue is given as $M_w 8.0$ for the whole observation time. Thus it seems unlikely that any larger event than the 365 AD event south-west of Crete occurred in this region within the last 2000 years. Thus, this $M_w 8.3$ event is adopted as the maximum magnitude event giving the rupture surface A for which $D_{seis}(t_1, t_2)$ is estimated.

The observation interval (t_1, t_2) for which $D_{seis}(t_1, t_2)$ is compared with $D_{total}(t_1, t_2)$ in the study region is given by the time interval of approximately 2000 years covered by the historic catalogue by Papazachos et al. (2000).

Using a b-value of 1.2 as well as an M_{wmax} of 8.5 in eq. (4.15) and the expressions for $D(M_w)$ and $a(M_w)$ as given in eqs. 4.9 and 4.12, respectively, generates a maximum cumulative seismic slip of approximately 39 m for a 2000 year interval. Compared to the 80 m expected from GPS measurements there is a considerable lack of seismic slip on the rupture surface of the 365 AD event even for this very conservative parameter estimation. Taking the relationships derived by Papazachos (1989) for the same parameter values yields a cumulative seismic slip of 68 m which is still smaller than but comparable to the geodetic data. However, this larger value reflects the large average displacements and small rupture areas obtained for large events using the relations of Papazachos (1989). Taking the best guess for the b-value in the area of the 365 AD event of 1.1 and the most likely magnitude of $M_w 8.3$ and the observation time of 2000 years given by the historic catalogue, both relations produce similar results (Figs. 4.5, 4.6) with estimates of the maximum seismic slip of about 21.5 and 32 m. Thus, a seismic coupling coefficient of 0.27 and 0.4, respectively, is obtained from these two relations for the last 2000 years. Thus, despite the 365 AD event there is a considerable seismic slip deficit on the plate contact south-west of Crete in the last 2000 years.

4.4.3 Maximum seismic slip obtained from 500 years of historic seismicity

If the analysis of the historic catalogue is limited to the time interval 1500 - 1999 the 356 AD event is excluded and the completeness of the catalogue is increased. Eq. (4.16) can be applied to estimate the maximum cumulative seismic slip on the presumed rupture surface of the 365 AD event. When summing over the events with $M_w \geq M_{wc}$ in eq. (4.16)

it is assumed that all these events in the area of the 365 AD event locate at the plate contact and exhibit thrust-type focal mechanisms in agreement with the subduction of the African plate below the Aegean-Anatolian plate. Furthermore, the area from which events are considered for the slip calculation is larger than the presumed rupture area of the $M_w 8.3$ event in order to account for possible location uncertainties in the historic hypocenter determination. It is indicated by the dashed box in Fig. 4.11. This means that the estimate obtained by applying eq. (4.16) represents an upper bound of the cumulative seismic slip. A completeness magnitude, M_{wc}, of $M_w = 7.0$ seems to be a reasonable choice from inspection of the historic catalogue (see Fig. 4.9a). A b-value for this catalogue can be estimated from the time interval 1910-1999 (Fig. 4.9b) for which the catalogue is believed to be complete above $M_w 5.0$ (Papazachos et al., 2000). Using a b-value of 1.1 for the 500 year period from 1500 till 2000 together with $M_{wc} = 7.0$ and $N_c = 5$ in eq. (4.16) and summing over the five events with $M_w \geq 7.0$ and integrating over the smaller magnitudes yields a maximum cumulative seismic slip of 2 m. This is much less than the 20 m expected from the extrapolated GPS data for the same time interval. Even when we assume that larger magnitudes are less likely than expected from the frequency magnitude relation for smaller events and compensate for this effect by doubling the value of N_c in the integral part of eq. (4.16), the resultant maximum cumulative seismic slip of little more than 3 m is far short of the 20 m total slip estimated for this time span. Using the relationships of Papazachos (1989) the corresponding values are 3 m and 4.7 m, respectively. Thus, the seismic coupling coefficient for this time span is of the order of 0.1 - 0.25.

4.4.4 Maximum seismic slip obtained from 34 years of instrumental seismicity

In order to study a time span which has the same order of magnitude as the GPS observation period and which also overlaps with a GPS observation campaign, the instrumental seismicity of the plate contact in the area of the 365 AD during the time period 1964-1998 is studied. Fig. 4.10a shows the MFD for the ISC catalogue of global seismicity (Engdahl et al., 1998) for this time interval in the area of the 365 AD rupture surface. Magnitudes in this catalogue are given in m_b and in order to calculate the corresponding moment magnitudes, M_w, the fomula $M_w = 1.28 m_b - 1.12$ derived by Papazachos (1997) for earthquakes in Greece was used. Because this relation only holds for events with $4.8 \leq m_b \leq 6.0$ only events with $m_b \geq 4.8$ are considered. Because the largest events in the ISC catalogue are $m_b 5.9$ events there is no problem with the upper limit of this relation. Thus, the investigation of the ISC catalogue is restricted to events with $M_w \geq 5.0$. The b-value calculated

from the moment magnitudes of these events is 1.04 (Fig. 4.10b). When calculating the maximum cumulative seismic slip on the presumed rupture surface of the 365 AD event using eq. (4.16) with a b-value of 1.1 for the events in the ISC catalogue we obtain a value of 11 cm. The total slip expected from geodetic measurements performed during the last 10 years of the observation period (1988-1998) is approximately 136 cm for 34 years. This leads to a seismic coupling coefficient of less than 0.1. We end up with similar results of slightly more than 0.1 for the seismic coupling coefficient when using the formulae given by Papazachos (1989). This means that while considerable relative motion was observed at the earths surface the observed seismic activity at the plate contact can account only for a small fraction of this motion.

4.5 Spatio-temporal seismicity variability in the area of the 365 AD event

Based on the ISC catalogue for 1964-1998 (Engdahl et al., 1998), the spatio-temporal distribution of events with magnitudes about $M_w 4.5$ and larger may be investigated. Fig. 4.11a shows a map view of the seismic activity in the vicinity of the rupture area of the Crete 365 AD event. As can be seen from Fig. 4.3 most of these events are close to the plate interface. The location uncertainty is of the order of 10 - 20 km and due to the application of a global velocity model depths are biased. Thus, most interplate activity locates below the presumed plate contact in the subducting slab. Interestingly, seismic activity is higher south of Crete compared to the region between Crete and the Peloponnese.

It is obvious that the presumed epicenter of the Crete 365 AD event is located in a region of elevated seismic activity when compared to the region to the north-west between Crete and the Peloponnese. This cannot be explained by regional differences of the detection threshold because Figs. 4.11c and d show that we have a deficit of large events towards the north-west of the 365 AD epicenter while smaller events are present in that region. Further high seismic activity is observed approximately 80 km to the south-east of the 365 AD epicenter originating from an active zone striking perpendicular to the trench axis. These observations are supported by Fig. 4.11d which shows the cumulative energy release calculated for parallel boxes of 20 km width oriented perpendicular to the line in Fig. 4.11a. The boxes are spanning the whole extent of the dashed region in Fig. 4.11a. The larger extent of the box when compared to the presumed rupture surface was chosen
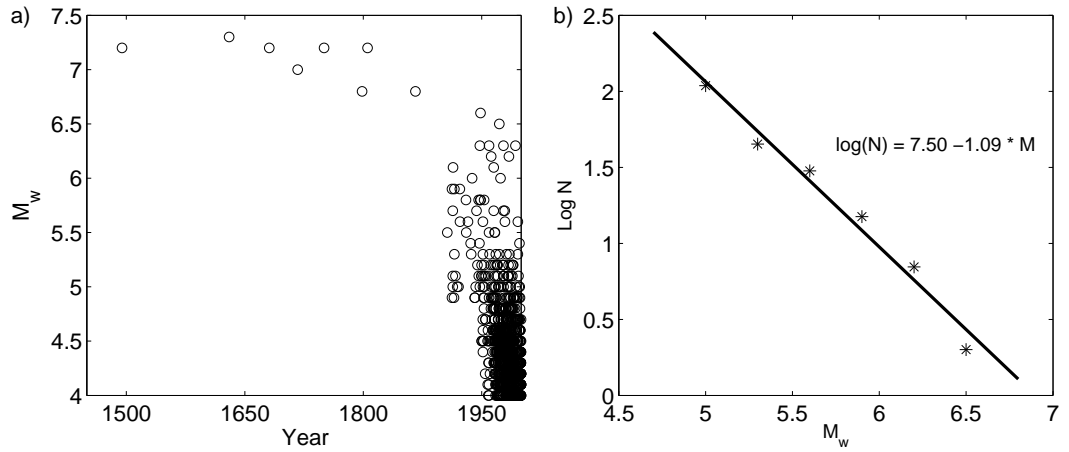
Figure 4.9: Historic seismicity in the area of the 365 AD event during the last 500 years. a) Magnitude-time plot of the seismic activity as given by the catalogue by Papazachos et al. (2000). b) b-value obtained from the time period 1910-1999 assuming a completeness magnitude of $M_w 5.0$.

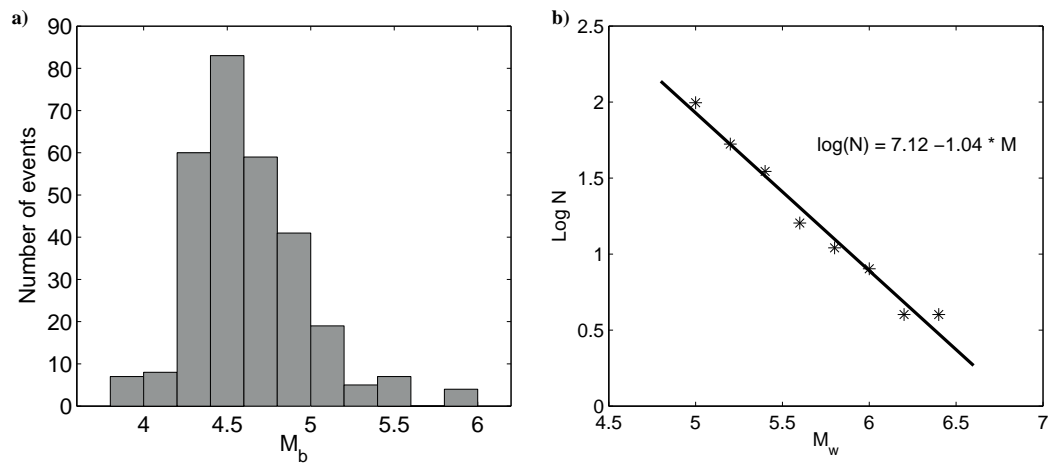

Figure 4.10: a) Magnitude-frequency distribution of the seismic activiy in the area of the 365 AD event during the time interval 1964-1998 as given by the ISC catalogue (Engdahl et al. (1998)). b) Determination of the b-value for this catalogue after conversion of the magnitude scale from m_b to M_w.
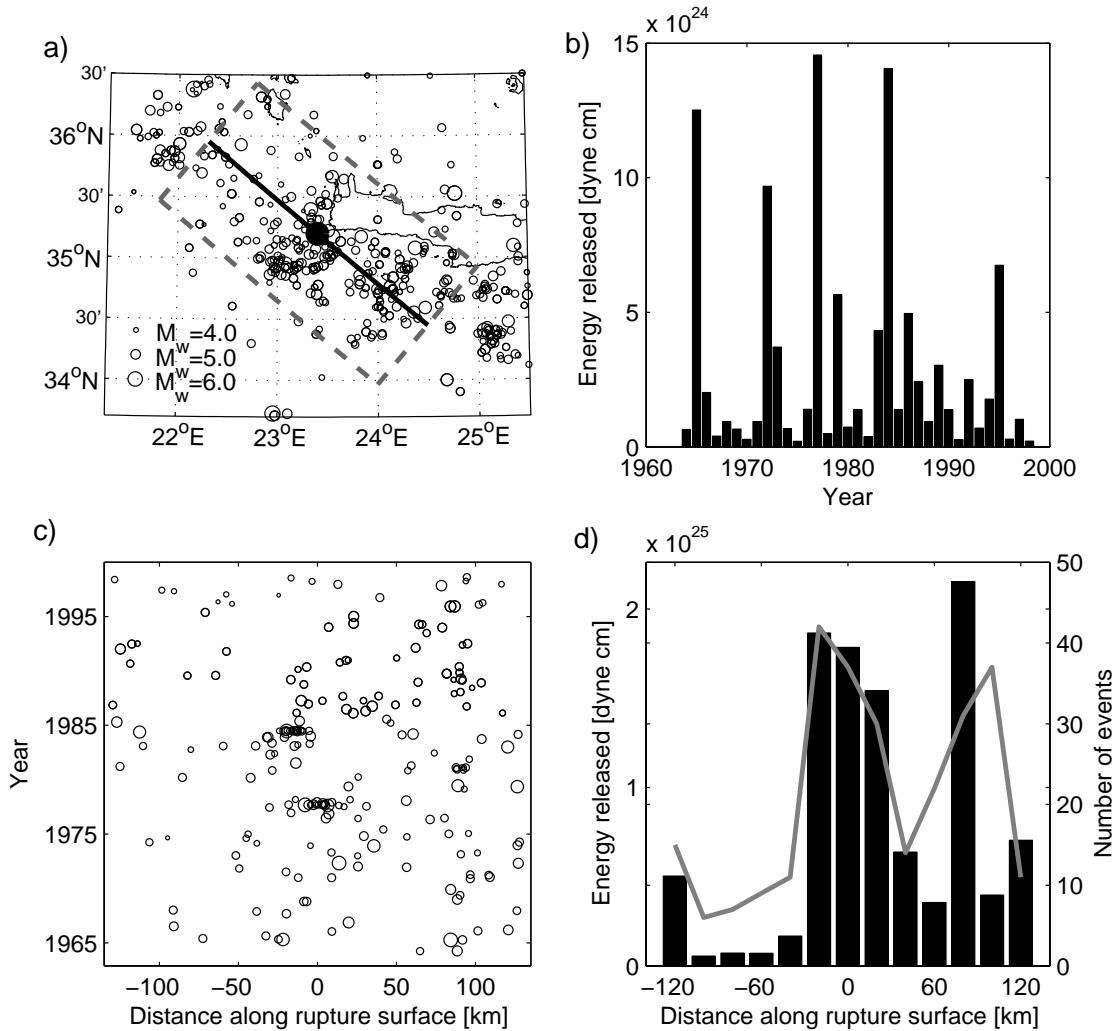
Figure 4.11: Seismic activity in the area of the Crete 365 AD event as observed by the global ISC catalog for 1964-1998. a) Mapview of the seismic activity. Black dot marks the center of the surface projection of the presumed rupture of the Crete 365 AD event which is indicated by the dashed box. Solid black line indicates strike of the rupture surface which was used for the projection in figure c). b) Annual seismic energy release in the area of the Crete 365 AD event. c) Projection of seismic events on the profile indicated in a) by the solid black line. d) Seismic energy release along the strike of the rupture surface indicated by the solid black line in a). Centre of projection corresponds to solid black dot in a).

in order to account for uncertainties in the determination of the rupture surface as well as possible location errors of the events. It is further assumed that every event contributes only to the energy release in the box containing its epicentre. This approach does not take into account possible location uncertainties or the finite extent of the rupture surface. However location uncertainty is of the order of 15 km and the rupture length of the largest event ($M_w 6.3$) is approximately 20 km (Wells and Coppersmith, 1994), thus, Fig. 4.11d can be regarded as a good approximation of the energy release for the period 1964-1998 in the vicinity of the rupture surface of the Crete 365 AD event. In agreement with Fig. 4.11a most energy is released at the centre of the profile and towards the south-east while the north-western part of the presumed rupture area exhibits an energy release which is an order of magnitude smaller. Because the velocity field of the Aegean lithosphere as calculated from GPS studies in the region (e.g. Cocard et al., 1999; Kahle et al., 2000; McClusky et al., 2000) appears homogeneous and thus does not indicate seismically locked zones, the above described behaviour hints at a spatial variability of the seismic coupling in this area or the events are located on an arc-normal fault within the overriding Aegean or the subducting African plate.

Fig 4.11b shows the annual energy release of all events contained within the dashed box shown in Fig. 4.11a. It is apparent that the energy release is not dominated by a single large event but more or less constant when averaged over a time period of 10 years or more. The nearly periodic recurrence of large events between 1965 and 1984 is not observed for the first 60 years of the last century when studying this time span in the Papazachos catalogue (see also Fig. 4.9a). Thus, this behaviour cannot be interpreted in terms of return periods especially when taking into account the large spatial separation of some of the individual events. Fig. 4.11c shows a time-plot of seismic activity projected on a line following the strike of the Ionian trench and approximating the lateral extent of the rupture surface of the Crete 365 AD event as given by Papazachos (2000). There is an obvious clustering of seismic activity close to the centre of the profile in the years 1977 and 1984 formed by the aftershock sequences of two $M_w 6.3$ events. The plot also indicates the absence of large seismically inactive zones that could hint at locked zones. The more or less temporally randomly and evenly distributed seismic activity in this time-plot hints at a currently conditionally stable and a steady state behaviour of the plate contact. That means randomly distributed subregions of the plate contact might be locked, accumulating strain that is released in moderate size earthquakes without complete failure of the entire rupture area of the 365 event.

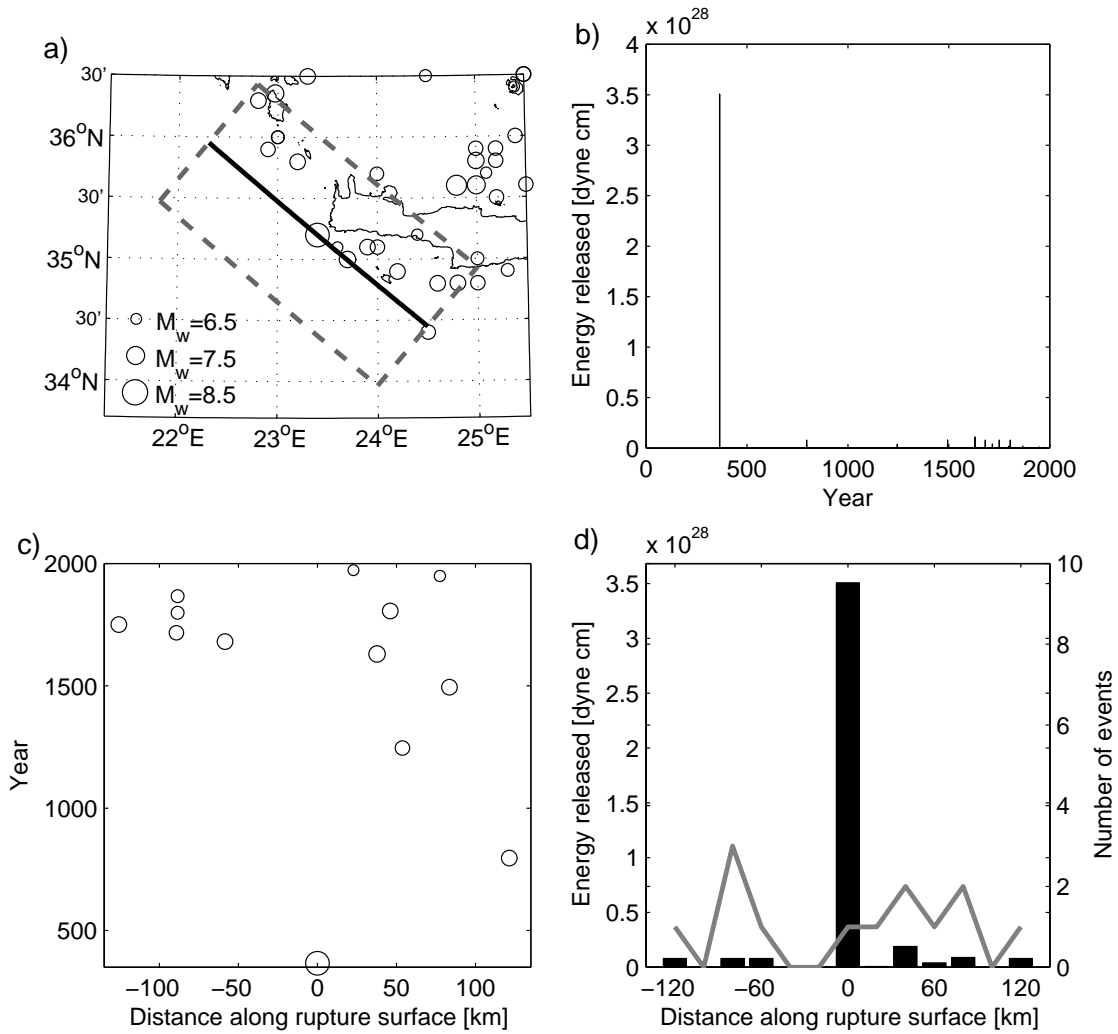For completeness, the study is extended to include all known historical earthquakes with

Figure 4.12: Historic seismic activity with $M_w \geq 6.5$ in the area of the Crete 365 AD event between 550 BC and 1999 AD as given by Papazachos et al. (2000). Same conventions as Fig. 4.11.

a magnitude of $M_w \geq 6.5$ (Fig. 4.12). However, the completness might vary spatially and the localization accuracy is only of the order of 50-100 km for most of the historical activity. As can be seen from Fig. 4.12 the catalogue in the western part only contains events after the beginning of the 18th century and thus activity prior to this date may fall below the detection threshold. We still observe a larger energy release towards the south-east of the 365 AD epicentre than towards the north-west compatible with the results mentioned above. However, the HSZ between the western coast of Crete and the Peloponnese also produced events with magnitudes larger $M_w 7.0$ in historic times (Fig. 4.12). This as well as the temporal distribution of large events during the last 500 years (Fig. 4.9a) indicates a temporal variability in the seismic energy release when considering longer time spans of hundreds or even thousands of year. Whether the absence of events with $M_w \geq 6.5$ for the last 500 years in the vicinity of the 365 AD epicentre 4.12c is real or caused by mislocated or missing historical events cannot be resolved.

4.6 Discussion

In this study a formula to calculate the maximum cumulative seismic slip on a rupture surface is derived and applied to the plate contact in the region of the Crete 365 AD $M_w 8.3$ event. For different time spans of 34, 500 and 2000 years covered by historic and instrumental catalogues the maximum cumulative seismic slip is estimated and a significant seismic slip deficit is found when the seismic slip is compared to the average relative plate motion. Table 4.1 summarizes the inferred seismic slip and seismic coupling obtained in this study for the respective time intervals. The results are in general agreement with studies using moment summation methods to calculate the moment release (e.g. North, 1974; Papadopoulos, 1989) or the rates of seismic deformation (e.g. Papazachos et al., 1992; Jenny et al., 2004) which found a deficit for the seismic moment release in the southern Aegean. To address possible uncertainties in case of an observed seismic slip deficit it is necessary to estimate the maximum possible seismic slip and the minimum total slip. As far as the seismic slip is concerned it may be underestimated by the omission of events in the used catalogues, the underestimation of magnitudes of listed events or the use of an underestimated b-value. It is very unlikely that any event with a magnitude of $M_w 8.0$ or larger was missed during the last 2000 years in the area of Crete given the rather complete historic reporting in this area of the Mediterranean, the tradition of archaeoseismology (e.g. Stiros

Time-interval (t_1, t_2)	$D_{seis}(t_1, t_2)$	$\bar{v}_{seis}(t_1, t_2)$	$D_{total}(t_1, t_2)$	$\bar{v}_{total}(t_1, t_2)$	$\nu(t_1, t_2)$
0 - 1998	21.5 m	1.1 cm/a	80 m	4 cm/a	0.27
1500 - 1998	2 m	0.4 cm/a	20 m	4 cm/a	0.1
1964 - 1998	11 cm	0.32 cm/a	134 cm	4 cm/a	<0.1

Table 4.1: Seismic slip, seismic slip rate, total slip, total slip rate and inferred seismic coupling for the considered time intervals

and Jones, 1996) and the exhaustive earthquake catalogue compiled by Papazachos et al. (2000) which also has a completeness threshold of $M_w 8.0$. For the shorter time intervals of 500 and 34 years, respectively, the completeness threshold was estimated from inspection of the catalogues (Engdahl et al., 1998; Papazachos et al., 2000). But even when we double the events above the assumed detection threshold we end up with a maximum seismic slip that can only account for less than half of the total slip. In section 4.4.2 it was shown that even when we assume a magnitude of $M_w 8.5$ for the 365 AD event and a b-value of 1.2 we are only able to account for roughly half of the expected total slip. An even larger magnitude of the 365 AD event is questionable (Papazachos, 1996; Papazachos and Papazachou, 1997) and a b-value of 1.2 can also be regarded as upper bound for this region (e.g. Hatzidimitriou et al., 1985; Papazachos, 1999; Manakou and Tsapanos, 2000; Papaioannou and Papazachos, 2000).

For the total slip a constant slip rate during the last 2000 years was assumed as given by the results of GPS studies in the end of the 20th century (Kahle et al., 2000; McClusky et al., 2000). These values of 40 mm/a for the relative motion between the plates are in good agreement with tectonic reconstructions spanning the last 10 Ma (tenVeen and Kleinspehn, 2003). However, a temporally variable total slip rate can not be ruled out. Especially in the time leading up to the 365 AD event for which studies of ancient shorelines (Pirazzoli et al., 1982, Pirazzoli et al., 1996) indicate a locking of the plate contact the total slip rate on the plate contact might have been much smaller than today. However, for the last 500 years e.g. the total slip rate at the plate contact must have been smaller than 10 mm/a in average to obtain complete seismic coupling. This scenario is very unlikely. Because strain accumulation started long before the 365 AD event even a ratio of seismic slip to total slip larger than one is theoretically possible. That means despite of the 365 AD event the plate contact of the rupture area of the event shows a seismic slip deficit for all considered time intervals.

This seismic slip deficit can be explained by different scenarios. First of all the plate con-

tact can be locked accumulating strain while the upper plate in the forearc is deformed aseismically. This scenario however seems unlikely because (1) no locked areas where detected in the evaluation of interplate seismicity, (2) most strong seismic activity is located at or close to the plate contact giving no indications for a strong internal deformation of the overiding plate in the broader vicinity of the plate contact, (3) the velocity field calculated from GPS studies (Kahle et al., 2000, McClusky et al., 2000) is rather homogeneous giving no indication for horizontal arc-normal internal deformation that could explain the seismic slip deficit, and (4) the rather high b-value of about 1 found in this region (Hatzidimitriou et al., 1985; Papazachos, 1999; Manakou and Tsapanos, 2000; Papaioannou and Papazachos, 2000). These observations hint more at steady slip conditions with an overall unlocked plate contact and large aseismic slip at the plate interface. Thus, a weak and unlocked plate contact seems to be present in the southwestern forearc of the HSZ. This would imply that the slip rate at the plate boundary can be equated with the far field GPS velocity and the plate contact is conditionally stable controlled by time and space dependent coupling. Whether some strain is accumulating at the plate contact despite the absence of large locked zones and reducing the amount of aseismic slip cannot be resolved. In order to address this problem it is necessary to quantify the amount of aseismic slip. Because aseismic slip may occure by small earthquakes, tremors, silent earthquakes or creep, a continuous microseismic monitoring, the search for non-volcanic tremors and silent earthquakes as well as a dense and continuous GPS measurement campaign in the area of Crete and towards the south is needed to estimate the aseismic component of the total slip. This is necessary to verify the assumption of an unlocked plate contact and to assess the seismic hazard caused by possible strain accumulation.

If we assume that the 365 AD event ruptured the plate contact, the behaviour of the plate contact can be characterize by three different phases: (1) A locked plate contact without relative plate movement ruptures in (2) sudden complete failure and is followed by the recent (3) steady slip regime with high rates of aseismic slip. Indications of a formerly locked plate contact were found in a stepwise subsidence of ancient shorelines (Pirazzoli et al., 1982, Pirazzoli et al., 1996) predating the up to 9 m of uplift accompanying the 365 AD event. The seismic slip deficit along the plate contact would be even larger if the 365 AD event occurred in the Aegean plate on a fault plane not parallel to the plate contact. Further palaeoseismological studies are needed to characterize the former behaviour of the plate contact.

The spatio-temporal variability of seismic coupling of the plate contact is further indicated by the rather random distribution of seismic events observed instrumentally. Subregions

of the plate contact may be locked and release subsequently seismic energy while most of the relative movement between the plates is accommodated aseismically. These properties may be influenced by a spatio-temporarily varying distribution of asperities and fluids as well as variations in pore pressure.

4.7 Conclusions

A formula to estimate the maximum seismic slip on a rupture surface from historical or instrumental catalogues is derived. The formulation uses empirical relations relating moment magnitude with rupture area as well as average seismic slip and extends the catalogues towards smaller magnitudes assuming a constant b-value. For catalogues with a known completeness threshold a summation over all events above this completeness threshold is performed. Alternatively, a maximum event can be chosen in conjunction with a constant b-value to estimate the cumulative seismic slip of all events on the rupture surface of this earthquake. Relating this cumulative seismic slip to the total slip obtained from geodetic or geologic studies gives the seismic coupling.

Application of this formula to the plate contact south-west of Crete shows the majority of the total slip at the rupture surface is currently accommodated aseismically despite of the $M_w 8.3$ event in the southwestern HSZ in 365 AD. When comparing the results for different time intervals of 2000, 500 and 34 years all ending in 1998 we find as most likely results values of about 0.25, 0.1 and less than 0.1, respectively, for the seismic coupling coefficient.

The seismicity distribution in catalogues of instrumental seismcity hints at a spatial variability of seismic energy release with activity in the proximity of the 365 AD epicentre an order of magnitude larger than towards the north-east between Crete and the Peleponnese. The spatio-temporal variability of the seismic energy release and seismic coupling hints at a conditionally stable behaviour of the plate contact. It is likely caused by non-stationary properties of the plate contact like the distribution of asperities and fluids or variations in pore pressure.

The occurrence of large earthquakes seems to depend on coeval locking of subregions of the plate contact that means on properties of the plate contact. Because of the spatio-temporal variability of the seismic coupling the concept of a fixed return period for exceptionally large events seems to be rather questionable. Continuous seismic and geodetic monitoring of the plate contact are needed to investigate the variable seismic and geodetic slip rates

in greater detail.

5 Concluding Remarks

The spatio-temporal seismicity clustering in the area of Crete was studied on different length and time scales spanning several orders of magnitude. On the one hand swarm-like microseismic activity lasting a few days and migrating with velocities of approximately 500 m/day was observed and taken as indication for the presence of fluids on the rupture surface triggering these microseismicity clusters on their way to the surface. On the other side of the time and length scales investigated in this work large magnitude seismicity with $M_w \geq 6.5$ was studied on the plate contact in the western part of the Hellenic forearc. Results indicate a temporal variability of the seismic energy release on the order of centuries and a plate contact in conditionally stable state. In the trantensional graben system in the eastern forearc a spatial clustering of microseismicity as well as intermediate magnitude seismicity is observed in the region of the Ptolemy and the Pliny trench with hardly any seismicity in between. This behaviour can be interpreted with the presence of a forearc sliver, a rigid block without significant internal deformation, that is bounded by the seismically active Ptolemy and Pliny trenches accomodating the left-lateral motion caused by the oblique subduction in that area.

Although the region of Crete and the Eastern Mediterranean in general is a focus of many research initiatives, projects and studies, important questions are not yet sufficiently answered. One of these questions is that of the source mechanism and fault zone of the 365 AD $M_w 8.3$ event. Although it is generally believed that is was a thrust event at the plate contact south-west of Crete it is not easy to model the observed vertical movements by such a scenario. Thus, further studies, using both a modelling approach and palaeoseismological invesigations, are needed to answer the question whether other fault planes may better explain the observed data. Another not entirely understood point is the character of the transtensional graben system in the eastern forearc. A GPS study including the island of Chrisi south of the Ptolemy trench as well as stations on Crete would provide valuable information about the character of the Ptolemy graben and might answer the question whether the high seismic activity observed from near surface depths down to the

plate interface is related to left lateral movement in that region. Also the hypothesis of cluster generation in the Ptolemy and possibly also the Pliny trench by ascending fluids can be addressed by detailed studies of the seafloor using ROVs or towed cameras.

Acknowledgements

Last but not least I thank Katrin, Marie and Helen for all the happy hours I have the privilege to spend with them.

Thank you!

Bibliography

R. E. Abercombie und J. N. Brune. Evidence for a constant b-value above magnitude 0 in the southern San Andreas, San Jacinto and San Miguel fault zones, and the Long Valley caldera, California. *Geophys. Res. Lett.*, 21:1647–1650, 1994.

N. N. Ambraseys. Comparison of frequency of occurence of earthquakes with slip rates from long-term seismicity data: the cases of Gulf of Corinth, Sea of Marmara and Dead Sea Fault Zone. *Geophys. J. Int.*, 165:516–526, 2006. doi:10.1111/j.1365-246X.2006.02858.x.

J. Angelier, N. Lyberis, X. LePichon, E. Barrier, und P. Huchon. The tectonic development of the Hellenic arc and the sea of Crete. *Tectonophysics*, 86:159–196, 1982.

D.F. Argus, R.G. Gordon, C.D. DeMets, und S. Stein. Closure of the Africa-Eurasia-North America plate motion circuit and the tectonics of the Gloria fault. *J. Geophys. Res.*, 94:5585–5602, 1989.

D.F. Argus und M.B. Heflin. Plate motion and crustal deformation estimated with geodetic data from GPS. *Geophys. Res. Lett.*, 22:1973–1076, 1995.

R.H. Armijo, H. Lyon-Caen, und D. Papanastassiou. East-west extension and Holocene normal-fault scarps in the Hellenic arc. *Geology*, 20:491–494, 1992.

R. C. Aster und J. Scott. Comprehensive Characterization of Waveform Similarity in Microearthquake Data Sets. *Bull. Seism. Soc. Am.*, 83:1307–1314, 1993.

W.H. Bakun und A.G. Lindh. The Parkfield, California, earthquake prediction experiment. *Science*, 229:619–624, 1985.

D. Becker. Mikroseismizität und Deformation der Kruste Ostkretas. 2000. Diploma Thesis, in German.

D. Becker, T. Meier, M. Bohnhoff, und H.-P. Harjes. Seismic coupling between the Aegean and African lithosphere in the Hellenic Subduction Zone. In *Tectonics on Human Time Scales*, pages 86–88, 2004. Bochumer Geowissenschaftliche Arbeiten, Heft 3.

Bibliography

D. Becker, T. Meier, M. Rische, M. Bohnhoff, und H.-P. Harjes. Spatio-temporal micro-seismicity clustering in the Cretan region. *Tectonophysics*, 423:3–16, 2006.

Y. Ben-Zion, V. Lyakhovsky, und H. Gvirtzman. Self-driven mode switching of earthquake activity on a fault system. *Earth Planet. Sci. Lett.*, 172:11–21, 1999.

M. Bohnhoff, J. Makris, G. Stavrakakis, und D. Papanikolaou. Crustal investigation of the Hellenic subduction zone using wide aperture seismic data. *Tectonophysics*, 343: 239–262, 2001.

M. Bohnhoff, T. Meier, und H.P. Harjes. Stress regime at the Hellenic Arc from focal mechanisms. *J. Seismology*, 9:341–366, 2005.

S. Bourouis und P. Bernard. Evidence for coupled seismic and aseismic fault slip during water injection in the geothermal site of Soultz (France), and implications for seismogenic transients. *Geophys. J. Int.*, 169:723–732, 2007.

M. Brönner. *Untersuchung des Krustenaufbaus entlang des Mediterranen Rückens abgeleitet aus geophysikalischen Messungen*. PhD thesis, Universität Hamburg, 2003. In German.

C.G. Bufe und D.M. Perkins. Evidence for a Global Seismic-Moment Release Sequence. *Bull. Seis. Soc. Am.*, 95:833–843, 2005.

G. Cifci, A. Limonov, L. Dimitrov, und V. Gaianov. Mud Volcanoes and Dome-Like Structures at the Eastern Mediterranean Ridge. *Mar. Geophys. Res.*, 19:421–438, 1997.

M. Cocard, H.-G. Kahle, Y. Peter, A. Geiger, G. Veis, S. Felekis, H. Billiris, und D. Paradissis. New constraints on the rapid crustal mozion of the Aegean region: Recent results inferred from GPS measurements (193-1998) across the West Hellenic Arc, Greece. *Earth Plant. Sci. Lett.*, 172:39–47, 1999.

J.B. de Chabalier, H. Lyon-Caen, A. Zollo, A. Deschamps, P. Bernard, und D. Hatzfeld. A detailed analysis of microearthquakes in western Crete from digital three-component seismograms. *Geophys. J. Int.*, 110:347–360, 1992.

N. Delibasis, M. Ziazias, N. Voulgaris, T. Papadopoulos, G. Stavrakakis, D. Papanastassiou, und G. Drakatos. Microseismic activity and seismotectonics of the Heraklion area (central Crete Island, Greece). *Tectonophysics*, 308:237–248, 1999.

C. DeMets, R. Gordon, D. Argus, und S. Stein. Current plate motions. *Geophys. J. Int.*, 101:425–478, 1994.

J. Dercourt, L.P. Zonenshain, L.-E. Ricou, V.G. Kazmin, X. LePichon, A.L. Knipper, C. Grandjacquet, I.M. Sbortshikov, J. Geyssant, C. Lepvrier, D.H. Pechersky, J. Boulin, J.-C. Sibuet, L.A. Savostin, O. Sorokhtin, M. Westphal, M.L. Bazhenov, J.P. Lauer, und B. Biju-Duval. Geological evolution of the Tethys belt from the Atlantic to the Pamirs since Lias. *Tectonophysics*, 123:241–315, 1986.

A.V. Deshcherevsky und V.I. Zhuravlev. Temporal regime of microearthquakes in the Garm research area. *Physics of the Solid Earth*, 40:66–82, 2004.

H.R. DeShon, S.Y. Schwartz, S.L. Bilek, L.M. Dorman, V. Gonzalez, J.M. Protti, E.R. Flueh, und T.H. Dixon. Seismogenic zone structure of the southern Middle America Trench, Costa Rica. *J. Geophys. Res.*, 108, 2003. doi:10.1029/2002JB002294.

A. di Vita. Archaeologists and earthquakes: the case of the 365 AD earthquake. *Ann. di Geofis.*, 38:971–976, 1996.

C.E. Duermeijer, W. Krijgsman, C.G. Langereis, und J.H. ten Veen. Post-early Messinian counterclockwise rotations on Crete; implications for late Miocene to recent kinematics of the southern Hellenic Arc. *Tectonophysics*, 298:177–189, 1998.

B. Endrun, T. Meier, M. Bischoff, und H.-P. Harjes. Lithospheric structure in the area of Crete constrained by receiver functions and dispersion analysis of Rayleigh phase velocities. *Geophys. J. Int.*, 158:592–608, 2004.

E.R. Engdahl, R. van der Hilst, und R. Buland. Global teleseismic earthquake relocation with improved travel times and procedures for depth determination. *Bull. Seismol. Soc. Am.*, 88:722–743, 1998.

B. Everitt. *Cluster Analysis*. Arnold, 1993.

C. Facenna, L. Jolivet, C. Piromallo, und A. Morelli. Subduction and the depth of convection in the Mediterranean mantle. *J. Geophys. Res.*, 108, 2003. doi:10.1029/2001JB0011690.

T. Fischer und J. Horalek. Refined locations of the swarm earthquakes in the Novy Kostel focal zone and spatial distribution of the January 1997 swarm in western Bohemia, Czech Republic. *Studia Geophys. et Geod.*, 44:210–226, 2000.

W.K. Gealey. Plate tectonic evolution of the Mediterranean - Middle East region. *Tectonophysics*, 155:285–306, 1988.

Bibliography

T.V. Gerya und B. Stöckhert. 2-D numerical modeling of tectonic and metamorphic histories at active continental margins. *Int. J. Earth Sciences*, 2006. in press.

T.V. Gerya, B. Stöckhert, und A.L. Perchuk. Exhumation of high-pressure metamorphic rocks in a subduction channel - a numerical simulation. *Tectonics*, 21:6–1 – 6–19, 2002.

D. Gillard, A. M. Rubin, und P. Okubo. Highly concentrated seismicity caused by deformation of Kilauea's deep magma system. *Nature*, 384:343–346, 1996.

J.-G. Got, J. Frechet, und F.W. Klein. Deep fault plane geometry inferred from multiplet relative relocation beneath the south flank of Kilauea. *J. Geophys. Res.*, 99:15375–15386, 1994.

B. Gutenberg und C.F. Richter. Frequency of earthquakes in California. *Bull. Seism. Soc. Am.*, 34:185–188, 1944.

S. Hainzl. Seismicity patterns of earthquake swarms due to fluid intrusion and stress triggering. *Geophys. J. Int.*, 159:1090–1096, 2004. doi:10.1111/j.1365-246X.2004.02463.x.

W. Hanka und R. Kind. The GEOFON Program. *Annali di Geofisica*, 33:1060–1065, 1994.

D. Hatzfeld, M. Besnard, K. Makropoulos, und P. Hatzdimitriou. Microearthquake seismicity and fault-plane solutions in the southern Aegean and its geodynamic implications. *Geophys. J. Int.*, pages 799–818, 1993.

P.M. Hatzidimitriou, E.E. Papadimitriou, D.M. Mountrakis, und B.C. Papazachos. The seismic parameter b of the frequency-magnitude relation and its association with the geological zones in the area of Greece. *Tectonophysics*, 120:141–151, 1985.

Y. Hayashi und Y. Morita. An image of a magma intrusion process inferred from precise hypocentral migrations of the earthquake swarm east of the Izu Peninsula. *Geophys. J. Int.*, 153:159–174, 2003.

P. Huchon, N. Lyberis, J. Angelier, X. LePichon, und V. Renard. Tectonics of the Hellenic Trench: A Synthesis of Sea-Beam and Submersible Observations. *Tectonophysics*, 86: 69–112, 1982.

C. Huguen, J. Mascle, E. Chaumillon, J.M. Woodside, J. Benkhelil, A. Kopf, und A. Volksonkaia. Deformation styles of the eastern Mediterranean Ridge and surroundings from combined swath mapping and seismic reflection profiling. *Tectonophysics*, 343:21–47, 2001.

S. Husen, E. Kissling, E. Flueh, und G. Asch. Accurate hypocenter determination in the seismogenic zone of the subducting Nazca Plate in northern Chile using a combined on-/offshore network. *Geophys. J. Int.*, 138:687–701, 1999.

T. Igarashi, T. Matsuzawa, und A. Hasegawa. Repeating earthquakes in interplate aseismic slip in the northeastern Japan subduction zone. *J. Geophys. Res.*, 108, 2003. doi:10.1029/2002JB001920.

J. Jackson und D. McKenzie. The relationship between plate motions and seismic moment tensors, and the rates of active deformation in the Mediterranean and the Middle East. *Geophysical J.*, 93:45–73, 1988.

S. Jenny, S. Goes, D. Giardini, und H.-G. Kahle. Earthquake recurrence parameters from seismic and geodetic strain rates in the eastern Mediterranean. *Geophys. J. Int.*, 157, 2004. doi:10.1111/j.1365-246X.2004.02261.x.

L. Jolivet. A comparison of geodetic and finite strain pattern in the Aegean, geodynamic implications. *Earth planet. Sci. Lett.*, 187:95–104, 2002.

M.L. Jost, O. Knabenbauer, J. Chang, und H.P. Harjes. Fault plane solutions of microearthquakes and small events in the Hellenic arc. *Tectonophysics*, 356:87–114, 2002.

H.-G. Kahle, M. Cochard, Y. Peter, A. Geiger, R. Reilinger, A. Barka, und G. Veis. GPS-derived strain rate field within the boundary zones of the Eurasian, African and Arabian Plates. *J. Geophys. Res.*, 105:23353–23370, 2000.

H.-G. Kahle, C. Straub, R. Reilinger, S. McClusky, R. King, K. Hurst, G. Veis, K. Kastens, und P. Cross. The strain rate field in the eastern Mediterranean region, estimated by repeated GPS measurements. *Tectonophysics*, 294:237–252, 1998.

H. Kanamori. Seismic and aseismic slip along subduction zones and their tectonic implications. In *Maurice Ewing Ser. 1*, pages 162–174, 1977.

N. Kato und T.Seno. Hypocenter depths of large interplate earthquakes and their relation to seismic coupling. *EPSL*, 210:53–63, 2003.

E. Kissling, W. Ellsworth, D. Eberhart-Phillips, und U. Kradolfer. Initial reference models in local earthquake tomography. *J. Geophys. Res.*, 99:19635–19646, 1994.

F. W. Klein. User's Guide to HYPOINVERSE-2000, a Fortran Program to Solve for Earthquake Locations and Magnitudes. Technical Report 02-171, U.S. Dep. Int., Geological Survey, 2002.

M. Knappmeyer und H.-P. Harjes. Geometry of the Aegean Benioff zones. *Ann. Geofis.*, 42:27–37, 1999.

A.J. Kopf. Significance of mud volcanism. *Rev. Geophys.*, 40, 2002. doi:10.1029/2000RG000093.

G. C. Koravos, I. G. Main, T. M. Tsapanos, und R. M. W. Musson. Maximum earthquake magnitudes in the Aegean area constrained by tectonic moment release rates. *Geophys. J. Int.*, 152:94–112, 2003.

V.V. Kostrov. Seismic moment and energy of earthquakes, and seismic flow of rocks. *Izv. Earth Physics*, 1:23–40, 1974.

S.A. Kovachev, I.P. Kuzin, und S.L. Soloviev. Spatial Distribution of Microearthquakes in the Frontal Part of the Hellenic Arc according to Observations of Bottom Seismographs. *Geotektonika*, 25:155–160, 1991.

S.A. Kovachev, I.P. Kuzin, und S.L. Soloviev. Microseismicity of the frontal Hellenic arc according to OBS observations. *Tectonophysics*, 201:317–327, 1992.

C. Kreemer und N. Chamot-Rooke. Contemporary kinematics of the southern Aegean and the Mediterranean Ridge. *Geophys. J. Int.*, 157:1377–1392, 2004. doi:10.1111/j.1365-246X.2004.02270.x.

J. H. Kurz, T. Jahr, und G. Jentzsch. Earthquake swarm examples and a look at the generation mechanism of the Vogtland/Bohemia earthquake swarm. *Phys. Earth Plant. Int.*, 142:75–88, 2004.

M. Laigle, M. Sachpazi, und A. Hirn. Variation of seismic coupling with slab detachment and upper plate structure along the western Hellenic subduction zone. *Tectonophysics*, 391:85–95, 2004.

S. Lallemant, C. Truffert, L. Jolivet, P. Henry, N. Chamot-Rooke, und B. de Voogd. Spatial transition from compression to extension in the Western Mediterranean Ridge accrettionary complex. *Tectonophysics*, 234:33–52, 1994.

K. Lambeck. Late Pleistocene and Holocene sea-level change in Greece and south-western Turkey: a separation of eustatic, isostatic and tectonic contributions. *Geophys. J. Int.*, 122:1022–1044, 1995.

T. Lay und H. Kanamori. Earthquake doublets in the Solomon islands. *Phys. Earth Planet. Inter.*, 21:283–304, 1981.

W. Lee und J. Lahr. HYPO71: A computer program for determining hypocentre, magnitude and first motion pattern of local earthquakes. Technical Report Open File Report 75-311, U.S. Geol. Surv., 1972.

X. LePichon, N. Chamot-Rooke, und S. Lallement. Geodetic determination of the kinematics of central Greece with respect to Europe: Implications for the eastern Mediterranean tectonics. *Geophys. Res.*, 100:12675 –12690, 1995.

X. LePichon, N. Lyberis, J. Angelier, und V. Renard. Strain distribution over the east Mediterranean Ridge: A synthesis incorporating new sea-beam data. *Tectonophysics*, 86:243–274, 1982.

X. Li, G. Bock, A. Vafidis, R. Kind, H.-P. Harjes, K. Wyllegalla, M. van der Meijde, und X. Yuan. Receiver function study of the Hellenic subduction zone; imaging crustal thickness variations and the oceanic Moho of the descending African lithosphere. *Geophys. J. Int.*, 155:733–748, 2003.

D.A. Lockner, J.D. Byerlee, V. Kuksenko, A. Ponomarev, und A. Sidorin. Quasi-static fault growth and shear fracture energy in granite. *Nature*, 363:39–42, 1991.

A. Lomax, J. Virieux, P. Volant, und C. Berge-Thierry. Probabilistic earthquake location in 3D and layered models. In C.H. Thurber und N. Rabinowitz, editors, *Advances in seismic event location*, Dordrecht, Netherlands, 2000. Kluwer Academic Publishers.

H. Lyon-Caen, R. Armijo, J. Drakopoulos, J. Baskoutas, N. Delibasis, R. Gaulon, V. Kouskouna, J. Latousakis, K. Makropoulos, P. Papadimitriou, D. Papanastasiou, und G. Pedotti. The 1986 Kalamata (South Peleponnesus) earthquake: Detailed Study of a Normal Fault, Evidences for East-West Extension in the Hellenic Arc. *J. Geophys. Res.*, 93:14967–15000, 1988.

I. G. Main. Earthquakes as Critical Phenomena: Implications for Probabilistic Seismic Hazard Analysis. *Bull. Seism. Soc. Am.*, 85:1299–1308, 1995.

I.G. Main. A characteristic earthquake model of the seismicity preceding the eruption of Mt St Helens on 18 May 1980. *Phys. Earth Planet. Int.*, 49:283–293, 1987.

K.C. Makropoulos und P.W. Burton. Greek tectonics and seismicity. *Tectonophysics*, 106: 275–304, 1984.

M. V. Manakou und T. M. Tsapanos. Seismicity and seismic hazard parameters evaluation in the island of Crete and the surrounding area inferred from mixed data file. *Tectonophysics*, 321:157–178, 2000.

J. Mascle, C. Huguen, J. Benkhelil, N. Chamot-Rooke, E. Chaumillon, J.P. Foucher, R. Griboulard, A. Kopf, G. Lamarche, A. Volkonskaia, J. Woodside, und T. Zitter. Images may show start of European-African plate collision. *EOS*, 80 (37):421,425,428, 1999.

S. McClusky, S. Ballassanian, A. Barka, C. Demir, S. Ergintav, I. Georgiev, O. Gurkan, M. Hamburger, K. Hurst, H. Kahle, K. Kastens, G. Kekelidze, R. King, V. Kotzev, O. Lenk, S. Mahmoud, A. Mishin, M. Nadariya, A. Ouzounis, D. Paradissis, Y. Peter, M. Prilepin, R. Reilinger, I. Sanli, H. Seeger, A. Tealeb, M.N. Toksöz, und G. Veis. Global Positionng System constraints on plate kinematics and dynamics in the eastern Mediterranean and Caucasus. *J. Geophys. Res.*, 105:5695–5719, 2000.

D.P. McKenzie. Plate tectonics of the Mediterranean region. *Nature*, 226:217–254, 1970.

T. Meier, K. Dietrich, B. Stöckhert, und H.-P. Harjes. One dimensional models for shear wave velocity for the Eastern Mediterranean obtained from the inversion of Reighley wave phase velocities and tectonic implications. *Geophys. J. Int.*, 156:45–58, 2004b. doi:10.1111/j.1365-246X.2004.92121.x.

T. Meier, M. Rische, B. Endrun, A. Vafidis, und H.-P. Harjes. Seismicity of the Hellenic subduction zone in the area of western and central Crete observed by temporary local seismic networks. *Tectonophysics*, 383:149–169, 2004a.

P. Meijer und M. Wortel. Temporal variation in the stress field of the Aegean region. *Geophys. Res. Lett.*, 23:439–442, 1996.

J.E. Meulenkamp, G.J. van der Zwaan, und W.A. van Wamel. On Late Miocene to recent vertical motions in the Cretan segment of the Hellenic arc. *Tectonophysics*, 234:53–72, 1994.

S.A. Miller. Fluid-mediated influence of adjacent thrusting on the seismic cycle at Parkfield. *Nature*, 382:799–802, 1996.

S.A. Miller und D.L. Olgaard. Modeling Seismicity Clustering and Fault Weakness due to High Pore Pressures. *Phys. Chem. Earth*, 22:43–48, 1997.

P. Molnar. Earthquake recurrence intervals and plate tectonics. *Bull. Seis. Soc. Am.*, 69: 115–133, 1979.

C. Monaco und L. Tortorici. Faulting and effects of earthquakes on Minoan archological sites in Crete (Greece). *Tectonophysics*, 382:103–116, 2004.

R. M. Nadeau und T. V. McEvilly. Seismological Studies at Parkfield V: Characteristic Microearthquake Sequences as Fault-Zone Drilling Targets. *Bull. Seis. Soc. Am.*, 87: 1463–1472, 1997.

R.M. Nadeau, W. Foxall, und T.V. McEvilly. Clustering and periodic recurrence of microearthquakes on the San Andreas fault near Parkfield. *Science*, 267:503–507, 1995.

R.M. Nadeau und J.R. Johnson. Seismological Studies at Parkfield IV: Moment Releaase Rates and Estimates of Source Parameters for Small Repeating Earthquakes. *Bull. Seis. Soc. Am.*, 88:790–814, 1998.

R. G. North. Seismic slip rates in the Mediterranean and Middle East. *Nature*, 252: 560–563, 1974.

Y. Ogata. Estimation of the parameters in the modified omori formula for aftershock frequencies by the maximum likelihood procedure. *J. Phys. Earth*, 31:115–124, 1983.

Y. Ogata. Statistical model for standard seismicity and detection of anomalies by residual analysis. *Tectonophysics*, 169:159–174, 1989.

J.F. Pacheco, L.R. Sykes, und C.H. Scholz. Nature of Seismic Coupling Along Simple Plate Boundaries of the Subduction Type. *J. Geophys. Res.*, 98:14133–14159, 1993.

G.A. Papadopoulos. Seismic and volcanic activities and aseismic movements as plate motion components in the Aegean area. *Tectonophysics*, 167:31–39, 1989.

Ch.A. Papaioannou und B.C. Papazachos. Time-Independent and Time-Dependent Seismic Hazard in Greece Based on Seismogenic Sources. *Bull. Seis. Soc. Am.*, 90:22–33, 2000.

B. Papazachos, A. Kiratzi, und E. Papadimitriou. Regional Focal Mechanisms for Earthquakes in the Aegean Area. *PAGEOPH*, 136:405–420, 1991.

B.C. Papazachos. Measures of earthquake size in Greece and surrounding areas. In Geophys. Soc. of Greece, editor, *Proc. of the 1st Scient. Conf. of Geophysics*, pages 438–447, Athens, 1989.

Bibliography

B.C. Papazachos. Large Seismic Faults in the Hellenic Arc. *Annal. di Geophys. XXXIX*, 5:891–903, 1996.

B.C. Papazachos und P.E. Comninakis. Geophysical and tectonic features of the Aegean arc. *J. Geophys. Res.*, 76:8517–853, 1971.

B.C. Papazachos, P.E. Comninakis, B.G. Karakaisis, B.G. Karakostas, C.A. Papaioannou, C.B. Papazachos, und E.M. Scordilis. *A catalog of earthquakes in Greece and Surrounding Area for the Period 550BC-1999.* Geophysics Laboratory, 2000a. University of Thessaloniki.

B.C. Papazachos, V.G. Karakostas, C.B. Papazachos, und E.M. Scordilis. The geometry of the Wadati-Benioff zone and the lithospheric kinematics in the Hellenic arc. *Tectonophysics*, 319:275–300, 2000b.

B.C. Papazachos, C.A. Papaioannou, C.B. Papazachos, und A.S. Savvaidis. Rupture zones in the Aegean region. *Tectonophysics*, 308:205–221, 1999.

B.C. Papazachos und C. Papazachou. *The earthquakes of Greece.* Ziti Publ., 1997.

C. Papazachos. An Alternative Method for a Reliable Estimation of Seismicity with an Application in Greece and the Surrounding Area. *Bull. Seis. Soc. Am.*, 89:111–119, 1999.

C.B. Papazachos, G.F. Karakaisis, E.M. Scordilis, und B.C. Papazachos. Probabilities of activation of seismic faults in critical regions of the Aegean area. *Geophys. J. Int.*, 159: 679–687, 2004. doi:10.1111/j.1365-246X.2004.02407.x.

C.B. Papazachos, A.A. Kiratzi, und B.C. Papazachos. Rates of active crustal deformation in the Aegean and the surrounding area. *J. Geodynamics*, 16:147–179, 1992.

C.B. Papazachos und G. Nolet. P and S deep velocity structure of the Hellenic area obtained by robust nonlinear inversion of travel times. *J. Geophys. Res.*, 102:8349–8367, 1997.

M. Parotidis, E. Rothert, und S.A. Shapiro. Pore-pressure diffusion: A possible triggering mechanism for the earthquake swarms 2000 in Vogtland/NW-Bohemia, central Europe. *Geophys. Res. Lett.*, 30, 2003. doi:10.1029/2003GL018110.

P. Pirazzoli, J. Laborel, und S. Stiros. Earthquake clustering in the Eastern Mediterranean during historical times. *J. Geophys. Res.*, 101:6083–6097, 1996.

P. Pirazzoli, J. Thommeret, Y. Thommeret, J. Laborel, und L. Montaggioni. Crustal block movements from Holocene shorelines, Crete and Antikythira (Greece). *Tectonophysics*, 86:27–43, 1982.

P. A. Pirazzoli. Uplift of Ancient Greek Coastal Sites: Study Methods and Results. In S. Stiros und R. E. Jones, editors, *Archaeoseismology*, pages 237–244, Athens, Greece, 1996.

P. Podvin und I. Lecomte. Finite difference computation of traveltimes in very contrasted velocity models: a massively parallel approach and its associated tools. *Geophys. J. Int.*, 105:271–284, 1991.

H.F. Reid. The mechanism of the earthquake. In Carnegie Institution, editor, *The California Earthquake of April 18, 1906, Report of the State Investigation Commission, Vol.2*, pages 1–192, Washington, DC, 1911.

R.E. Reilinger, S.C. Mc Clusky, M.B. Oral, R.W. King, M.N. Toksöz, A.A. Barka, I. Kinik, O. Lenk, und I. Sanli. Global Positioning System measurements of present-day crustal movements in the Arabia-Africa-Eurasia plate collision zone. *J. Geophys. Res.*, 102: 9983–9999, 1997.

E.A. Robinson. *Statistical communication and detection with special reference to digital data processing of radar and seismic signals.* Charles Griffin and Company, Ltd., 1967. London.

E. Roeloffs und J. Langbein. The earthquake prediction experiment at Parkfield. *Rev. Geophys.*, 32:315–336, 1994.

A. M. Rubin, D. Gillard, und J.-L. Got. Streaks of microearthquakes along creeping faults. *Nature*, 400:635–641, 1999.

L. Ruff und H. Kanamori. Seismicity and the Subduction Process. *Phys. Earth Planet. Int.*, 23:240–252, 1980.

D. P. Schaff und G. C. Beroza. Coseismic and postseismic velocity changes measured by repeating events. *J. Geophys. Res.*, 109, 2004. doi:10.1029/2004JB003011.

C.H. Scholz. Mechanics of Seismic Coupling in Subduction Zones. *EOS*, 69, 1988.

C.H. Scholz. *Mechanics of Earthquakes anf Faulting.* Cambridge University Press, 2002. Cambbridge.

C.H. Scholz und J. Campos. On the mechanism of seismic decoupling and back arc spreading at subduction zones. *J. Geophys. Res.*, 100:22103–22115, 1995.

D. Schorlemmer und S. Wiemer. Microseismicity data forecast rupture area. *Nature*, 434: 1086, 2005.

D. Schorlemmer, S. Wiemer, und M. Wyss. Earthquake statistics at Parkfield: 1. Stationarity of b values. *J. Geophys. Res.*, 109, 2004. doi:10.1029/2004JB003234.

E. M. Scordilis, G.F. Karakaisis, B.G. Panagiotopoulos, P.E. Comninakis, und B.C. Papazachos. Evidence for transform faulting in the Ionian Sea: the Cephalonia island earthquake sequence of 1983. *Pure Appl. Geophys.*, 123:388–397, 1985.

T. Senshu. On the time interval distribution of aftershocks. *Zisin, Ser. 2*, 12:149–161, 1959. in Japanese.

P. M. Shearer. Parallel fault strands at 9-km depth resolved on the Imperial Fault, Southern California. *Geophys. Res. Lett.*, 29:19–22, 2002.

K. Sieh, M. Stuiver, und D. Brillinger. A More Precise Chronology of Earthquakes produced by the San Andreas Fault in Southern California. *J. Geophys. Res.*, 94:603–623, 1989.

W. Spakman, S. van der Lee, und R. van der Hilst. Travel-time tomography of the European-Mediterranean mantle down to 1400 km. *Phys. Earth Planet. Int.*, 79:3–74, 1993.

A. Spicak und J. Horalek. Possible role of fluids in the process of earthquake swarm generation in the West Bohemia/Vogtland seismoactive region. *Tectonophysics*, 336: 151–161, 2001.

R.S. Stein. The role of stress-transfer in earthquake occurrence. *Nature*, 402:605–609, 1999.

S. Stiros und R.E. Jones. *Archaeoseismology.* Institute of Geology and Mineral Exploration and The British School at Athens, 1996. Fitch Laboratory Occasinal Paper 7.

S.C. Stiros. The AD 365 Crete earthquake and possible seismic clustering during the fourth to sixth centuries AD in the Eastern Mediterranean: a review of historical and archaeological data. *J. Struct. Geol.*, 23:545–562, 2001.

T. Taymaz, J. Jackson, und R. Westaway. Earthquake mechanisms in the Hellenic Trench near Crete. *Geophys. J. Int.*, 102:695–731, 1990.

J.H. ten Veen und K.L. Kleinspehn. Incipient continental collision and plate-boundary curvature: Late Pliocene-Holocene transtensional Hellenic forearc. *J. Geol. Soc.*, 160: 161–181, 2003.

J.H. ten Veen und P.T. Meijer. Late Miocene to recent tectonic evolution of Crete (Greece): geological observations and model analysis. *Tectonophysics*, 298:191–208, 1998.

S.N. Thomson, B. Stöckhert, und M.R. Brix. Thermochronology of the high-pressure metamorphic rocks of Crete, Greece: Implications for the speed of tectonic processes. *Geology*, 26:259–262, 1998.

M.N. Toksöz, A.F. Shakal, und A.J. Michael. Space-time migration of earthquakes along the North Anatolian fault zone and seismicity gaps. *Pageoph.*, 117:1258–1270, 1979.

T. Utsu, Y. Ogata, und R.S. Matsu'ura. The centenary of the Omori formula for a decay law of aftershock activity. *J. Phys. Earth*, 43:1–33, 1995.

F. Waldhauser und W.L. Ellsworth. A Double Difference Earthquake Location Algorithm: Method and Application to the Northern Hayward Fault. *Bull. seis. Soc. Am.*, 90:1353–1368, 2000.

S.N. Ward. Pacific-North America plate motions: new results from very long baseline interferometry. *J. Geophys. Res.*, 95:21965–21981, 1990.

D.L. Wells und K.J. Coppersmith. New Empirical Relations among Magnitude, Rupture Length, Rupture Width, Rupture Area and Surface Displacement. *Bull. Seism. Soc. Am.*, 84:974–1002, 1994.

M. West, J.J. Sanchez, und S.R. McNutt. Periodically Triggered Seismicity at Mount Wrangell, Alaska, After the Sumatra Earthquake. *Science*, 308:1144–1146, 2005.

S. Wiemer. A Software Package to analyze Seismicity: ZMAP. *Seis. Res. Lett.*, 72:373–382, 2001.

S. Wiemer und M. Wyss. Spatial and temporal variability of the b-value in seismogenic volumes: an overview. *Adv. Geophys.*, 45:259–302, 2002.

M. Wyss. Locked and creeping patches of the Hayward fault, California. *Geophys. Res. Lett.*, 28:3537–3540, 2001.

M. Wyss und M. Baer. Seismic quiescence in the Western Hellenic Arc may foreshadow large earthquakes. *Nature*, 289:785–787, 1981.

M. Wyss und R. Stefansson. Nucleation Points of Recent Mainshocks in Southern Iceland, Mapped by b-Values. *Bull. Seism. Soc. Am.*, 96:599–608, 2006. doi:10.1785/0120040056.

T. Yamashita. Pore Creation due to Fault Slip in a Fluid-permeated Fault Zone and its Effects on Seismicity: Generation Mechanism of Earthquake Swarm. *Pure Appl. Geophys.*, 155:625–647, 1999.

A. Ziv und A.M. Rubin. Static stress transfer and earthquake triggering: No lower threshold in sight? *J. Geophys. Res.*, 105:13631–13642, 2000.